The interaction of CENP-C-Mis12 complex is crucial for chromosome segregation fidelity and genome stability

CENP-C と Mis12 複合体の相互作用は染色体分配の正確性とゲノム安定性に重要である

Weixia Kong

Graduate School of Frontier Biosciences

Osaka University

September 2024

Abstract

The precise segregation of chromosomes during mitosis is vital for preserving genetic stability, a process tightly regulated by the kinetochore formed on centromeric region. CENP-C is an essential kinetochore component; its N-terminal region contains a conserved domain that directly associates with the Mis12 complex (Mis12C) to bridge the outer kinetochore and microtubules. This interaction appears to be crucial for cell viability. However, my lab previous demonstrated that the deletion of the Mis12C-binding domain of CENP-C was found to be dispensable in chicken DT40 cells. As this region is conserved in other species, this raises the questions: is this domain essential for cell growth in mammalian cells? or does the CENP-C-Mis12C interaction have an unclarified functional role in mammalian cells?

To address these questions, I generated mice (with a collaborator), mouse embryonic fibroblasts (MEFs) and human RPE-1 cells lacking the Mis12C-binding domain. I found that while the region is dispensable for growth in mouse and human cells, the CENP-C-Mis12C interaction is essential for precise chromosome segregation, mediated by the Aurora B kinase in human RPE-1 cells. The absence of the Mis12C-binding region in CENP-C resulted in reduced centromeric localization of Aurora B through the Bub1-H2AT120ph pathway, leading to weaker error correction and diminished chromosome oscillation in human RPE-1 cells. Additionally, I found that forced binding of Mis12C to CENP-C enhanced Aurora B localization and error correction activity in human HeLa cells with low Aurora B activity. Given that Aurora B facilitates the binding of CENP-C to Mis12C, I propose a positive feedback loop of Aurora B regulation mediated by the CENP-C-Mis12C interaction. Further cooperative work indicates that mice lacking the Mis12C-binding domain are prone to cancer. My findings link the CENP-C-Mis12C interaction to the regulation of Aurora B activity, which is crucial for ensuring chromosome segregation fidelity and maintaining cellular fitness.

CONTENTS

Chapter 1: General Introduction

The process of mitosis, characterized by its precise orchestration of events leading to the faithful segregation of chromosomes, has fascinated scientists for centuries. Integral to mitosis is the centromere, a specialized chromosomal region critical for the proper attachment and movement of chromosomes during cell division.

1.1 Centromere: Foundation of Chromosome Segregation

The journey to unraveling the mysteries of mitosis began with the pioneering observations of early microscopists. In the 19th century, scientists such as Walther Flemming and Eduard Strasburger (reviewed in Paweletz N. 2001) utilized advancements in microscopy to document the dynamic process of cell division. Their detailed descriptions of mitotic stages, including prophase, metaphase, anaphase, and telophase, laid the groundwork for subsequent investigations into the mechanisms governing chromosome segregation.

The identification of the centromere as a crucial component of chromosome structure and function emerged from a combination of cytological studies and genetic analyses. In the early 20th century, researchers like Theodor Boveri and Thomas Hunt Morgan (reviewed in O'Connor C and Miko I. 2008) provided evidences, suggesting the existence of specialized regions on chromosomes responsible for their segregation during mitosis and meiosis. Subsequent experiments employing techniques such as chromosome staining and electron microscopy further elucidated the morphological characteristics of centromeres, highlighting their importance in chromosome organization and movement.

The centromere, originally designated by Cyril Darlington in 1936 (Darlington CD. 1936), is a specialized region of the chromosome that plays a fundamental role in ensuring accurate chromosome segregation during cell division. It serves as the attachment site for microtubules emanating from the mitotic or meiotic spindle apparatus. This attachment is essential for proper chromosome alignment and segregation.

1.1.1 Structure of the Centromere

At a structural level, centromeres exhibit significant diversity across various organisms. In the majority of eukaryotes, centromeres manifest as monocentric chromosomes, identifiable as constriction points under microscopy. Plants and some insects, centromere diffuse or spread the whole chromosome defined as holocentromere (Drinnenberg IA et al., 2014; Cuacos M et al., 2015). To date, active centromeres are known epigenetically marked by the histone H3 variant CENP-A found in native and neocentromere (reviewed in Fukagawa T et al., 2014; McKinley KL et al., 2016; Musacchio A et al., 2017; Hara M et al., 2017). Monocentric chromosomes may possess either point centromeres, as observed in S. cerevisiae (a species of budding yeast), or regional centromeres, as found in humans (see Figs. 1A-B) (Hara M et al., 2017). Point centromeres represent specific DNA sequences consist of three elements (CDEI, II, and III) sufficient for centromere function, recruit of CENP-A (Cse4 in yeast) (Fig. 1B). CDEI and II are conservable while CDEII variable in sequence. Conversely, the regional centromere in humans comprises repetitive alpha-satellite DNA sequences, referred to as high-order repeats, which alone are insufficient for centromere function (Fig. 1B) (Clarke L et al.,1983; Carbon J et al.,1984). The incorporation of CENP-A replaces canonical histone H3 in nucleosomes, determining the active centromere, which spans a range from 340 kilobases (Chromosome 21) to 4.8 megabases (Chromosome 18) (reviewed in Sundararajan K et al., 2022).

1.1.2 Epigenetic Centromere Marker: CENP-A

Centromere in most organisms was defined by epigenetic mechanisms. Centromere identity is conferred by CENP-A, which is a histone H3 variant and is essential for centromere function. Human centromere protein A, CENP-A, was first identified using the serum of scleroderma CREST patients (Moroi Y et al., 1980; Earnshaw WC and Rothfield N. 1985). Molecular structural analysis of CENP-A reveals that the histone-fold domain in the C-terminal region shares approximately 57% amino acid identity with histone H3 and RG loop in the N-terminal tail. This stucture conformation is critical for

CENP-A incorporation and function (Sullivan KF, 1994; Sullivan KF, 2001; Tian T et al., 2018; Ariyoshi M et al., 2021). Deletion or mislocalization of CENP-A due to overexpression can lead to improper chromosome segregation, underscoring the importance of CENP-A in maintaining genome stability (Régnier V et al., 2005; Shrestha RL et al., 2017).

CENP-A is loaded exclusively onto the active centromere in dicentric chromosomes, suggesting it is an epigenetic marker (Warburton PE et al., 1997). Furthermore, in non-repetitive sequences, functional centromeres containing CENP-A can be established via the LacO/LacI system, providing a valuable tool for chromosome engineering and centromere studies (Hori T et al., 2013). In addition to marking the centromere, CENP-A associates with other centromere proteins, shedding light on the mechanism of chromosome segregation.

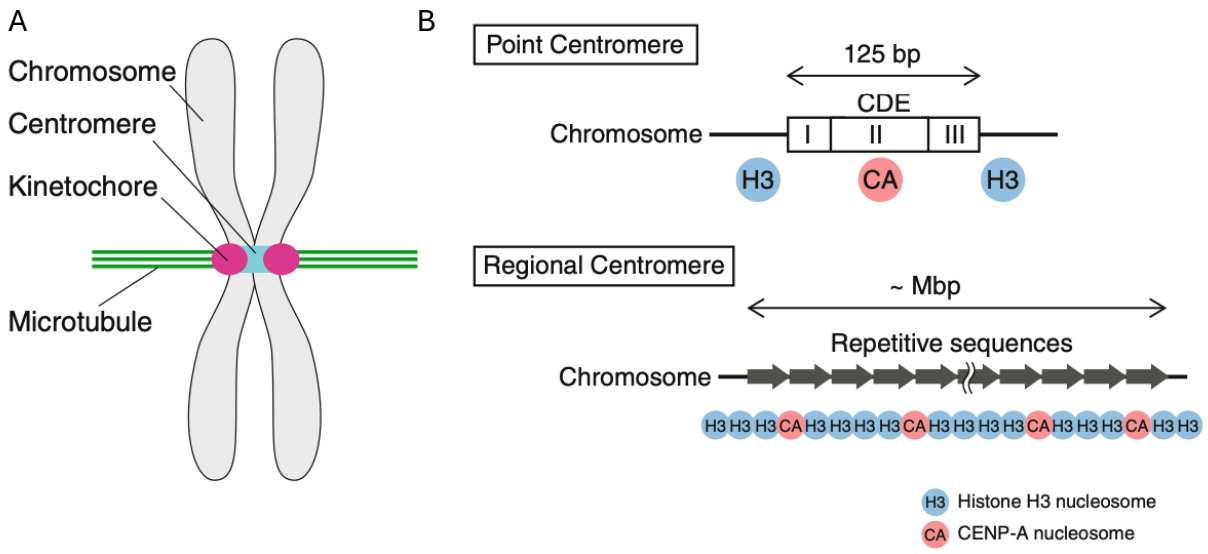

Figure.1 A schematic of the structure and arragement of the centromere.

(A) The centromere denotes a distinct genomic locus where the kinetochore assembles, establishing a microtubule-binding interface crucial for accurate chromosome segregation.

(B) A schematic of the point centromere and the regional centromere. The budding yeast, *Saccharomyces cerevisiae*, exhibits a distinctive point centromere structure, characterized by a compact 125-bp DNA sequence housing centromere DNA elements (CDE) I, II, and III. This concise DNA motif is occupied by a nucleosome containing the centromere-specific histone H3 variant, known as CENP-A (termed Cse4 in Saccharomyces cerevisiae). Conversely, regional centromeres span broader genomic regions and are typified by repetitive sequences, such as alpha-satellite repeats DNA in humans. While these repetitive elements aid in centromere assembly, the positioning of regional centromeres is primarily governed by the presence of CENP-A nucleosomes, serving as epigenetic markers for centromeric identity.

Figure 1 was adapted from Hara M and Fukagawa T. 2017.

1.2 The Kinetochore: Molecular Machinery for Chromosome Segregation

The kinetochore represents a sophisticated proteinaceous assembly that forms upon the centromere and orchestrates the binding of microtubules to chromosomes. This structure serves as the primary interface facilitating the interaction between chromosomes and the mitotic or meiotic spindle apparatus, thereby facilitating the transmission of forces requisite for accurate chromosome segregation.

Comprising numerous protein subcomplexes, the kinetochore is a multifaceted entity. In vertebrates, over 100 kinetochore proteins were identified up to date and were divided into subcomolexes. These subcomplexes encompass the constitutive centromere-associated network (CCAN), the KMN network (consisting of the KNL1 complex (KNL1C), Mis12 complex (Mis12C), and Ndc80 complex (Ndc80C)), alongside various regulatory proteins (reviewed in Nagpal H and Fukagawa T. 2016). Each constituent element plays a pivotal role in shaping the overall architecture and functionality of the kinetochore.

1.2.1 The Constitutive Centromere-Associated Network (CCAN): Scaffold for Kinetochore Assembly

The CCAN constitutes a pivotal structural framework within the kinetochore, orchestrating the assembly of diverse kinetochore proteins. It functions as a pivotal linkage between the centromeric chromatin and the outer kinetochore, notably the KMN (Knl1C-Mis12C-Ndc80C) network (DeLuca JG and Musacchio A. 2012), thereby conferring structural integrity and promoting accurate microtubule engagement to ensure proper chromosome segregation during cell division. Visualized through electron microscopy, the vertebrate kinetochore manifests as a trilaminar architecture, serving as a conduit between the centromeric region and microtubular elements (Fig. 2). Specifically, it exhibits a discernible middle layer of translucent appearance, flanked by densely stained inner and outer plates. Notably, the distal aspect of the outer plate interfaces with the fibrous corona, thereby completing the intricate architecture of the kinetochore complex (McEwen BF et al., 1998; Cheeseman IM and Desai A. 2008).

The CCAN comprises a diverse array of proteins, each with distinct roles in kinetochore assembly. This complex encompasses at least 16 members, including CENP-C, CENP-TWSX complex, CENP-LN complex, CENP-HIKM complex, and CENP-OPQUR complex (Fig. 3). The CCAN, along with the KMN netowork, is recruited to the centromere through CENP-C and CENP-T assembly pathway (McKinley KL et al., 2015; Nagpal H and Fukagawa T. 2016; Hara M et al., 2017).

A

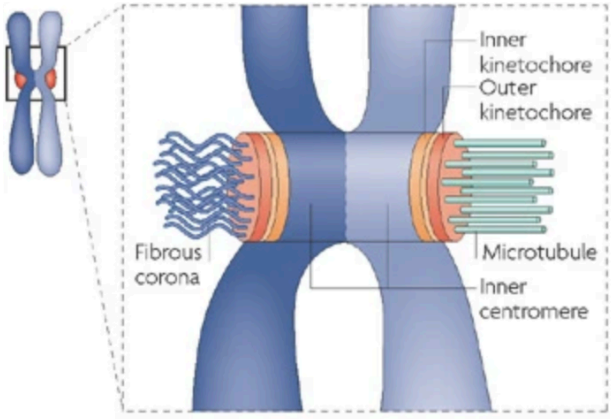

B

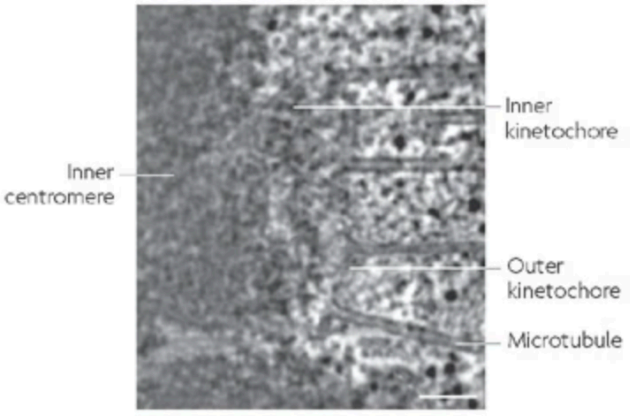

Nature Reviews | Molecular Cell Biology

Figure.2 Ultrastructure of vertebrate kinetochore by electron micrograph.

(A) A schematic of a chromosome with the unattched chromatid (left) and the attached chromatid (right) to microtubules at mitosis. Highlighted with the fibrous corona, the inner centromere, the inner kinetochore and the outer kinetochore.

(B) Human kinetochore under electron microscopy. The electron micrograph depicts a singular section extracted from a tomographic dataset of mitotic cell cryo-fixed under high pressure conditions. It has undergone labeling to pivotal architectural attributes of the kinetochore as in (A).

Figure 2 was adapted from Cheeseman IM and Desai A. 2008.

1.2.1.1 CENP-C

CENP-C is a key component of the CCAN and plays a central role in kinetochore assembly and function. It helps to maintain the stability of kinetochore-microtubule attachments and ensures proper chromosome alignment and segregation during cell division (Fukagawa T and Brown WR. 1997; Kwon MS et al., 2007; Klare K et al., 2015; Hara M et al., 2017).

CENP-C is a multi-domain protein with distinct regions that mediate its various functions within the kinetochore (Figs. 4A-B). These include regions involved in bindings to CENP-A, CCAN , and KMN and spindle checkpoint signaling (Mis12C binding domain) (Przewloka MR et al., 2011; Screpanti E et al., 2011; Petrovic A et al., 2016), CENP-A nucleosome-binding domains for centromere localization (central domain and CENP-C motif) (Carroll CW et al., 2010; Kato H et al., 2013; Ariyoshi M et al., 2021), and protein-binding domains for interactions with other kinetochore components (PEST domain) (Pentakota S et al., 2017; Klare K et al., 2015).

The dynamic regulation of the interaction between the CENP-A nucleosome and CENP-C occurs throughout the cell cycle. The presence of the CENP-H complex and the CENP-C motif is essential for the localization of CENP-C and the formation of functional centromeres (Watanabe R et al., 2019; Kwon MS et al., 2007; Fukagawa T et al., 2001).

Phosphorylation by CDK1 at a conserved site, T734 in humans and T651 in chickens, facilitates the binding of CENP-A nucleosomes to CENP-C (Watanabe R et al., 2019). During M-phase, CENP-C localizes to the centromere in cells lacking CENP-H or -K (members of the CENP-H complex), while CENP-C binding to the centromere requires the CENP-H complex during interphase (Fukagawa T et al., 2001). The interaction between CENP-A and CENP-C is crucial for the functioning of CENP-C during mitosis in human cells, although it appears to be non-essential in DT40 cells (Watanabe R et al., 2019). It is hypothesized that in DT40 cells, the CENP-T pathway assumes dominance and compensates for the absence of the CENP-A-CENP-C interaction, thereby mitigating the deficiencies arising from its absence within the CENP-C pathway (Watanabe R et al., 2019). Additionally, the CENP-LN complex directly binds to the CENP-A nucleosome and is required for the interaction of CENP-C with CENP-A nucleosomes during interphase (McKinley KL et al., 2015; Nagpal H et al., 2015). During M-phase, DSN1, a component of the Mis12 complex (Mis12C), undergoes phosphorylation at S100 and S109 by Aurora B kinase, facilitating its binding to CENP-C (Welburn JP et al. ,2010; Kim S and Yu H. 2015; Petrovic A et al., 2016; Dimitrova YN et al., 2016; Hara M et al., 2018). These pieces of evidence elucidate the dynamic alterations in CENP-C localization at the centromere during mitotic progression.

Disruption of cupin domain, which facilitates dimerization, attenuates the functionality of CENP-C in vertebrates (Klare K et al., 2015; Hara M et al., 2023). While the N-terminal region of CENP-C, Mis12C-binding domain is conserved from yeast to vertabrates and mammalian cells, the absence of the Mis12C-binding domain of CENP-C does not appear to affect cell proliferation and viability (Hara M et al., 2018; Watanabe R et al., 2019). However, the necessity of Mis12C-binding domain for CENP-C function during mitotic progression remains unclear.

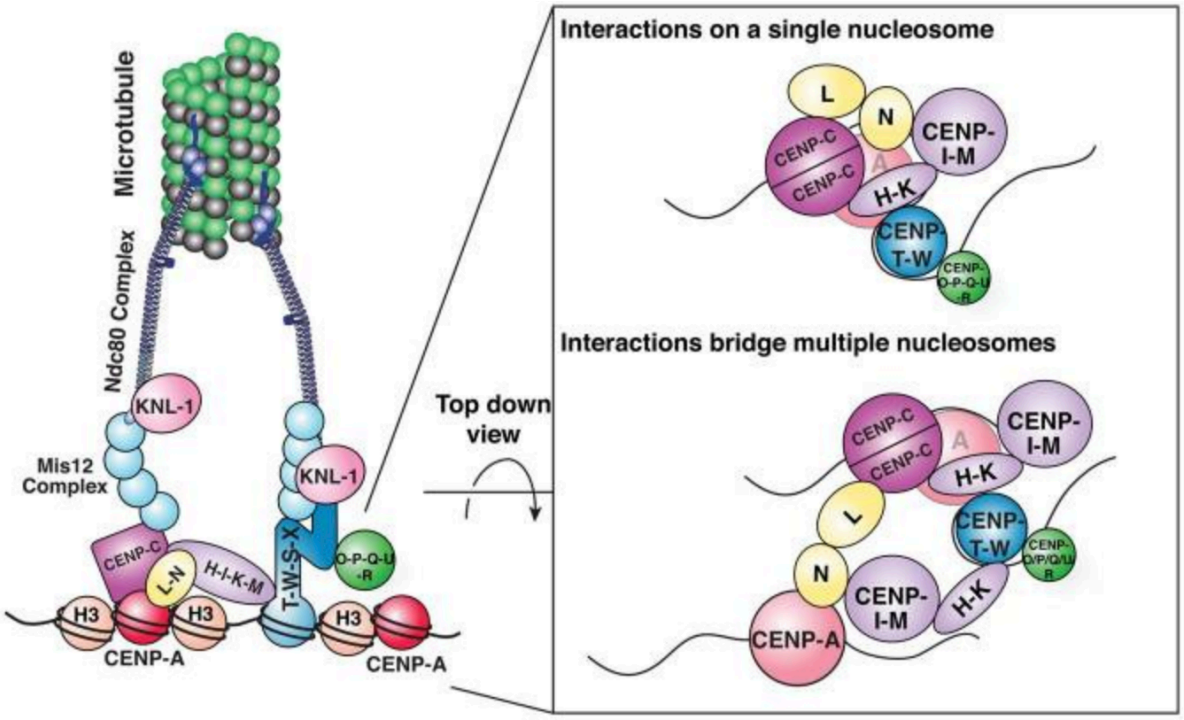

Figure.3 A schematic of the structure of the CCAN. Left: The interactions of the CCAN to the KMN network and centromere. Right: The CCAN sub-complexes engage in direct interactions when observed from an overhead perspective of the CENP-A nucleosome, either on a singular nucleosome (top) or between distinct nucleosomes (bottom).

Figure 3 was adapted from McKinley KL et al., 2015.

1.2.1.2 CENP-TWSX

CENP-T is a multi-domain protein with an elongated structure consisting of multiple alpha-helical repeats. It localizes to the inner kinetochore, contains N-terminal and C-terminal regions that are involved in interactions with other CCAN components and plays a role in recruiting kinetochore proteins (Fig. 3) (Hori T et al., 2008a; Nishino T et al., 2012; Takeuchi K et al., 2014). CENP-T does not exhibit direct binding with the centromere epigenetic marker CENP-A nucleosome (Hori T et al., 2008a). Instead, it

forms a heterodimer with CENP-W, and the CENP-T and CENP-W subsequently forms a heterotetramer, with histone-fold domain proteins CENP-S and CENP-X. Through biochemical, structural, and functional assays, it has been demonstrated that the CENP-TW and CENP-SX heterotetrameric structure capable of directly binding to DNA, thus facilitating the formation of a functional kinetochore (Nishino T et al., 2012).

The N-terminus of CENP-T harbors directly binding sites for Ndc80C, with two binding sites identified in humans and one in chickens (Nishino T et al., 2013; Huis In 't Veld PJ et al., 2016). Multiple CDK1 phosphorylation events regulate the association of CENP-T with outer kinetochore proteins, including the KMN network and the subcomplex Spc24-Spc25. In chicken cells, phosphorylation sites of Thr72 and Ser88 were identified as facilitating the association with Spc24-Spc25 (Nishino T et al., 2013). Subsequently, in human cells, phosphorylation of Thr195 or Ser201 were found enhances the binding affinity of CENP-T to the Mis12C, with Thr195 phosphorylation likely being effective only in vivo. Additionally, phosphorylation of Thr11 or Thr85 is sufficient for CENP-T binding to the subcomplex Spc24-Spc25 of Ndc80C. Alanine mutation of Thr11, Thr85, and Ser201 can abolish the recruitment of Mis12C and Ndc80C (Huis In 't Veld PJ et al., 2016). With the presence of Aurora B also promote the binding of CENP-T with Mis12C (Walstein K et al., 2021). CENP-C and CENP-T play pivotal roles in assembling the outer kinetochore in distinct ways that essential for the formation of functional centromere. Notably, in chicken cells, CENP-T assumes a predominant role in compensating for the absence of Mis12C binding in CENP-C, thereby ensuring proper kinetochore function (Hara M et al., 2018). Moreover, it has been observed that two copies of Ndc80C binding via the CENP-T pathway are sufficient for adequate kinetochore function (Takenoshita Y et al., 2022).

1.2.1.3 CENP-HIKM

CENP-H, initially discovered in mouse (Sugata N., 1999), is a small kinetochore protein. Mis6 was first identified in fission yeast (Saitoh S et al., 1997), and its homolog, CENP-I, later found in chicken and human cells, which interact with CENP-H (Nishihashi A et al., 2002; Okada M et al., 2006). Further evidence revealed that CENP-H and CENP-K form

a dimer, while CENP-I link the CENP-HK dimer and CENP-M to form a stabilized complex (Basilico F et al., 2014). The CENP-HIKM complex associates with CENP-A nucleosomes and plays a role in the incorporation of CENP-A nucleosomes into the centromere. The localization of each member of the CENP-HIKN complex is interdependent, and their presence contribute to the faithful progression of mitosis. Deletion of any factor within this complex results in chromosome segregation defects (Foltz DR et al., 2006; Okada M et al., 2006).

1.2.1.3 CENP-LN

CENP-N recognizes the CENP-A targeting region of CENP-A nucleosomes, facilitating their incorporation into the centromere (Carroll CW et al., 2009; Fang J et al., 2015). Biochemical analysis has revealed that CENP-L directly binds to the C-terminal region of CENP-N and interacts with CENP-C, thereby contributing to the localization of the CENP-LN complex at the centromere (McKinley KL et al., 2015). The CENP-LN complex also interacts with the CENP-HIKM complex. However, the hierarchy of recruitment of CENP-C, CENP-LN, and CENP-HIKM does not occur in a linear manner; instead, functional analysis suggests simultaneous interactions that stabilize the localization of CENP-C (McKinley KL et al., 2015). The interplay between CENP-L and CENP-N serves dual importance, not only in constructing the kinetochore but also in ensuring the accurate segregation of chromosomes during mitosis (Liu R et al., 2023). The complexity of associations among kinetochore components provides insight into the orchestrated localization at the centromere throughout the cell cycle progression.

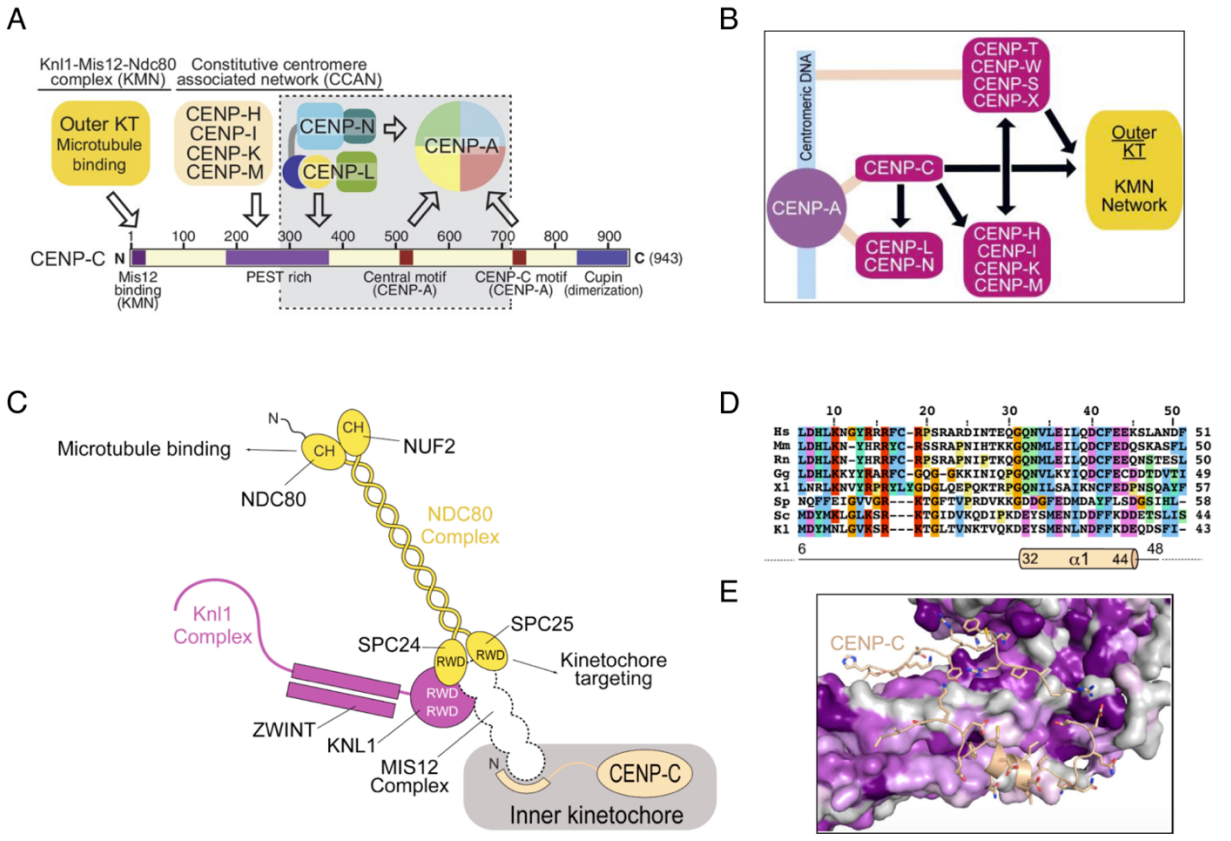

Figure. 4 A schematic of the interaction of CENP-C to centromere and KMN network.

(A) Schematic of the multifunctional domains of human CENP-C.

(B) A diagram illustrating the assembly scheme of the kinetochore.

(C) The interaction of CENP-C with KMN network.

(D) Alignment of the Mis12C binding domain within CENP-C orthologs across various species: Hs (Homo sapiens), Mm (Mus musculus), Rn (Rattus norvegicus), Gg (Gallus gallus), Xl (Xenopus laevis), Sp (Schizosaccharomyces pombe), Sc (Saccharomyces cerevisiae), Kl (Kluyveromyces lactis).

(E) The conservation scores derived from sequences of various species including Homo sapiens, Bos taurus, Ovis aries, Ornithorhynchus anatinus, Gallus gallus, Pseudopodoces humilis, Python bivittatus, Gekko japonicus, Xenopus laevis, Danio rerio, Drosophila busckii, Drosophila melanogaster, Saccharomyces cerevisiae, Kluyveromyces lactis, and Schizosaccharomyces pombe are mapped onto the MIS12C structure. Conservation levels are represented by a color gradient ranging from purple

(indicating highly conserved amino acid positions) to gray (indicating variable amino acid positions).

Figure 4A was adapted from Pentakota S et al., 2017; Figure 4B was adapted from Klare K et al., 2015; Figures 4C, D, E was adapted from Petrovic A et al., 2016.

1.2.1.4 CENP-OPQUR

The CENP-OPQUR complex interacts with a composite interface present on both the CENP-LN and CENP-HIKM complexes (Pesenti ME et al., 2018). Expressed human or chicken CENP-O, -P, -Q, or -U was immunoprecipitated with the CENP-HI complex (Okada M et al., 2006). In further studies, proteins of CENP-O, -P, -Q, and -U were found to associate with CENP-R, categorizing them as CENP-O class kinetochore proteins. Subunits of CENP-O, -P, -Q, and -U are interdependent on each other and participate in the recovery from spindle damage to prevent premature separation of duplicated chromatids, although they are dispensable for cell viability (Hori T et al., 2008). Structural analysis reveals that CENP-OP serves as a bridge between the CENP-HIKM complex and the CENP-LN complex, as well as other subunits of the CENP-OPQUR complex. It has been observed that CENP-QU pelleted with microtubules, indicating its binding affinity for microtubules. While CENP-R also associates with microtubules, the incorporation of CENP-R into the CENP-OPQUR complex did not lead to an apparent enhancement in binding affinity. The structures of CENP-QU and CENP-OP resemble that of Ndc80C (SPC24:SPC25 and Ndc80:NUF2), with the N-terminal region of CENP-Q replaced by the Ndc80 tail, which is functional in microtubules association. However, unlike the Ndc80 tail, which can be phosphorylated at up to nine sites by Aurora A and B and CDK1, the N-terminal of CENP-Q has only one to two consensus sites for Aurora kinase, but not for CDK1 (Pesenti ME et al., 2018). Further studies are needed to elucidate the functional implications of the CENP-OPQUR complex and its relationship with Ndc80C.

Understanding the structure, function, and orchestration of the CCAN proteins is crucial for elucidating the molecular mechanisms underlying kinetochore biology and may offer

insights into therapeutic strategies for diseases associated with chromosomal instability, such as cancer.

1.2.2 The KMN Network: Bridge the CCAN and Microtubules

The segregation of sister chromatids necessitates the bridging of the centromere to microtubules by kinetochore proteins. Acting as a linker between the CCAN-centromeric DNA and spindle microtubules, the KMN network of the outer kinetochore components provides a binding interface for microtubules. The KMN network comprises 10 subunits organized into three super-complexes: Mis12C, KNL1C, and Ndc80C (Cheeseman IM et al., 2008; Varma D et al., 2012; Pesenti ME et al., 2016; Hara M et al., 2017). The three-dimensional structure of these complexes has been elucidated through cryoEM imaging techniques (Fig. 5) (Ariyoshi M and Fukagawa T. 2023).

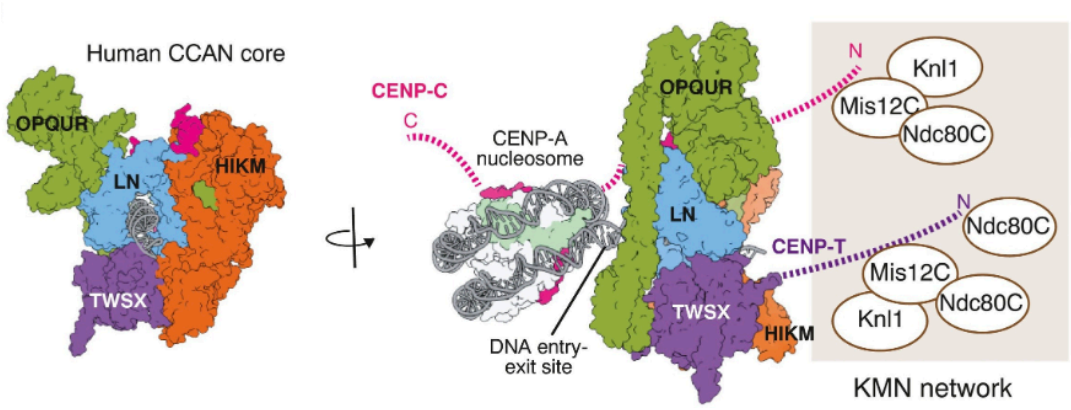

Figure.5 The core structure of the CCAN [Protein Data Bank (PDB) entry; 7ywx] connects centromeric chromatin housing the CENP-A nucleosome with the KMN network. Within the CCAN core, linker DNA extending from the CENP-A nucleosome is securely bound. The N-terminal domains of both CENP-C and CENP-T contain KMN network binding sites.

Figure 5 was adapted from Ariyoshi M and Fukagawa T. 2023.

The Mis12C contains four components (MIS12, PMF1, NSL1, DSN1) like a cylindrical structure (Fig. 6B) serves as a platform for KMN network assemble under EM analysis (Fig. 4C; Fig. 6A) (Pesenti ME et al., 2016; Petrovic A et al., 2016; Dimitrova YN et al., 2016; Yatskevich S et al., 2024; Polley S et al., 2024). The Mis12C exhibits an approximate length of 23 nanometers (Petrovic A et al., 2010). Each unit of the construct extends across the entire longitudinal dimension of the complex, maintaining uniform orientation. This arrangement yields two discernible subcomplexes: MIS12:PMF1 pair and DSN1:NSL1 pair. MIS12 and NSL1, and the helical connector of DSN1:NSL1 provide the interphase for CENP-C interacting (Dimitrova YN et al., 2016; Petrovic A et al., 2016).

However, the motif presents in DSN1, housing residues Ser100 and Ser109, demonstrates alignment capability with segment 10-17 of the human CENP-C. This alignment suggests that DSN1 potentially disrupts the interaction between the N-terminal region of CENP-C and the Mis12C. And deletion of this motif or phosphorylation of residues $DSN1^{Ser100}$ and $DSN1^{Ser109}$ by Aurora B kinase can enhance the binding affinity (Petrovic A et al., 2010; Hara M et al., 2018; Welburn JP et al., 2010; Akiyoshi B et al., 2013).

The crystalline structure of the C-terminal region of NSL1 demonstrates interaction with the corresponding C-terminal segment of KNL1 (Petrovic A et al., 2010, 2016). Additionally, NSL1, in conjunction with DSN1 (residues 209-213 and 323-348, respectively), has a direct interaction surface for the subcomplex Spc24-Spc25 of the Ndc80C binding machinery. This interaction surface is exemplified by the enhanced microtubule binding capabilities demonstrated by the chimeric $Ndc80^{Bonsai}$ construct (Fig. 6C), as evidenced by high-resolution 3D images acquired through electron microscopy (Ciferri C et al., 2008; Petrovic A et al., 2016; Pesenti ME et al., 2016).

The C-terminal domain of KNL1 has been identified to interact with Zwint-1 through the yeast two-hybrid system, forming the KNL1C complex (Kiyomitsu T et al., 2007). While KNL1 indeed directly binds to Mis12C, this interaction necessitates support from Zwint-1 (Cheeseman IM et al., 2006; Petrovic A et al., 2010). Notably, the contribution of KNL1C

extends beyond the formation of the KMN network; it also serves as a scaffold for spindle assembly checkpoint (SAC) docking (Cheeseman IM et al., 2006). Zwint-1 facilitates the assembly of ROD-ZW10-ZWILCH, which crucial for the binding of Mad1 and Mad2 (Karess R. 2005; Varma D et al., 2013). Furthermore, KNL1 directly associates with Bub1 and BubR1 through two consensus KI motifs (KI(D/N)XXXF(L/I)XXLK) located at regions aa 151-200 and aa 201-250 (Kiyomitsu T et al., 2011). KI motifs cooperate with MELT repeats of N-terminal KNL1 to enhance the Bub1 and BubR1 recruitment (Krenn V et al., 2014). The localization of BubR1 at KNL1 is essential for the functional SAC. Mutant BubR1 deprived of the ability to bind Mad2, Cdc20 to KNL1 results in SAC failure (Bolanos-Garcia VM et al., 2011).

Ndc80C compose four subunit, Ndc80 (Hec1 in human), Nuf2, Spc24 and Spc25, major component of kinetochore for microtubule binding (Tooley J and Stukenberg PT. 2011). Ndc80/Hec1 was first identified by Lee and colleagues (Chen Y et al., 1997), and immunoprecipitated with Spc24-Spc25 as spindle pole components together with earlier identified Nuf2 a component of spindle pole body (Wigge PA et al., 2001; Osborne MA et al., 1994). The Ndc80C complex is conserved across a broad range of organisms, spanning from yeasts to vertebrates. Within this complex, Hec1:Nuf2 and Spc24:Spc25 constitute two distinct subcomplexes. These subunits tetramerize via their C- and N-terminal regions, resulting in a structure characterized by an elongated shape with globular formations at both ends (Kiyomitsu T et al., 2007, 2011; Wei RR et al., 2005, 2006). The globular domains of Ndc80 and Nuf2 form a dual calponin homology domain (CHD) serve as a mediator in facilitating the attachment between kinetochore and microtubules. Mutations in several residues within this domain have been shown to disrupt the binding affinity of microtubules. Additionally, the N-terminal tail of Ndc80 plays a regulatory role in modulating the stability of kinetochore-microtubule attachments (Miller SA et al., 2008; Ciferri C et al., 2008). Ndc80 harbors multi-phosphorylation sites (Ser4, Ser5, Ser8, Ser15, Ser44, Tyr49, Ser55, Ser62, and Ser69). Phosphorylation events catalyzed by Aurora B kinase lead to destabilization of kinetochore-microtubule attachments (DeLuca JG et al., 2006; Ciferri C et al., 2008).

Taken together, the centromere, CENP-C, and CENP-T, through their coordinated actions, along with other CCAN proteins and the outer kinetochore, constitute a tightly regulated molecular machinery, ensure the faithful distribution of genetic material to daughter cells during cell division. Understanding the molecular mechanisms underlying their functions is not only crucial for basic cell biology but also has implications for human health, as defects in these processes can lead to genomic instability and contribute to the development of diseases such as cancer. Further investigation into the structure and function of these pivotal components involved in chromosome segregation is essential.

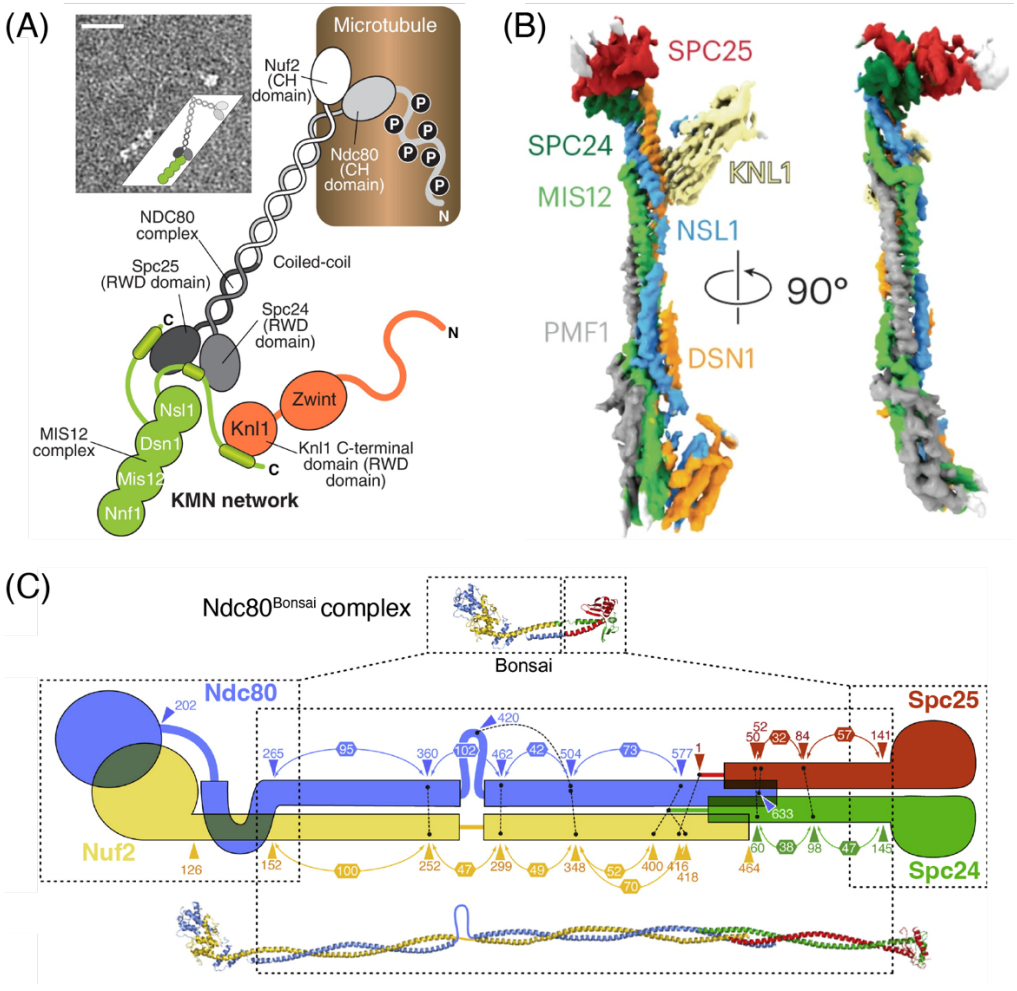

Figure.6 Schematic of sub-units interaction within the KMN network.

(A) The image in the top left corner displays a negative-stain electron micrograph (EM) capturing a reconstituted sample featuring the Mis12C and Ndc80C (adapted from the

reference Screpanti E et al., 2011). Scale bar: 50nm. Adjacent to the EM image is a model illustrating the EM of the Mis12C and Ndc80C as observed in the EM. Based on the EM analysis, the Mis12C overlaps approximately 30 residues with the Ndc80C, the latter adopting a long rod structure with two globular regions at each end (Wei RR et al., 2005; Ciferri C et al., 2008; Maure JF et al., 2011).

(B) A 3D structure of a single particle of the KMN network (Mis12C:Ndc80$^{Bonsai:}$ KNL1$^{2106-2311}$) illustrated by EM map. The full length of Ndc80C is about 55 nm. And the side segment about 5~7 nm length is part of KNL1.

(C) The structure model of Ndc80^{bonsai}. The model is a fusion construct where residues 1-286 of Ndc80 are combined with residues 118-224 of Spc25. Additionally, residues 1-169 of Nuf2 are fused with residues 112-197 of Spc24. This fusion results in a chimeric structure, combining elements from four components of Ndc80C.

Figures 6A was adapted from Pesenti ME et al., 2016; figure 6B was adapted from Polley S et al., 2024; figure 6C was adapted from Ciferri C et al., 2008.

1.3 The Coordinator of Kinetochore-Microtubule Attachment

The molecular mechanism of chromosome segregation involves a complex interplay of various proteins and molecular motors that ensure accurate distribution of chromosomes to daughter cells during cell division. The kinetochore's functionality hinges on its interaction with the microtubule plus ends, which are integrated into the outer plate of the kinetochore (McEwen BF et al., 2011). In human cells, approximately 20 microtubules can attach to kinetochores, whereas yeast typically bind to a single microtubule (O'Toole ET et al., 1999; Dudka D et al., 2018). The intrinsic preference of kinetochore-microtubule attachments tends toward biorientation, wherein sister kinetochores connect to microtubules extending from opposite spindle poles (Indjeian VB et al., 2007; Tanaka TU. 2005). However, mal-orientations of chromosome attachments frequently occur during early prometaphase (Ault JG et al., 1992; Cimini D et al., 2003). Mal-orientations or improper attachments may include monotelic, syntelic,

and merotelic attachment (Compton DA. 2007). Monotelic attachment refers to an interim phase wherein a kinetochore connects to microtubules originating from one spindle pole before achieving biorientation or proper amphitelic attachment. Syntelic attachment resembles monotelic attachment in being mono-oriented, yet it differs in that both sister kinetochores bind to microtubules extending from the same pole. Merotelic attachment occurs when one sister kinetochore binds to microtubules emanating from opposing poles (Fig. 7) (Gregan J et al., 2011; Ricke RM et al., 2011; Wimbish RT and DeLuca JG. 2020). Merotelic attachment is believed to be a major source of aneuploidy (abnormal DNA contents), a condition associated with lethality and frequently accompanying disease and tumor formation (Cimini D et al., 2001; Torres EM et al., 2008). For accurate chromosome segregation, the correction of improper attachments between kinetochores and microtubules is crucial. Two pivotal mechanisms, the error correction machinery and the spindle assembly checkpoint, play pivotal roles in ensuring the fidelity of this process (Tanaka K et al., 2009; Banerjee A et al., 2020).

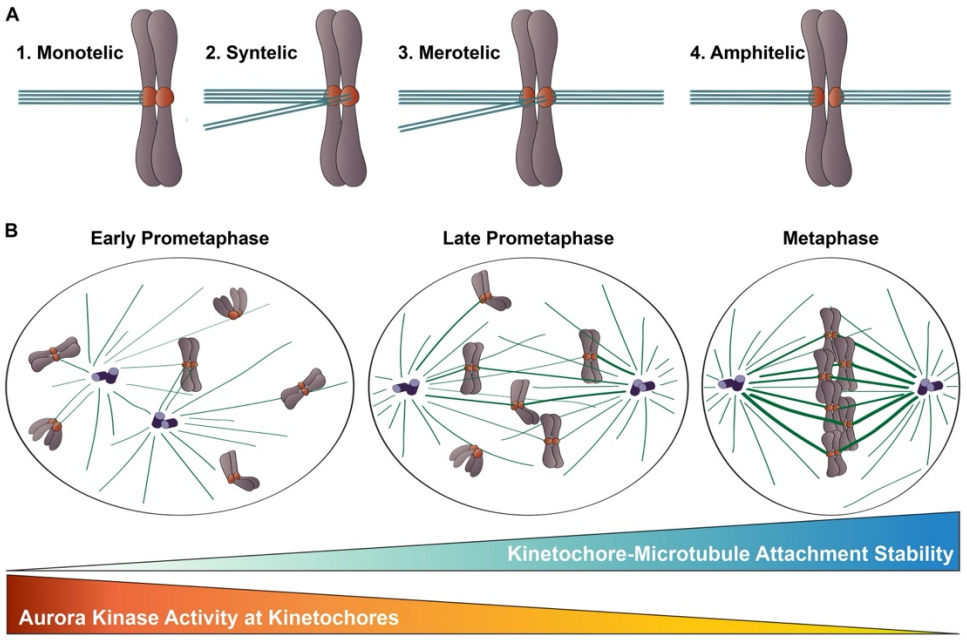

Figure.7 Models of bi-orientation (amphiltelic) and mal-orientations. (A) Since microtubules are captured by kinetochores in a stochastic manner, it's susceptible to generating mal-orientations known as monotelic, syntelic or merotelic attachments. (B)

Aurora B kinase mediate the correction mechanism, inhibiting Aurora B activity leads to an increased incidence of such erroneous attachments.

Figure 7 was adapted from Wimbish RT and DeLuca JG. 2020.

1.3.1 Aurora B-Dependent Error Correction

For accurate chromosome segregation, kinetochores on duplicated chromatids need to attach to dynamic microtubules from opposite spindle poles, creating tension. At the early prometaphase, kinetochores demonstrate indiscriminate binding to microtubules, predisposing them to frequent attachment errors that necessitate corrective measures. The Aurora B kinase, a Serine/Threonine (S/T) kinase, plays a pivotal role by phosphorylating the N-terminal tail of the Ndc80/Hec1, thereby inducing destabilization of kinetochore-microtubule attachments (DeLuca JG et al., 2006; Cimini D et al., 2006). Research efforts have elucidated nine phosphorylation sites (S4, S5, S8, S15, S44, T49, S55, S62, and S69) within the tail region, with one site (T31) currently identified as a target of Cdk1, while the others are substrates of Aurora B or both Aurora B and A kinases (Zaytsev AV et al., 2015; Kucharski TJ et al., 2022). Noteworthy is the observation that mutants of the Ndc80/Hec1 tail, such as Hec1^{9A}, display significantly erroneous attachments in error correction experiments (DeLuca KF et al., 2011).

The spatial arrangement of Aurora B in close proximity to its substrates is pivotal for its regulatory function. Aurora B functions as an enzymatic subunit within the Chromosomal Passenger Complex (CPC), a protein assembly crucial for various mitotic processes (reviewed in Hindriksen S et al., 2017). Comprising three additional members, namely INCENP, Borealin, and Survivin, the CPC orchestrates its activities through intricate interactions. INCENP serves as a scaffold within the complex, with its conserved IN-box region at the C-terminal end facilitating interaction with Aurora B. Concurrently, the N-terminal domain of INCENP associates with Borealin and Survivin play a pivotal role in modulating Aurora B kinase activity and ensuring its localization at the centromere before anaphase transition (Klein UR et al., 2006; Carmena M et al., 2012).

The inner-centromeric localization of Aurora B relies on the activities of two kinases, Bub1 and Haspin. Bub1 phosphorylates histone H2A at threonine 120 (H2AT120ph), a modification crucial for recruiting Sgo1/2 proteins to the centromere. Subsequently, Borealin interacts with Sgo1/2 to facilitate it association with the centromere (Kitajima TS et al., 2005; Kawashima SA et al., 2007). Meanwhile, Haspin mediates the phosphorylation of histone H3 at threonine 3 (H3T3ph), which directly promotes the binding of Survivin to the CPC, thereby enhancing its localization at the centromere (Kelly AE et al., 2010; De Antoni A et al., 2012).

1.3.2 chTOG-Mediated Error Correction

Biggins and colleagues have uncovered a novel pathway governing error correction, distinct from the mechanisms reliant on Aurora B. This pathway involves chTOG-mediated error correction via its basic linker (Herman JA et al., 2020). chTOG, a non-motor protein, harbors domains that engage with microtubules (Spittle C et al., 2000; van der Vaart B et al., 2011; Hood FE et al., 2013). Deleting either the wild-type form or the linker region of chTOG leads to cell death in both yeast and human cells. Mutating two specific residues in the basic linker (chTOG$^{TT/AA}$) doesn't disrupt microtubule dynamics and maintains cell viability. Investigation into the chTOG$^{TT/AA}$ mutant cell model reveals that the basic linker is crucial for mitotic bi-orientation, potentially by competing with Ndc80/Hec1-microtubule binding rather than directly destabilizing erroneous attachments. Yet, the mechanism by which the chTOG-linker distinguishes low-tension attachments and interacts with Aurora B activity remains elusive. It's also unclear whether the linker region plays a role in impeding the recruitment of other microtubule-binding effectors to the Ndc80C (Fig. 8) (Herman JA et al., 2020).

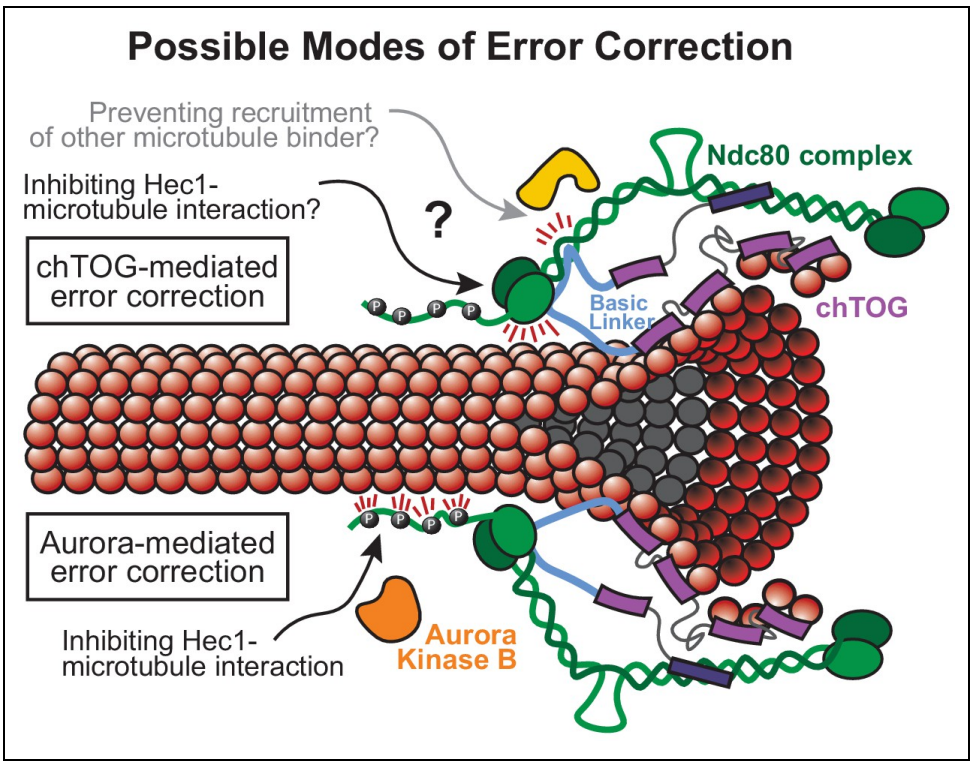

Figure.8 Proposed error correction mechanisms. chTOG-mediated correction (top), the C-terminal region of chTOG preserves its microtubule binding capability in a 'bent' conformation. This conformation may position the basic linker in proximity to the CH domain of Ndc80/hec1. While the basic linker could directly influence Ndc80/Hec1-microtubule attachment, an alternative possibility is that chTOG obstructs the recruitment of additional microtubule binding effectors. Notably, this pathway operates independently of Aurora B-dependent error correction (below), wherein phosphorylation of the tail of Ndc80/Hec1 by Aurora B serves to destabilize erroneous bindings.

Figure 8 was adapted from Herman JA et al., 2020.

1.3.3 The Spindle Assembly Checkpoint

Kinetochores capturing microtubules require sufficient time to reach the proper amphitelic attachment. The spindle assembly checkpoint (SAC) serves as a surveillance system crucial for ensuring enough time for faithful chromosome segregation during

mitosis in eukaryotes (Musacchio A et al., 2007., Vleugel M et al., 2012; Musacchio A. 2015; Lara-Gonzalez P et al., 2021).

Hartwell LH and Weinert TA first proposed the existence of checkpoints to ensure the fidelity of chromosome distribution in 1989 (Hartwell LH and Weinert TA, 1989). Following their work, majority of components were identified in budding yeast (Saccharomyces cerevisiae) and named Bub1, Bub3, Mad1, Mad2, Mad3, and MPS1 (Hoyt MA et al., 1991; Li R et al., 1991; Weiss E et al., 1996). The SAC monitors the onset of anaphase by inhibiting the activation of the anaphase-promoting complex/ cyclosome (APC/C) to prevent chromosome segregation (Fig. 10) (Musacchio A, 2015). The APC/C, functioning as an E3 ubiquitin ligase, targets two major substrates, securin and B-type cyclin (cyclin B), and its activation requires Cdc20 (Schrock MS et al., 2020). Cdc20 can be co-immunoprecipitated with Mad2, Mad3 (the human homologue of BubR1), and Bub3, indicating their physical interaction. The interaction of Mad2-BubR1-Bub3 with Cdc20, termed the mitotic checkpoint complex (MCC), which corresponds Mad2-Mad3-Cdc20 in *S.pombe* (reviewed in Liu ST et al., 2016), blocks the coactivator Cdc20 from binding to or activating APC/C arrest cells at mitosis (Hwang LH et al., 1998; Fraschini R et al., 2001; Sudakin V et al., 2001).

The mitotic checkpoint becomes activated and localized specifically at unattached kinetochores. In classical research methodologies, the SAC is triggered by the administration of drugs targeting microtubule dynamics, such as nocodazole and taxol, or Eg5 inhibitors, which induce monopolar attachment (Wilson L et al., 1999; Sarli V et al., 2005). Investigating how the SAC concentrates at kinetochores in the absence of microtubules remains an ongoing area of research. This process entails the involvement of kinetochore proteins interacting with components of the checkpoint system. Additionally, tension exerted by microtubules plays a role in coordinating checkpoint signaling, along with Aurora-B-dependent error-correction mechanisms, regulating the initiation of anaphase (Bunning AR and Gupta ML Jr. 2023). However, extended periods of mitotic arrest can be deleterious for the cell with constant the spindle checkpoint activity. Therefore, proper chromosome segregation also requires the eventual silencing of SAC signaling (Fig. 9) (Gascoigne KE and Taylor SS. 2008; Pines J. 2005).

Cdc20 engages in physical interaction with the APC/C (APC/C^{Cdc20}), to initiate the E3 ligase activity of APC/C^{Cdc20}. APC/C^{Cdc20} selectively recognizes substrates harboring a destruction box (D-box), such as securin and cyclin at metaphase, primarily through the WD40 domain of Cdc20 (Pines J. 2005). Securin's pivotal function lies in safeguarding the cohesin complex from cleavage by separase. Both securin and cyclin B1 undergo ubiquitination, facilitated by APC/C^{Cdc20}, resulting in their degradation. This action result in release separase, enabling the initiation of anaphase (Hagting A et al., 2002).

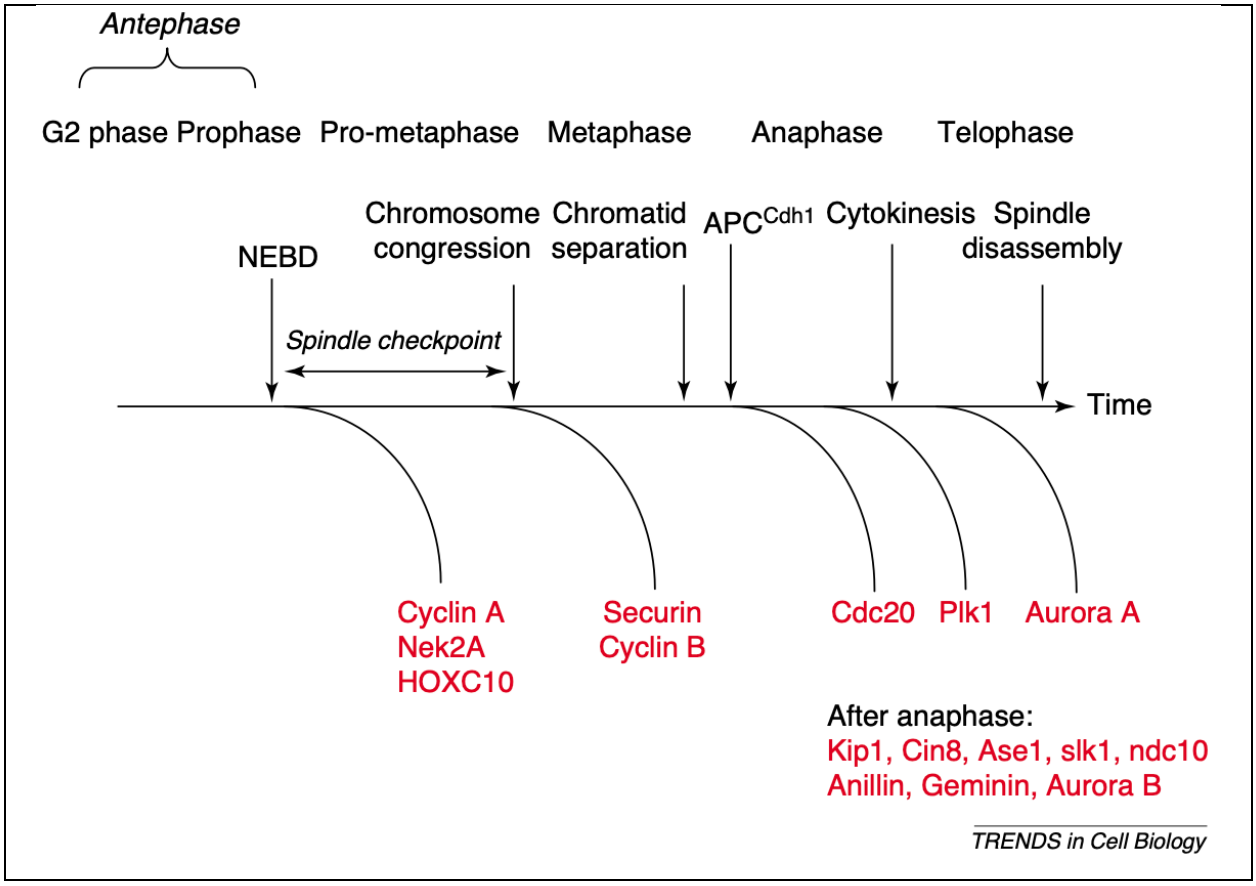

Figure.9 Schematic of cell cycle progression with destruction of specific substrates. When APC/C activation after nuclear envelope breakdown (NEBD), degradation of specific proteins at specific time for different purposes.

Figure 9 was adapted from Pines J. 2005.

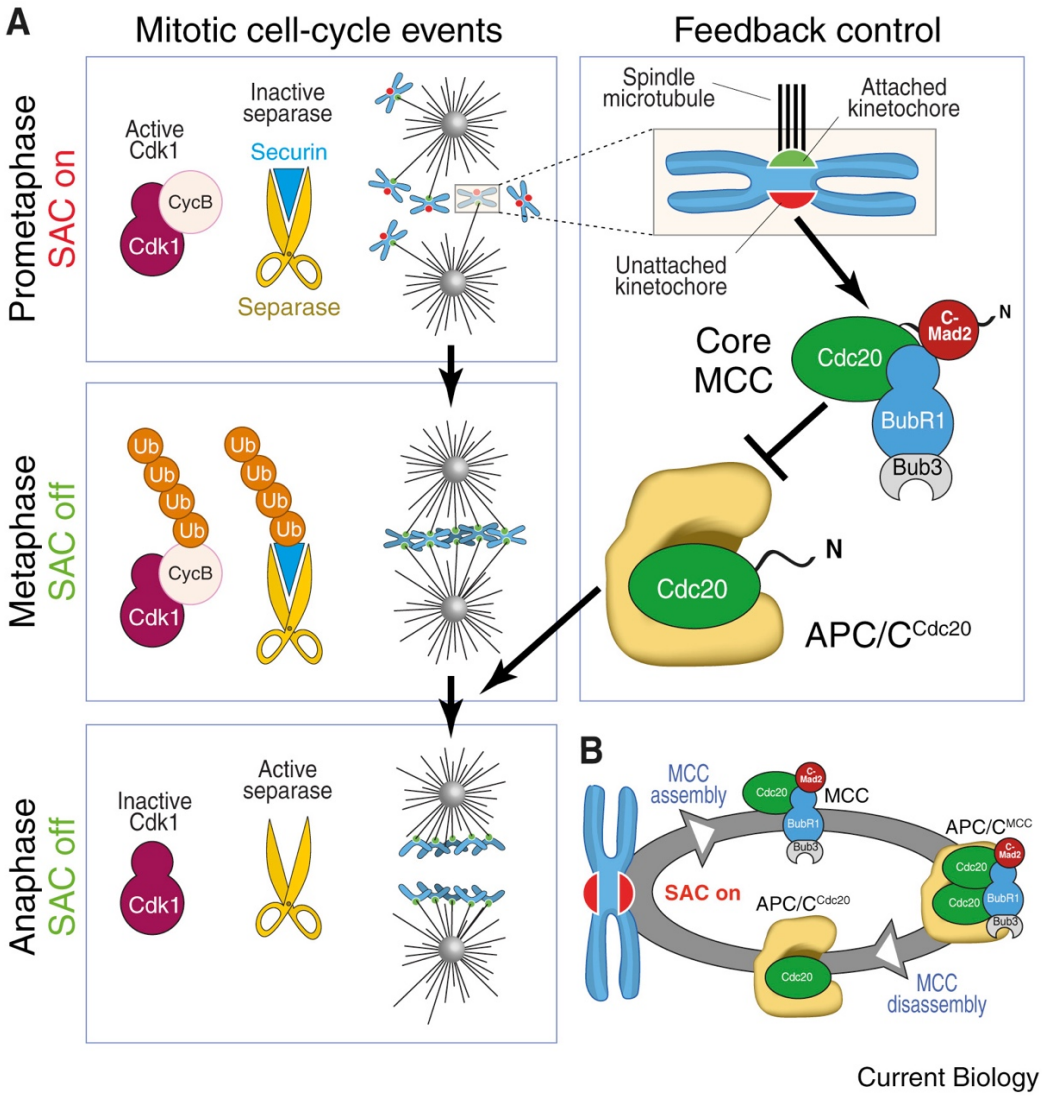

Figure.10 Trigger the mitotic transition is driven by the activation of Cdk1-Cyclin B complex. The SAC becomes active during prometaphase, a stage characterized by the attachment of chromosomes to the mitotic spindle, a process that involves kinetochores. Correctly kinetochore-microtubule attachment (depicted in green), when satisfy the SAC leading to the cessation of signaling. Unattached or incorrect attached kinetochores (depicted in red) emit the SAC signal. The SAC effector, known as the MCC, locate at the red kinetochore. It binds to and inhibits the APC/C^{Cdc20}, which is essential for the transition from metaphase to anaphase, therefore preventing anaphase transition. Once the SAC is satisfied across all kinetochores (during metaphase), activation of APC/C^{Cdc20} promotes the ubiquitination and degradation of Cyclin B and Securin. Their

degradation initiates mitotic exit and the separation of sister chromatids, facilitated by the activation of the separase (cohesion-protease).

(B) Even when the SAC is active, the cell simultaneously operates pathways for both the production and inactivation of the MCC. This dual process is crucial for an effective SAC response: the ongoing presence of "red" kinetochores is essential to maintain a sufficiently elevated rate of MCC production, which is necessary to offset MCC disassembly.

Figure 10 was adapted by Musacchio A. 2015.

1.3.3.1 Assembly of Spindle Checkpoint Components

MCC is a direct effector for SAC signaling and is recruited at unattached kinetochores. The component of MCC, as mentioned above, BubR1, Bub3, Mad2, and Cdc20 form a tetrameric complex (Chao WC et al., 2012).

BubR1 is the largest component of the MCC composed of structural domains and functional motifs (Fig. 11) (Lara-Gonzalez P et al., 2021). The N-terminal region of BubR1 is crucial for SAC function, where the TPR region and KEN box 1 (KEN1) recruit Cdc20 for binding, while the D-box followed by KEN2 prevents the recruitment of APC/C^{Cdc20} substrates. The GLEBS domain facilitates Bub3 binding, promoting the dimerization of Bub1, which contributes to BubR1 localization. The KARD (kinetochore attachment regulatory domain) motif serves as the site for PP2A interaction (Musacchio A et al., 2015; Lara-Gonzalez P et al., 2021). Bub1 (Fig. 11) initially recruits to the kinetochore, where it forms a heterocomplex with BubR1, facilitating the latter's localization. Bub3 binds to the equivalent region of both Bub1 and BubR1. Importantly, Bub1, rather than BubR1, promotes the localization of Bub3 to the phospho-MELT repeats of KNL1 (Fig. 12) (Lara-Gonzalez P et al., 2021).

A well-established role of the Mps1 kinase involves its direct association with Ndc80C, which is necessary for phosphorylating the Met-Glu-Leu-Thr (MELT) repeats on KNL1

(Musacchio A and Desai A. 2017). Phosphorylation of the MELT motifs creates docking sites for the Bub1-Bub3 complex, as discussed earlier. The recruitment of Mps1 is contingent on CDK1 phosphorylation, as discussed in the CDK1 section (Morin V et al., 2012). Additionally, Aurora B may play a role in Mps1 recruitment; however, the precise mechanism remains a topic of debate (Santaguida S et al., 2010; Lara-Gonzalez P et al., 2021). Mps1 also contributes to the release of Mad1-Mad2 from nuclear pore complexes (NPCs) during prophase, facilitating the localization of Mad1-Mad2 to unattached kinetochores (Cunha-Silva S et al., 2020). The localization of Mad1-Mad2 (Fig. 11) to unattached kinetochores in human cells is dependent on the RZZ complex, which comprises ROD, ZW10, and Zwilch, interconnected by the KNL1C component Zwint1. This complex directly interacts with Cdc20 (Dou Z et al., 2019). Bub1 also aids in recruiting and positioning Mad1 at kinetochores through the ABBA motif and the CM1 motif (Lara-Gonzalez P et al., 2021). The localization of Mad1 at the kinetochore is adequate for activating the signaling of the SAC (Ballister ER et al., 2014; Heinrich S et al., 2014).

Cdc20 (Fig. 11) play a dual role during prometa-meta phase, serving as a component of spindle checkpoint and an effector of the APC/C. To formation of MCC, Cdc20 recognizes the ABBA motif in both Bub1 and BubR1 to locate at kinetochores (Di Fiore B et al., 2015). Cdc20 localizes to the kinetochores temporally but predominantly acts in the cytoplasm, suggesting that the interactions involving Bub1 with Cdc20 and BubR1 with Cdc20 exhibit high dynamics (Lara-Gonzalez P et al., 2021). All components of the MCC gather at unattached kinetochores, instigating the signaling cascade of the SAC. Moreover, MCC acts as a potent inhibitor for the APC/C by preventing the association of substrates (Chao WC et al., 2012). Cdc20, another identity as an effector when it undergoes interaction with the APC/C. APC/C is a massive molecular machine, consisting of at least 13 subunits, which collectively confer a substantial molecular weight approaching 1 MDa (McLean JR et al., 2011). This interaction is facilitated by distinct structural motifs located at the N-terminal and C-terminal regions of Cdc20. Specifically, the N-terminal region of Cdc20 contains a conserved motif known as the C-box, which acts as a binding site for the APC/C. Furthermore, at the C-terminal end, Cdc20 harbors an Isoleucine-Arginine (IR) tail. This tail structure is implicated in

mediating the interaction between Cdc20 and the APC/C (Rudner AD et al., 2000; Chao WC et al., 2012).

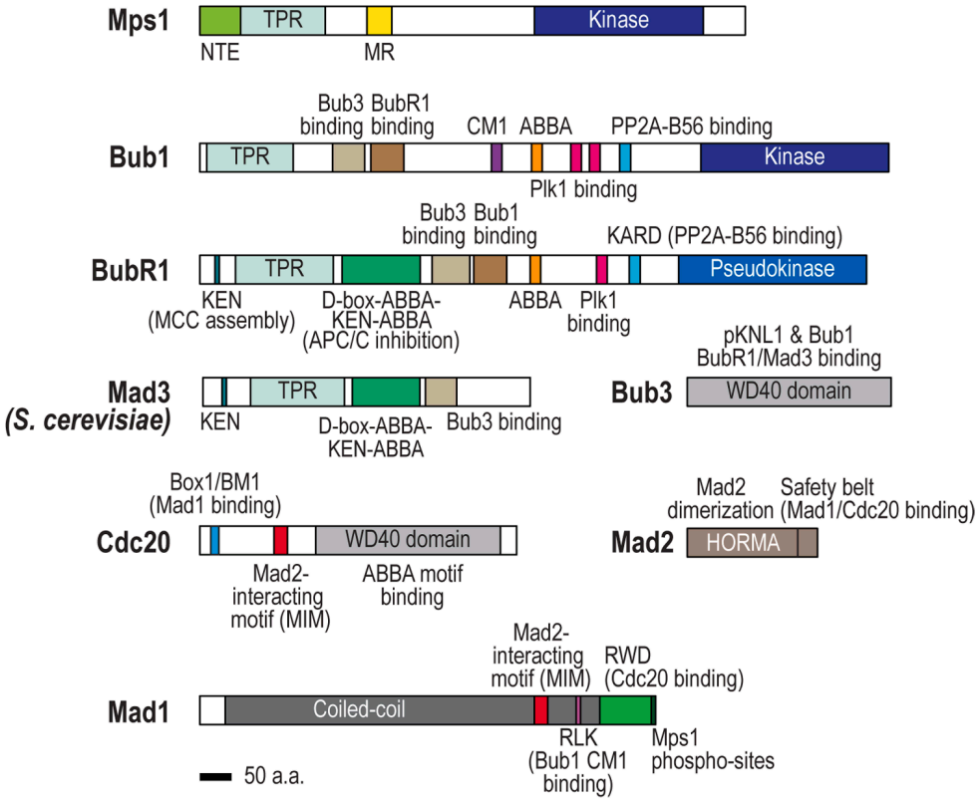

Figure.11 Schematic of SAC subunits. The models represent human proteins, except for Mad3 (S.cerevisiae). NTE: N-terminal extension; MR: middle region; TPR: tetratricopeptide repeat region; CM1: conserved motif 1; Scale bar = 50 amino acids.

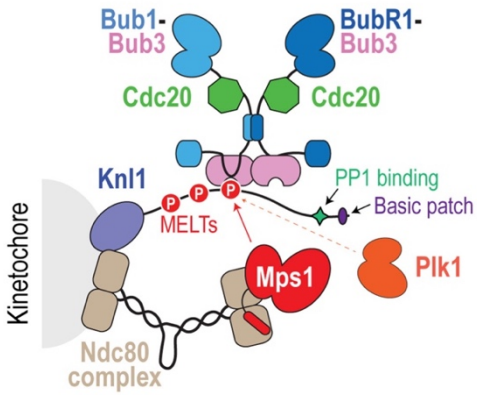

Figure.12 The MCC localizes at the phospho-MELT repeats of KNL1. The Plk1 kinase, with its diverse functions, can also play a role in regulating the SAC.

Figures 11 and 12 were adapted from Lara-Gonzalez P et al., 2021.

CDK1 also play an important role in establishment of the SAC machinery. To initiate the M-phase, Cyclin B forms a complex with the cell cycle regulator cyclin-dependent kinase 1 (CDK1) to execute its catalytic function in most eukaryotes. Phosphorylation of Cyclin B-CDK1 at Tyr15 and Thr14 maintains its inactivity to prevent premature entry, with subsequent activation by Cdc25 phosphatases (Parker LL et al., 1992; Mueller PR et al., 1995; Boutros R et al., 2006). The activity of Cyclin B-CDK1 gradually increases from the onset of prophase to prometaphase (approximately 6.5 minutes in RPE-1 cells) and remains sustained during prometa-meta phase, catalyzing a cascade of events (Gavet O et al., 2010).

Phosphorylation of Mps1 by Cyclin B-Cdk1 at residue Ser283 in its noncatalytic region enhances its activity, crucially facilitating the assembly of Mad1-Mad2 at kinetochores and thereby activating the SAC (Morin V et al., 2012). Cdk1 also phosphorylates Thr609 of Bub1 or Thr620 of BubR1 to aid in the localization of Plk1 (Qi W et al., 2006; Wong OK et al., 2005; Elowe S et al., 2007). Plk1 collaborates with MPS1 to phosphorylate the MELT repeats of KNL1, thereby regulating the spindle checkpoint (von Schubert C et al., 2015).

Furthermore, Cyclin B-Cdk1 facilitates the association of Cdc20 by phosphorylating the APC/C, thereby stimulating its E3 ligase function (Kraft C et al., 2003; Fujimitsu K et al., 2016; Zhang S et al., 2016). This activation leads to the targeting and degradation of APC/C substrates as discussed above.

1.3.3.3 Disassembly of Spindle Checkpoint Components

Upon microtubule attachment to kinetochores during mitosis, timely suppression of the SAC signal is crucial for facilitating mitotic exit. Failure to promptly silence the SAC can lead to a phenomenon termed mitotic ‘slippage’ or ‘escape,’ wherein the cell prematurely exits mitotic arrest. The repercussions of insufficient SAC suppression are severe and may include cell death or arrest in the subsequent interphase. Hence, upon proper attachment of kinetochores to microtubules, the cell must deactivate the SAC

signaling to progress into anaphase (Brito DA et al., 2006; Gascoigne KE et al., 2008). There exist two pathways responsible for disassembly mitotic checkpoints.

The first pathway involves the ubiquitination of Cdc20, leading to its degradation within the MCC. This degradation prompts the dissociation of Mad2 from the MCC, resulting in the dismantling of spindle checkpoints (Reddy SK et al., 2007; Jia L et al., 2011).

The second pathway orchestrates the disassembly of mitotic checkpoints via the TRIP13 ATPase. $P31^{comet}$ functions as an inhibitor of Mad2, dampening Mad2 activation and the formation of the MCC (Jia L et al., 2013). The binding of the MCC to APC/C is notably stable, necessitating the energy provided by TRIP13 ATPase for reversal mediated by $P31^{comet}$ (Miniowitz-Shemtov S et al., 2015).

Collectively, the coordinated assembly of kinetochores, coupled with error correction mechanisms and spindle checkpoints, is indispensable for the accurate segregation of chromosomes, as any dysregulation in these processes carries the risk of generating aneuploid cells.

Chapter 2: Mis12C-Binding Domain of CENP-C Is Required for Proper Mitotic Progression

2.1 Introduction

Duplicated chromosomes must be accurately distributed to two daughter cells during mitosis. Errors in this process can lead to chromosomal instability, harm cell proliferation, and even result in aneuploidy, a hallmark of cancer (Santaguida S et al., 2015; Bakhoum SF et al., 2018).

The kinetochore is a large protein complex containing two major subcomplex CCAN and KMN network (KMN for short) as introduced above which assembled on the centromere. Correctly esbalishment of a bi-oriented chromosome-microtubule attachment via the kinetochore is crutial for faithful chromosome segregation during mitotic progression (Fukagawa T et al., 2014; McKinley KL et al., 2016; Hara M et al., 2017, 2018; Mellone BG et al., 2021).

CENP-C, a CCAN protein, stabilizes kinetochore-microtubule attachments and ensures accurate chromosome alignment and segregation during cell division (Earnshaw WC et al., 1985; Tomkiel J et al., 1994; Fukagawa T et al., 1997; Fukagawa T et al., 1999; Klare K et al., 2015; Hara M et al., 2017). Each functional domain of CENP-C plays distinct role: binding to the centromere marker CENP-A, recruiting other CCANs, and also directly associating with Mis12C of KMN at G2 and M phase (Nagpal H and Fukagawa T. 2016; Hara M et al., 2017).

The N-terminal region, Mis12C-binding domain (M12BD), is highly conserved among vertabrates and mammals (Dimitrova YN et al., 2016; Petrovic A et al., 2016). This region was thought to be important for CENP-C function and also cell viability during cell division, however, our privious results showed that disrupting this interaction is dispensable for cell proliferation in chicken DT40 cells (Hara M et al., 2018). Disruption of the interaction of Mis12C with CENP-C and CENP-T leads to cell death, but CENP-T-KMN interaction is sufficient to rescue cell defects (Hara M et al., 2018). This raises several questions: why is Mis12C assembled by CENP-C at the kinetochore? Is the

M12BD a redundant part of CENP-C function? Or does the M12BD of CENP-C play different roles in different cell types?

To address these questions, co-work with Dr. Fujijmori group (National Institute for Basic Biology, NIBB) and Dr. Wakabayashi group (Chiba Cancer Center), mice lacking the M12BD of CENP-C (*Cenpc*$^{\Delta M12BD}$) were generated and characterized. Embryonic fibroblasts (MEFs) were isolated from *Cenpc*$^{\Delta M12BD/\Delta M12BD}$ embryos and their phenotype was characterized. To further explore the molecular mechanisms involved, I constructed CENP-C$^{\Delta M12BD}$ human RPE-1 cell and examined mitotic progression in these cells.

2.2 Results

2.2.1 Mis12C-binding domain of CENP-C is dispensable for mouse development but is required for proper mitotic progression in mouse embryonic fibroblasts (MEFs)

CENP-C binds to Mis12C via its N-terminal region (Screpanti E et al., 2011; Dimitrova YN et al., 2016; Petrovic A et al., 2016; Hara M et al., 2018; Przewloka MR et al., 2011) (Mis12C-binding domain: M12BD; Figs. 13A and B). In my group's prior investigations, it was established that M12BD does not play a crucial role in the proliferation of chicken DT40 cells (Hara M et al., 2018). However, given the amino acid (aa) sequence conservation of M12BD among species and its importance in KMN interactions (Figs. 13A and B), I wondered whether this finding was specific to DT40 cells.

To test whether CENP-C requires M12BD for its functions in other species and to determine the physiological importance of the CENP-C-Mis12C interaction, co-work with collaborating research groups (Fujimori Lab and Wakabayashi Lab) generated a mutant mouse model lacking the M12BD of CENP-C. Exons 2–4 of the *Cenpc1* (*Cenpc*) gene, encoding amino acids 7-75, were deleted using the CRISPR/Cas9 system (Fig. 13C). Their deletion removed most of the M12BD, including the key conserved residues for Mis12C-binding (CENP-C$^{\Delta M12BD}$) (Fig. 13A-B) (Screpanti E et al., 2011; Petrovic A et al., 2016). In contrast to *Cenpc* null mice, which do not survive embryonic development

(Kalitsis P et al., 1998), intercrossing heterozygous (*Cenpc*$^{+/\Delta M12BD}$) mice produced homozygous progeny (*Cenpc*$^{\Delta M12BD/\Delta M12BD}$), despite a slight reduction in female offspring (Figs. 13C, D, and E). These results suggest that M12BD of CENP-C is largely dispensable in mouse development; however, female embryos are sensitive to the loss of M12BD.

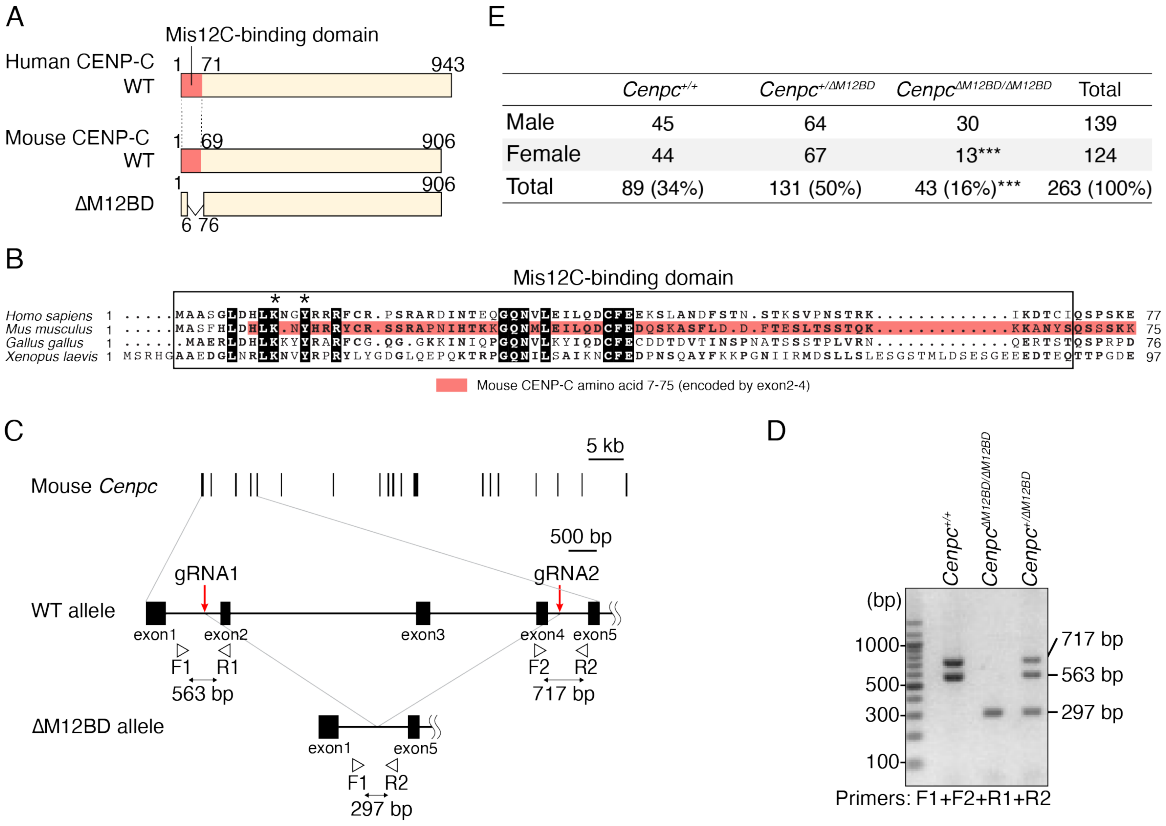

E

	Cenpc$^{+/+}$	*Cenpc*$^{+/\Delta M12BD}$	*Cenpc*$^{\Delta M12BD/\Delta M12BD}$	Total
Male	45	64	30	139
Female	44	67	13***	124
Total	89 (34%)	131 (50%)	43 (16%)***	263 (100%)

Figure.13 Mis12C-binding domain of CENP-C is conservable among species but dispensable for mouse development.

(A) Schematic representation of human and mouse CENP-C proteins. The Mis12-binding domain (M12BD) of human CENP-C and its homologous region in mouse CENP-C are highlighted in each CENP-C wild-type (WT). To establish *Cenpc1* (*Cenpc*) mutant mice lacking M12BD (*Cenpc*$^{\Delta M12BD}$), using CRISPR/Cas9 genome editing, exon2-4 encoding amino acids 7-75 were deleted from the *Cenpc* gene locus (CENP-C ΔM12BD).

(B) Alignment of the amino acid sequence of the CENP-C N-terminus including Mis12C-binding domain. The Mis12C-binding domain of human CENP-C and the corresponding region in CENP-C of other species are boxed. Asterisks show the conserved amino acids in CENP-C essential for Mis12C binding (lysine 10 and tyrosine 13) (Screpanti E et al., 2011). In mouse CENP-C, most of the Mis12C-binding domain, including the conserved amino acid for Mis12C-binding, are encoded in exon2-4 (aa 7-75). Homo sapience CENP-C: NP_001803, Mus musculus CENP-C: NP_031709, Gallus gallus CENP-C: NP_001376225.2, Xenopus laevis CENP-C: NP_0011594.

(C) Schematic representation of the exon 2-4 deletion from mouse *Cenpc* gene. mouse *Cenpc1* (*Cenpc*) gene has 19 exons. Using the CRISPR-Cas9 system with two gRNAs, the exon2-4 is deleted to make the Mis12C-binding domain deletion mutant (ΔM12BD). The position of gRNAs and PCR primers for genotyping PCR are shown. The amplicon sizes are approximately 563 bp (F1/R1), 717 bp (F2/R2), 297 bp (F1/R2).

(D) Genotyping PCR of Δ*M12BD Cenpc* mutant mice ($Cenpc^{\Delta M12BD}$).

(E) Genotype of offspring from $Cenpc^{+/\Delta M12BD}$ intercross (Chi-squared test. ***, $p < 0.001$).

The observed female-biased lethality in mouse embryos, attributed to chromosomal instability and ensuing micronuclei formation (McNairn AJ et al., 2019), served as impetus for exploring mitotic progression in MEFs derived from E14.5 $Cenpc^{\Delta M12BD/\Delta M12BD}$ embryos (Figs. 14A-B). MEFs were derived from $Cenpc^{+/+}$ and $Cenpc^{+/\Delta M12BD}$ mice and their genotypes were confirmed along with the expression of CENP-C protein (Fig. 14B).

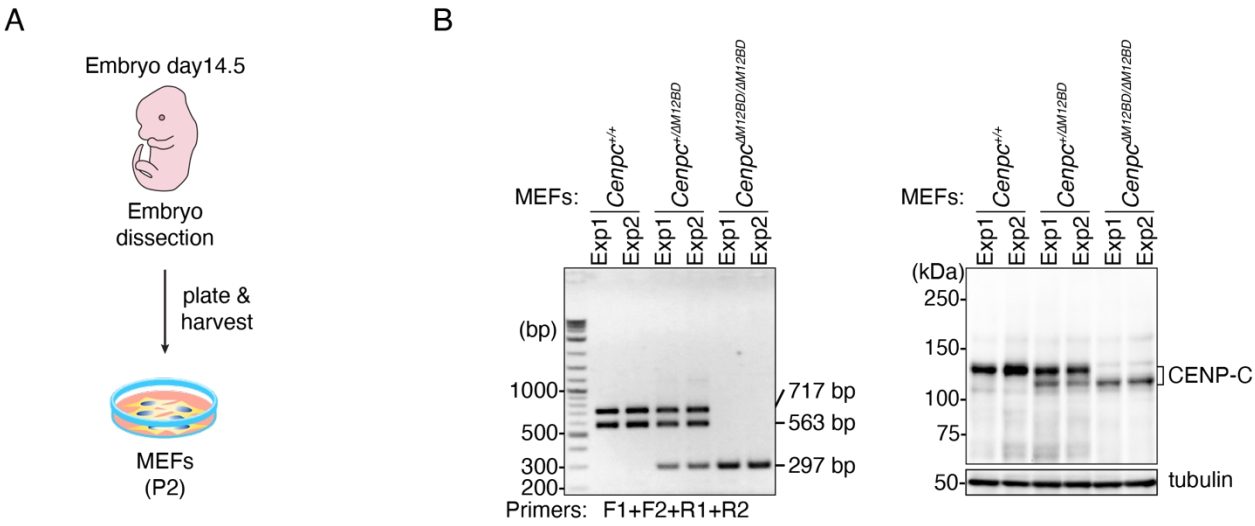

Figure.14 Generation of CENP-C mutant MEFs.

(A) Schematic representation of the establishment of MEFs from embryos.

(B) Genotyping PCR and immunoblotting for CENP-C of *Cenpc*$^{\Delta M12BD}$ MEFs. The MEFs isolated from two independent experiments were tested. In immunoblots, mouse CENP-C was detected by an antibody against mouse CENP-C, and α-tubulin was probed as a loading control.

Upon assessing the growth of MEFs, it was evident that the proliferation rate of *Cenpc*$^{\Delta M12BD/\Delta M12BD}$ MEFs lagged behind that of both *Cenpc*$^{+/+}$ and *Cenpc*$^{+/\Delta M12BD}$ MEFs (Fig. 15A). Subsequently, an investigation into mitotic progression through time-lapse imaging (Fig. 15B) revealed a discernible delay, albeit slight yet significant, from nuclear envelope breakdown (NEBD) to anaphase onset in *Cenpc*$^{\Delta M12BD/\Delta M12BD}$ MEFs compared to their counterparts (Figs. 15B-C). Furthermore, an increase in the occurrence of chromosome mis-segregation events during anaphase (e.g., lagging chromosomes or

chromosome bridges) and micronuclei formation was observed in *Cenpc*$^{\Delta M12BD/\Delta M12BD}$ MEFs (Figs. 15D-E). Consistent with these findings, there was an escalation in the proportion of cells exhibiting DNA content exceeding 4C in *Cenpc*$^{\Delta M12BD/\Delta M12BD}$ MEFs (Fig. 15F). Notably, chromosome spread analysis following nocodazole treatment demonstrated a rise in the frequency of cells harboring ≥ 80 chromosomes in *Cenpc*$^{\Delta M12BD/\Delta M12BD}$ MEFs (Figs. 16A-B). However, it is pertinent to acknowledge the possibility of discrepancies arising from variations in cell collection or limitations in technique, as the observed frequency of ~80 chromosomes in *Cenpc*$^{+/+}$ and *Cenpc*$^{+/\Delta M12BD}$ MEFs appears notably higher than the results obtained via flow cytometry. These results showed that *Cenpc*$^{\Delta M12BD/\Delta M12BD}$ MEFs exhibited chromosomal instability, suggesting that the M12BD of CENP-C contributes to accurate chromosome segregation in mouse cells despite being largely dispensable for development.

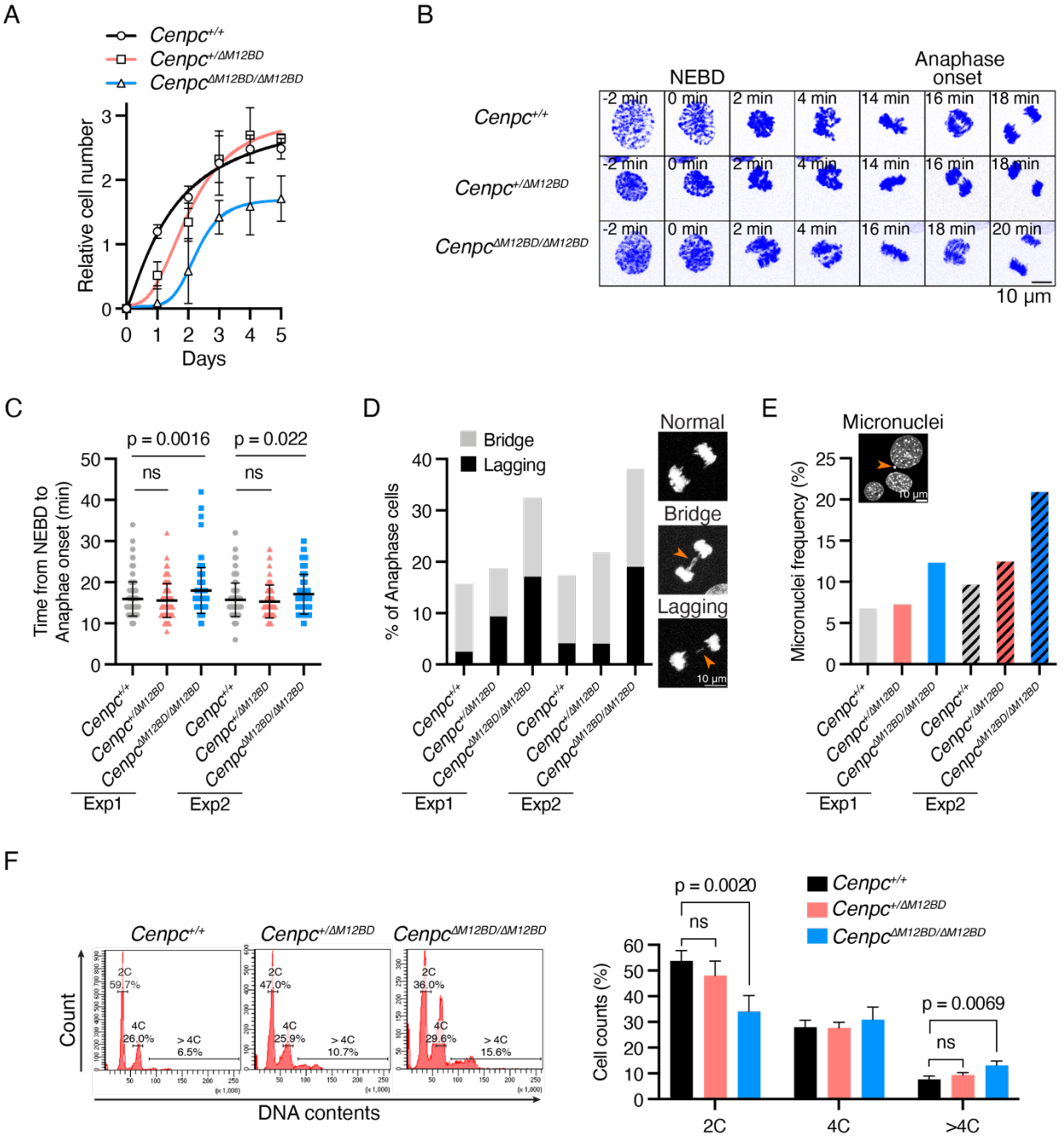

Figure.15 Mis12C-binding domain of CENP-C is required for proper mitotic progression in MEFs.

(A) The growth curve of the MEFs isolated from *Cenpc*$^{+/+}$, *Cenpc*$^{+/\Delta M12BD}$, or *Cenpc*$^{\Delta M12BD/\Delta M12BD}$ embryos. The cell numbers were normalized to those at Day 0 of each line. Error bars indicate the mean and standard deviation (SD).

(B) Representative time-lapse images of mitotic progression in *Cenpc*$^{+/+}$, *Cenpc*$^{+/\Delta M12BD}$, or *Cenpc*$^{\Delta M12BD/\Delta M12BD}$ MEFs. DNA was visualized by staining with SPY650-DNA. Images were projected using maximum intensity projection and deconvoluted. Time is relative to nuclear envelope breakdown (NEBD). Scale bar, 10 μm.

(C) Mitotic duration from NEBD to anaphase onset in *Cenpc*$^{+/+}$, *Cenpc*$^{+/\Delta M12BD}$, or *Cenpc*$^{\Delta M12BD/\Delta M12BD}$ MEFs. The time-lapse images were analyzed to measure the time from NEBD to anaphase onset. Two independent experiments were performed (Mean and SD, one-way ANOVA with Dunnett's multiple comparison test, exp1: n = 121 (*Cenpc*$^{+/+}$), 107 (*Cenpc*$^{+/\Delta M12BD}$), 117 (*Cenpc*$^{\Delta M12BD/\Delta M12BD}$), exp2: n = 121 (*Cenpc*$^{+/+}$), 124 (*Cenpc*$^{+/\Delta M12BD}$), 121 (*Cenpc*$^{\Delta M12BD/\Delta M12BD}$)).

(D) Chromosome segregation errors in *Cenpc*$^{+/+}$, *Cenpc*$^{+/\Delta M12BD}$, or *Cenpc*$^{\Delta M12BD/\Delta M12BD}$ MEFs. The lagging chromosomes and chromosome bridges during anaphase in the cells analyzed in (C) were scored. Representative images are shown. Scale bar, 10 μm.

(E) Micronuclei formation in *Cenpc*$^{+/+}$, *Cenpc*$^{+/\Delta M12BD}$, or *Cenpc*$^{\Delta M12BD/\Delta M12BD}$ MEFs. MEFs were fixed and the interphase cells with micronuclei were scored (exp1: n = 1570 (*Cenpc*$^{+/+}$), 1753 (*Cenpc*$^{+/\Delta M12BD}$), 1679 (*Cenpc*$^{\Delta M12BD/\Delta M12BD}$), exp2: n = 818 (*Cenpc*$^{+/+}$), 754 (*Cenpc*$^{+/\Delta M12BD}$), 765 (*Cenpc*$^{\Delta M12BD/\Delta M12BD}$)). Representative images are shown. Scale bar, 10 μm.

(F) Flow cytometry analysis of DNA contents in *Cenpc*$^{+/+}$, *Cenpc*$^{+/\Delta M12BD}$, or *Cenpc*$^{\Delta M12BD/\Delta M12BD}$ MEFs. MEFs from exp1 were fixed and stained with propidium iodide and analyzed by flow cytometry. Representative results are shown on the left. Each cell line was tested in triplicate and analyzed (Mean and SD, one-way ANOVA with Dunnett's multiple comparison test).

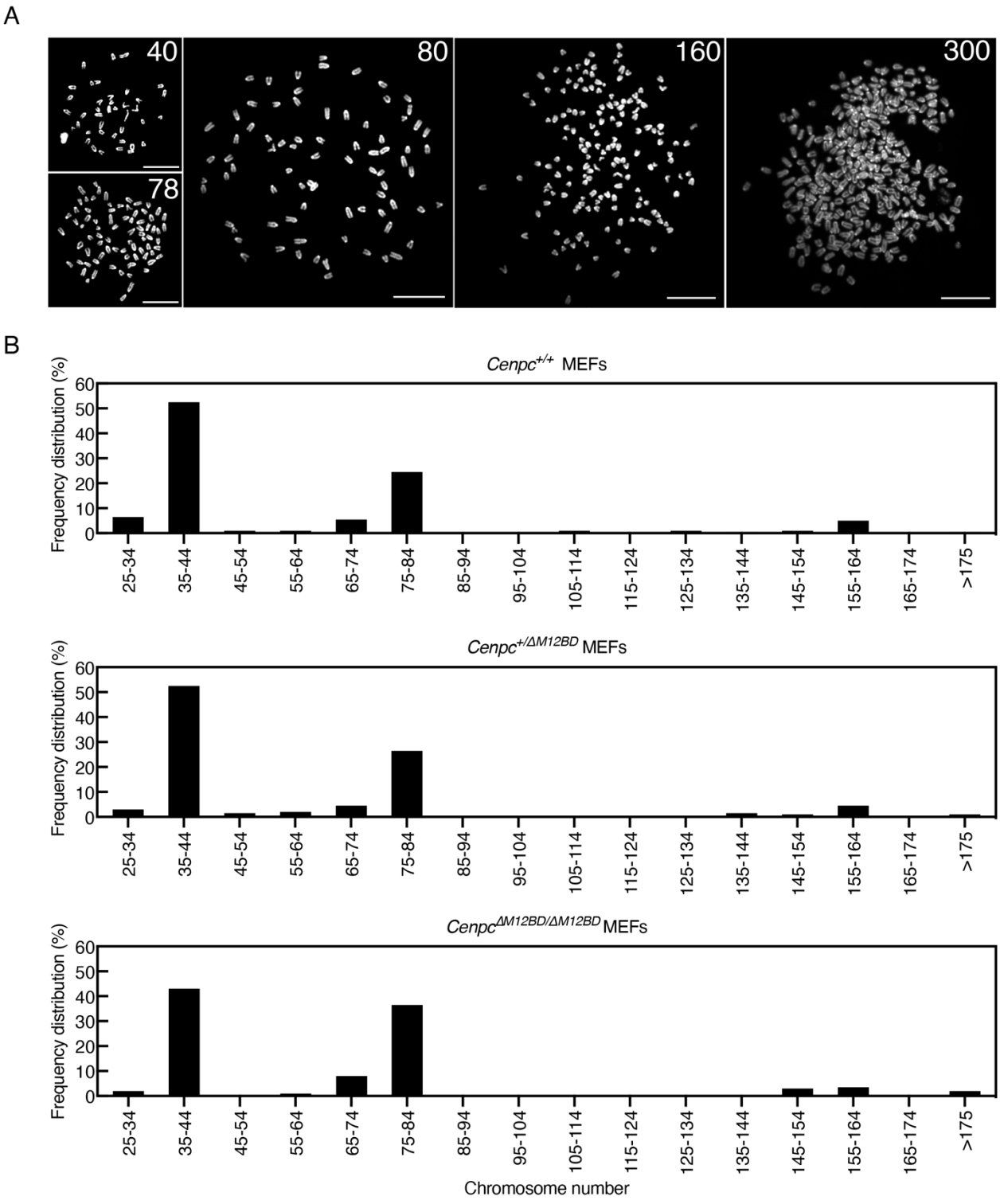

Figure.16 Chromosome number shift in Mis12C-binding domain mutant CENP-C MEFs.

(A) Representative images illustrating cells displaying distinct chromosome numbers following chromosome spread analysis. Chromosome numbers are indicated at the top right of each image. Scale bar: 10 μm.

(B) Frequency distribution of chromosome numbers observed in MEFs. Cell number: n = 200 of each cell type.

2.2.2 Deletion of M12BD of CENP-C accelerates tumor formation and malignant conversion in the two-stage skin carcinogenesis model

(Collaborative work with the Wakabayashi Lab)

The chromosomal instability is a hallmark of cancer (Bakhoum SF et al., 2018; Girish V et al., 2023). Since deleting the M12BD from CENP-C increased chromosomal instability in MEFs, the Wakabayashi Lab examined the cancer susceptibility of *Cenpc*$^{\Delta M12BD/\Delta M12BD}$ mice using a two-stage skin carcinogenesis model as a collaborative study (Fig. 17A) (Kemp CJ et al., 2005; Abel EL et al., 2009). Between 14 and 20 weeks after the initial 7,12-dimethylbenz(a)anthracene (DMBA)/12-O-tetradecanoylphorbol-13-acetate (TPA) treatment, *Cenpc*$^{\Delta M12BD/\Delta M12BD}$ mice developed significantly more papillomas than *Cenpc*$^{+/+}$ or *Cenpc*$^{+/\Delta M12BD}$ mice (Figs. 17B-C). Mice were continuously monitored for a duration exceeding 20 weeks, revealing a notable enhancement in malignant conversion was significantly promoted in *Cenpc*$^{\Delta M12BD/\Delta M12BD}$ mice by 36 weeks compared to that in *Cenpc*$^{+/+}$ or *Cenpc*$^{+/\Delta M12BD}$ mice (Fig. 17D). These results demonstrate that *Cenpc*$^{\Delta M12BD/\Delta M12BD}$ mice are cancer-prone, suggesting that M12BD of CENP-C contributes to cancer prevention.

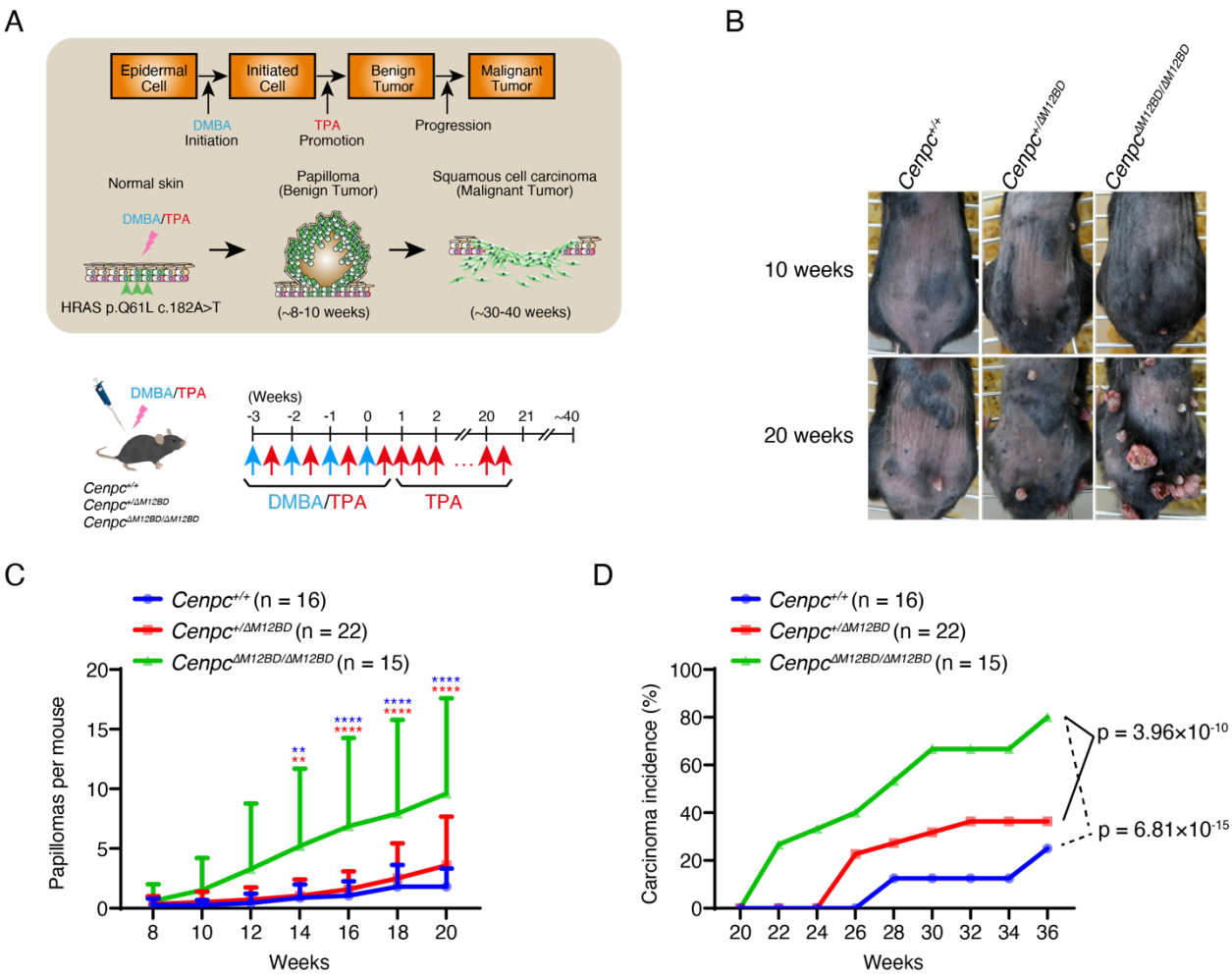

Figure.17 Deletion of the Mis12C-binding domain of CENP-C exacerbates tumor formation and malignant conversion in two-stage skin carcinogenesis model.

(A) Schematic representation of the two-stage skin carcinogenesis model. 7,12-dimethylbenz(a)anthracene (DMBA) and 12-O-tetradecanoylphorbol-13-acetate (TPA) were applied to the shaved dorsal back skin. After four rounds of DMBA/TPA treatment, the mice were further treated with TPA to promote papilloma formation and malignant conversion. The pipette and mouse images are adapted from Togo TV (https://togotv.dbcls.jp/en).

(B) Representative images of papillomas on the back skin of *Cenpc*$^{+/+}$, *Cenpc*$^{+/\Delta M12BD}$, or *Cenpc*$^{\Delta M12BD/\Delta M12BD}$ mice at 10 and 20 weeks after the DMBA/TPA cycles.

(C) Papilloma development in *Cenpc*$^{+/+}$, *Cenpc*$^{+/\Delta M12BD}$, or *Cenpc*$^{\Delta M12BD/\Delta M12BD}$ mice. The numbers of papillomas on the back skin were counted for each mouse (Mean and SD, two-way ANOVA with Tukey's test, **: $p < 0.01$, ****: $p < 0.0001$, Blue: *Cenpc*$^{+/+}$ vs *Cenpc*$^{\Delta M12BD/\Delta M12BD}$, Red: *Cenpc*$^{+/\Delta M12BD}$ vs *Cenpc*$^{\Delta M12BD/\Delta M12BD}$).

(D) Malignant conversion in *Cenpc*$^{+/+}$, *Cenpc*$^{+/\Delta M12BD}$, or *Cenpc*$^{\Delta M12BD/\Delta M12BD}$ mice. Mice with squamous cell carcinoma were scored from 20 to 36 weeks after the DMBA/TPA cycles (Fisher's exact test, *Cenpc*$^{+/+}$: n = 16, *Cenpc*$^{+/\Delta M12BD}$: n = 22, *Cenpc*$^{\Delta M12BD/\Delta M12BD}$: n = 15).

2.2.3 M12BD deletion from CENP-C causes chromosome mis-segregation, leading to mitotic defects in human RPE-1 cells

I aimed to understand the molecular mechanisms by which CENP-C M12BD prevents chromosomal instability. Since MEFs are heterogeneous and their cell proliferation is sensitive to replicative senescence, which limits detailed analyses of mitotic regulation, I used human retinal epithelial cells (RPE-1) for further investigation. RPE-1 is a widely used noncancerous cell line with a stable near-diploid karyotype. I generated RPE-1 cells in which endogenous CENP-C was replaced with FLAG-human CENP-C lacking the Mis12C-binding domain (aa 1-75 region; M12BD; Fig. 18A-G and Fig. 18A). These cells were referred to as CENP-C$^{\Delta M12BD}$ cells (Figs. 18A-G; Fig. 19A). I also generated RPE-1 cells expressing wild-type FLAG-human CENP-C (CENP-C^{WT} cells) as controls (Figs. 18A-G; Fig. 19A).

First, I quantified the Mis12C levels in the kinetochores of CENP-C$^{\Delta M12BD}$ cells. For this, I immunostained DSN1, a component of Mis12C, in CENP-C$^{\Delta M12BD}$ or CENP-C^{WT} cells expressing mScarlet-CENP-A as a kinetochore marker. As shown in Fig. 19B, the punctate DSN1 signals found in CENP-C^{WT} cells were significantly reduced in CENP-C$^{\Delta M12BD}$ cells. I also examined the levels of KNL1C and Ndc80C by immunostaining with antibodies against their components (KNL1 and Hec1, respectively) and found that the signals of both KNL1C and Ndc80C were reduced in CENP-C$^{\Delta M12BD}$ cells (Figs. 19C-D). The reduction of Ndc80C levels was mild compared with that of Mis12C and KNL1C. This can be explained by three additional Ndc80C binding sites in CENP-T (Rago F et al., 2015; Huis In 't Veld PJ et al., 2016; Takenoshita Y et al., 2022).

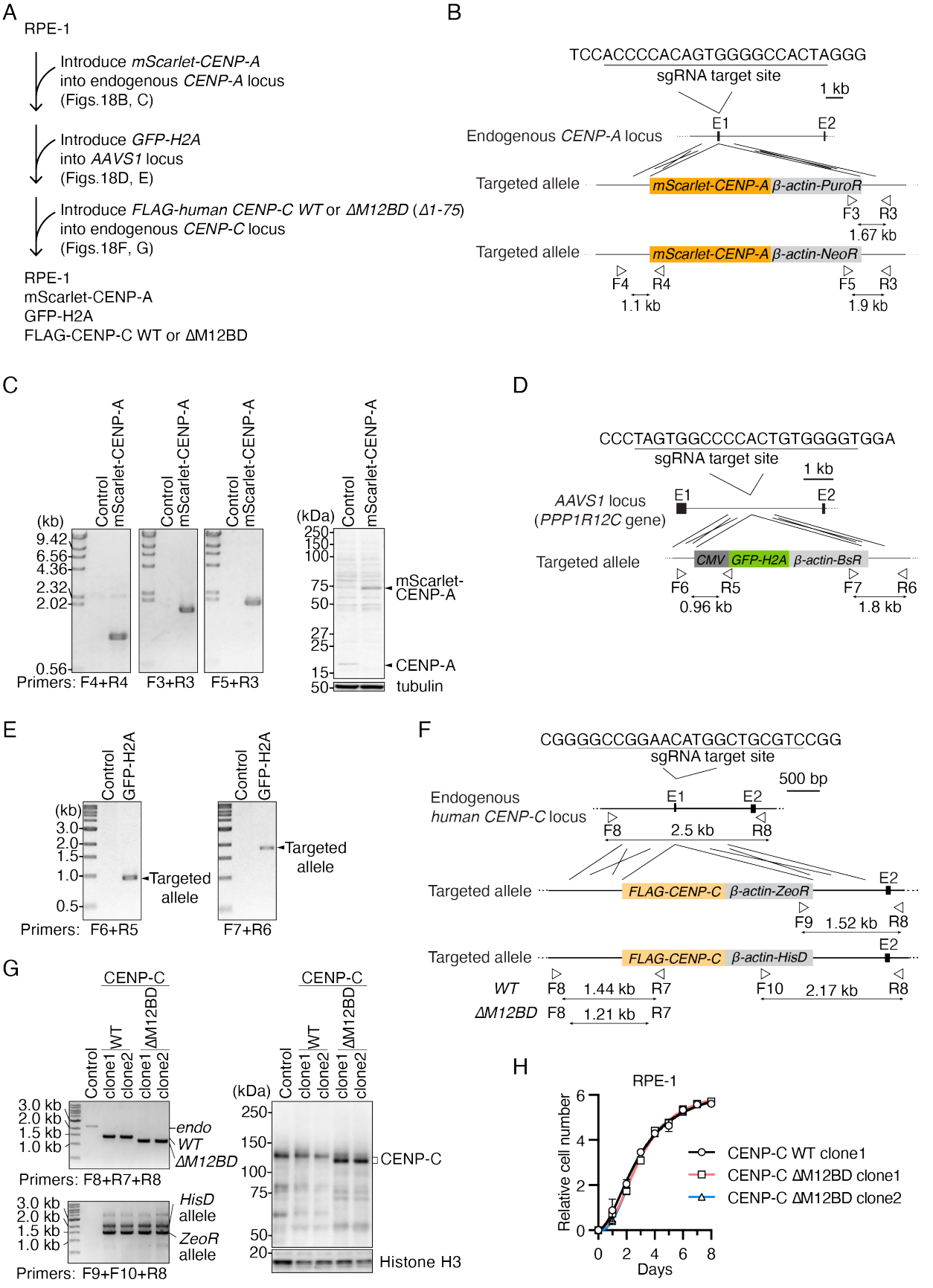
A
RPE-1
Introduce mScarlet-CENP-A into endogenous CENP-A locus (Figs.18B, C)
Introduce GFP-H2A into AAVS1 locus (Figs.18D, E)
Introduce FLAG-human CENP-C WT or ΔM12BD (Δ1-75) into endogenous CENP-C locus (Figs.18F, G)
RPE-1
mScarlet-CENP-A
GFP-H2A
FLAG-CENP-C WT or ΔM12BD
B
TCCACCCCACAGTGGGGCCACTAGGG
sgRNA target site
1 kb
E1
E2
Endogenous CENP-A locus
Targeted allele
mScarlet-CENP-A β-actin-PuroR
F3
R3
1.67 kb
Targeted allele
mScarlet-CENP-A β-actin-NeoR
F4
R4
1.1 kb
F5
R3
1.9 kb
C
Control
mScarlet-CENP-A
(kb)
9.42
6.56
4.36
2.32
2.02
0.56
Primers: F4+R4
F3+R3
F5+R3
(kDa)
250
150
100
75
50
27
25
15
50
mScarlet-CENP-A
CENP-A
tubulin
D
CCCTAGTGGCCCCACTGTGGGGTGGA
sgRNA target site
1 kb
AAVS1 locus (PPP1R12C gene)
E1
E2
Targeted allele
CMV GFP-H2A β-actin-BsR
F6
R5
0.96 kb
F7
R6
1.8 kb
E
Control
GFP-H2A
(kb)
3.0
2.0
1.5
1.0
0.5
Targeted allele
Primers: F6+R5
F7+R6
F
CGGGGCCGGAACATGGCTGCGTCCGG
sgRNA target site
500 bp
Endogenous human CENP-C locus
E1
E2
F8
2.5 kb
R8
Targeted allele
FLAG-CENP-C β-actin-ZeoR
E2
F9
1.52 kb
R8
Targeted allele
FLAG-CENP-C β-actin-HisD
E2
WT
F8
1.44 kb
R7
F10
2.17 kb
R8
ΔM12BD
F8
1.21 kb
R7
G
CENP-C
Control
WT clone1
WT clone2
ΔM12BD clone1
ΔM12BD clone2
3.0 kb
2.0 kb
1.5 kb
1.0 kb
endo
WT
ΔM12BD
Primers: F8+R7+R8
HisD allele
ZeoR allele
Primers: F9+F10+R8
(kDa)
250
150
100
75
50
20
CENP-C
Histone H3
H
RPE-1
Relative cell number
Days
CENP-C WT clone1
CENP-C ΔM12BD clone1
CENP-C ΔM12BD clone2

Figure.18　Generation of CENP-C mutant RPE1 cell lines.

(A) Strategy to generate CENP-C^{WT} or CENP-C$^{\Delta M12BD}$ RPE1 cells expressing mScarlet-CENP-A and GFP-H2A.

(B) Schematic representation of *mScarlet-CENP-A* cDNA targeting into the endogenous *CENP-A* locus. To express mScarlet-fused CENP-A under the control of the endogenous *CENP-A* promoter, *mScarlet-CENP-A* cDNA was targeted into the exon1 by CRISPR/Cas9-mediated homologous recombination. Since the targeting constructs have puromycin resistance genes (*PuroR*) or neomycin resistance genes (*NeoR*), targeted cells were selected using these selection markers. The gRNA sequence and position of primers for genotyping are shown.

(C) Genotyping PCR and immunoblotting for mScarlet-CENP-A in *mScarlet-CENP-A*-introduced RPE-1 cells. The genotype in isolated single clones was examined using the primers shown in (B). In immunoblots, CENP-A was detected by an antibody against CENP-A, and α-tubulin was probed as a loading control.

(D) Schematic representation of *GFP-H2A* cDNA targeting into the *AAVS1* locus (*PPP1R12C* gene). To express GFP-fused histone H2A from the *AAVS1* locus, *GFP-H2A* cDNA was targeted into the intron1 by CRISPR/Cas9-mediated homologous recombination. Since the targeting construct has blasticidin resistance genes (*BsR*), targeted cells were selected using the *BsR* marker. The gRNA sequence and position of primers for genotyping are shown.

(E) Genotyping PCR of *GFP-H2A*-introduced RPE-1 cells. The genotype in an isolated single clone was examined using the primers shown in (D).

(F) Schematic representation of *FLAG-human CENP-C* cDNA targeting into the endogenous *human CENP-C* locus. To express FLAG-tagged CENP-C wiled-type (WT) or a Mis12C-binding domain deletion mutant (ΔM12BD: Δ1-75) under the control of the endogenous *CENP-C* promoter, *FLAG-CENP-C WT* or *ΔM12BD* cDNA was targeted into the exon1 by CRISPR/Cas9-mediated homologous recombination. Since the targeting constructs have Zeocin resistance genes (*ZeoR*) or histidinol resistance genes

(*histidinol dehydrogenase*: *HisD*), targeted cells were selected using these selection markers. The gRNA sequence and position of primers for genotyping are shown.

(G) Genotyping PCR and immunoblotting for FLAG-CENP-C in *FLAG-CENP-C*-introduced RPE-1 cells. The genotype in isolated single clones was examined using the primers shown in (F). In immunoblots, CENP-C was detected by an antibody against human CENP-C, and histone H3 was probed as a loading control.

(H) The growth curve of CENP-C^{WT} or CENP-C$^{\Delta M12BD}$ RPE1 cells. The cell numbers were normalized to those at Day 0 of each line. Error bars indicate the mean and standard deviation. Two clones of CENP-C$^{\Delta M12BD}$ RPE1 cells were examined.

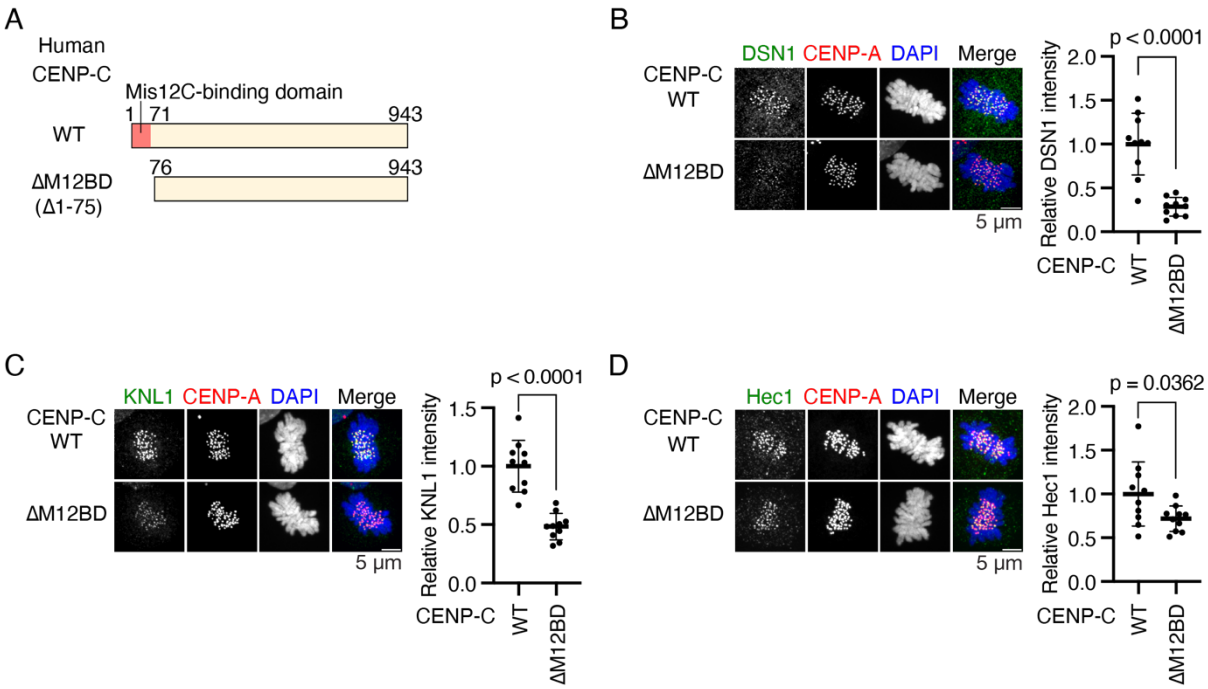

Figure.19　KMN network reduction in Mis12C mutant CENP-C RPE-1 cells.

(A) Schematic representation of human CENP-C. The Mis12C-binding domain (M12BD, amino acids 1-71) is highlighted in CENP-C wild-type (WT). The N-terminus region (amino acid 1-75) was deleted in CENP-C$^{\Delta M12BD}$. FLAG-tagged CENP-C WT or

ΔM12BD was introduced into the *CENP-C* locus in RPE-1 cells expressing mScarlet-CENP-A and GFP-H2A (CENP-C^{WT} or CENP-$C^{\Delta M12BD}$ cells, respectively.

(B) DSN1 localization in CENP-C^{WT} or CENP-$C^{\Delta M12BD}$ cells. DSN1, a subunit of the Mis12 complex, was stained with an antibody against DSN1 (green). mScarlet-CENP-A is a kinetochore marker (CENP-A, red). DNA was stained with DAPI (blue). Scale bar, 5 μm. DSN1 signal intensities at mitotic kinetochores were quantified (Mean and SD, two-tailed Student's t-test, CENP-C^{WT} cells: n = 10, CENP-$C^{\Delta M12BD}$ cells: n = 10).

(C) KNL1 localization in CENP-C^{WT} or CENP-$C^{\Delta M12BD}$ cells. KNL1, a subunit of the KNL1 complex, was stained with an antibody against KNL1. KNL1 localization at mitotic kinetochores was examined and quantified as in (B). Scale bar, 5 μm. Mean and SD, two-tailed Student's t-test, CENP-C^{WT} cells: n = 10, CENP-$C^{\Delta M12BD}$ cells: n = 10.

(D) Hec1 localization in CENP-C^{WT} or CENP-$C^{\Delta M12BD}$ cells. Hec1, a subunit of the Ndc80C, was stained with an antibody against Hec1. Hec1 localization at mitotic kinetochores was examined and quantified as in (B). Scale bar, 5 μm. Mean and SD, two-tailed Student's t-test, CENP-C^{WT} cells: n = 10, CENP-$C^{\Delta M12BD}$ cells: n = 10.

Next, I examined whether CENP-$C^{\Delta M12BD}$ cells showed mitotic defects as observed in *Cenpc*$^{\Delta M12BD/\Delta M12BD}$ MEFs. In contrast to MEFs, in which the deletion of M12BD from CENP-C delayed cell growth, CENP-$C^{\Delta M12BD}$ cells grew comparably to CENP-C^{WT} cells (Fig. 18H). However, time-lapse imaging showed that the mitotic progression from NEBD to anaphase onset was significantly delayed in CENP-$C^{\Delta M12BD}$ cells, as observed in *Cenpc*$^{\Delta M12BD/\Delta M12BD}$ MEFs (Figs. 20A-B). I also observed an increase in chromosome mis-segregation with lagging or bridging chromosomes in CENP-$C^{\Delta M12BD}$ cells (Fig. 20C). In addition, the cell population with micronuclei was increased in CENP-$C^{\Delta M12BD}$ cells (Fig. 20D). However, the DNA content did not exhibit a shift in CENP-$C^{\Delta M12BD}$ RPE-1 cells, which differs from the observed phenomenon in *Cenpc*$^{\Delta M12BD/\Delta M12BD}$ MEFs (Fig. 21).

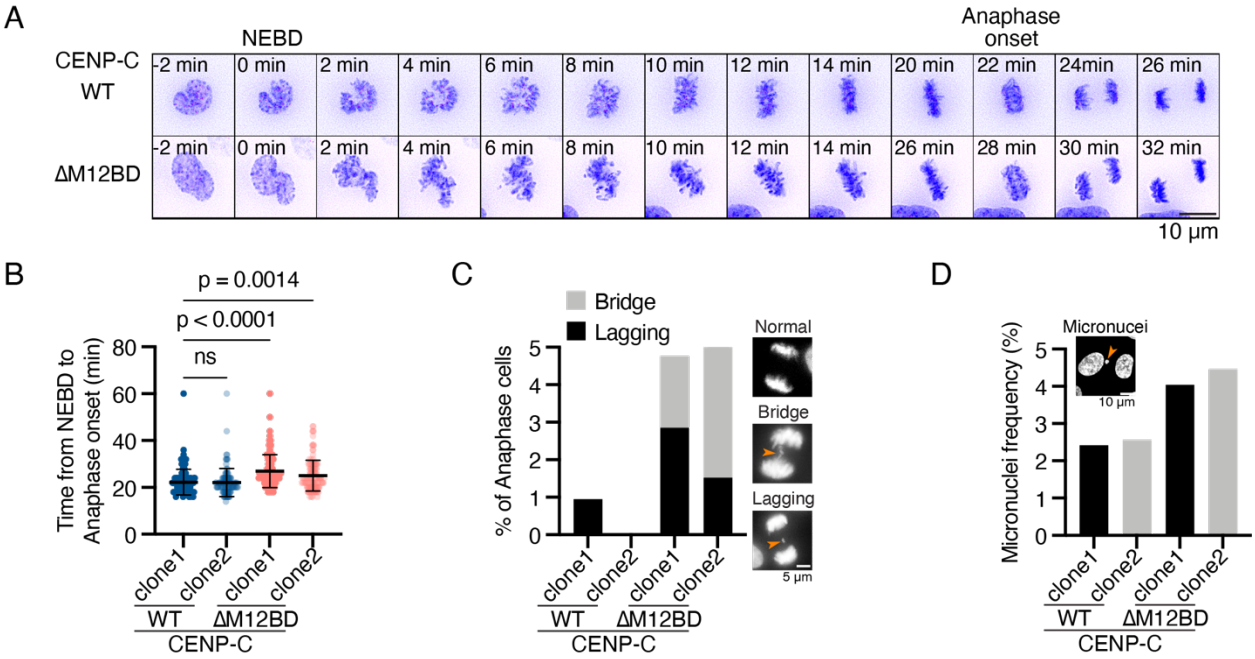

Figure.20 Mis12C-binding domain of CENP-C is required for proper mitotic progression in RPE-1 cells.

(A) Representative time-lapse images of mitotic progression in CENP-C^{WT} or CENP-C$^{\Delta M12BD}$ cells. DNA was visualized with GFP-H2A. Images were projected using maximum intensity projection and deconvoluted. Time is relative to nuclear envelope breakdown (NEBD). Scale bar: 10 μm.

(B) Mitotic duration from NEBD to anaphase onset in CENP-C^{WT} or CENP-C$^{\Delta M12BD}$ cells. The time-lapse images were analyzed to measure the time from NEBD to anaphase onset. Two independent clones of CENP-C^{WT} or CENP-C$^{\Delta M12BD}$ cells were tested (Mean and SD, two-tailed Student's t-test, CENP-C^{WT} cells clone1: n = 120, CENP-C^{WT} cells clone2: n = 105, CENP-C$^{\Delta M12BD}$ cells clone1: n = 105, CENP-C$^{\Delta M12BD}$ cells clone2: n = 132).

(C) Chromosome segregation errors in CENP-C^{WT} or CENP-C$^{\Delta M12BD}$ cells. The lagging chromosomes and chromosome bridges during anaphase in the cells analyzed in (B) were scored. Representative images are shown. Scale bar: 5 μm.

(D) Micronuclei formation CENP-C^{WT} or CENP-C$^{\Delta M12BD}$ cells. The cells were fixed and the interphase cells with micronuclei were scored (CENP-C^{WT} cells clone1: n = 1527,

CENP-C^{WT} cells clone2: n = 976, CENP-C$^{\Delta M12BD}$ cells clone1: n = 1633, CENP-C$^{\Delta M12BD}$ cells clone2: n = 1076). Scale bar: 10 μm.

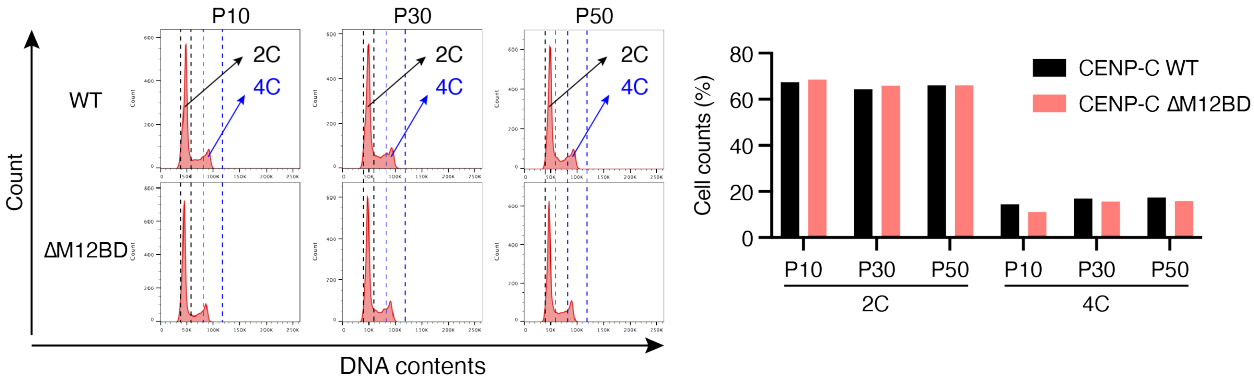

Figure.21 Flow cytometry analysis of DNA contents in CENP-C WT or ΔM12BD RPE-1 cells at different passages. RPE-1 cells were fixed and stained with propidium iodide and analyzed by flow cytometry. Representative results are shown on the left. P: passage time.

2.3 Discussion

The interaction of CENP-C-Mis12C has been extensively studied through structural analysis, revealing its role in mediating the assembly of Ndc80C-microtubules at the centromere (Dimitrova YN et al., 2016; Petrovic A et al., 2016). This association is important for mitotic progression. Contrary to expectations, the deletion of M12BD is largely dispensable for the development of *Cenpc*$^{\Delta M12BD/\Delta M12BD}$ mouse embryos and the survival of their littermates. This suggests that CENP-T-KMN interaction might be sufficient to support microtubule binding and allow cell cycle progression, as observed in chicken DT40 cells (Hara M et al., 2018).

Mitotic progression is a precise and coordinated process that requires each component to function correctly in both space and time. Even minor defects can result in abnormal progeny cells, leading to cell death or increased vulnerability to environmental changes (Santaguida S et al., 2015; Potapova T et al., 2017). This may explain why

Cenpc$^{\Delta M12BD/\Delta M12BD}$ offspring were less number than their counterparts. Chemical treatment revealed that *Cenpc*$^{\Delta M12BD/\Delta M12BD}$ mice were more susceptible to cancer induction and have a higher incidence of malignant transformation in a two-stage skin carcinogenesis model. This indicates that the interaction between CENP-C and Mis12C is crucial for accurate chromosome segregation under stress conditions.

MEFs derived from *Cenpc*$^{\Delta M12BD/\Delta M12BD}$ embryos exhibited notable chromosome segregation errors and the formation of micronucleited cells. Notably, the culture conditions in my experiment were not optimized as reported for MEFs (Parrinello S et al. 2003), likely contributing to elevated basal levels of $\geqslant$4C DNA contents in control cells. Additionally, CENP-C$^{\Delta M12BD}$ RPE-1 cells displayed similar mitotic defects to *Cenpc*$^{\Delta M12BD/\Delta M12BD}$ MEFs, although the CENP-C-Mis12C interaction was found to be dispensable for cell proliferation in RPE-1 cells. These results demonstrate that M12BD was essential for proper chromosome segregation in mitosis. However, unlike MEFs, flow cytometry analysis in my study showed no significant difference in DNA content between CENP-C ΔM12BD and WT RPE-1 cells during longer continuous passages. This phenomenon may be attributed to minor nucleotide changes undetectable by flow cytometry or the activation of the p53 pathway, which is responsible for arresting cells in the subsequent G1 phase to facilitate repair or elimination when cells endure anaphase delay and segregation mistakes (Janssen A et al., 2011; Santaguida S et al., 2015; Potapova T et al., 2017).

My group's earlier research found that the interaction between CENP-C and Mis12C did not affect the proliferation of chicken DT40 cells (Hara M et al., 2018). This could be due to technical limitations in detecting subtle differences in chromosome segregation in these cells, similar to observations of proliferation ability of RPE-1 cells. Another possibility is that the differences in CENP-C characteristics between mammals and chickens explain this result. In human cells, CENP-C depletion causes the CCAN complex to disassemble (McKinley KL et al., 2015). However, in CENP-C-knockout chicken DT40 cells, CCAN proteins, including CENP-T, remain attached to the centromeres (Hori T et al., 2008). This suggests that other kinetochore proteins may compensate for the lack of CENP-C in chicken DT40 cells.

Chapter 3: Ndc80C and K-fiber Reduction Are Dispensable for Mitotic Progression in CENP-C$^{\Delta M12BD}$ Cells

3.1 Introduction

The Mis12C binding region is crucial for faithful chromosome segregation, as illustrated above. Structural analysis has revealed that Mis12C directly associates with the N-terminal region of CENP-C and recruits KNL1C and Ndc80C at kinetochores (Ciferri C et al., 2008; Alushin GM et al., 2012; Petrovic A et al., 2016; Dimitrova YN et al., 2016). The Ndc80/Hec1-Nuf2 subcomplex of Ndc80C contributes to kinetochore-microtubule interactions. Deletion of the N-tail of Ndc80/Hec1 or the CH modules of Ndc80/Hec1-Nuf2 results in a reduction in the number of microtubules (DeLuca JG et al., 2005; Alushin GM et al., 2012).

To establish a functional chromosome segregation machinery, microtubules extending from two opposite poles are required to bind to kinetochores at sister chromatids. These kinetochore-associated microtubule bundles are defined as K-fibers (reviewed in Tolić IM, 2018). K-fibers play a crucial role in chromosome alignment (congression) during metaphase and are essential for chromosome separation during anaphase (Mitchison T et al., 1986; Zhai Y et al., 1995; Tanaka TU et al., 2008). In human RPE-1 cells, approximately 20 microtubules can attach to each kinetochore, reducing K-fiber occupancy with low-dose tubulin-binding drugs (BAL27862) can decrease inter-kinetochore distance and slightly delay anaphase onset in RPE-1 as reported previously (Dudka D et al., 2018).

K-fibers are highly dynamic, frequently undergoing polymerization (elongation) and depolymerization (shortening), yet are quite stable under cold or calcium buffer treatment compared to non-K-fibers, maintaining characteristics such as length and number (Rieder CL, 1981; Zhai Y et al., 1995). Thus, I supplement buffer containing calcium and quantify the signal intensity of K-fiber in cells with deletion of M12BD.

3.2 Results

3.2.1 M12BD deletion from CENP-C causes K-fiber reduction

To clarify the cause of chromosome segregation errors and mitotic delay in CENP-C$^{\Delta M12BD}$ RPE-1 cells, I first examined the K-fiber, which is the microtubule bundles associated with kinetochores (Tolić IM, 2018). The level of K-fiber, along with Ndc80C, a critical microtubule-binding complex, were significantly reduced in CENP-C$^{\Delta M12BD}$ cells. Following calcium treatment to depolymerize the highly dynamic microtubules, I stained the remaining stable microtubules, which corresponded to K-fiber, and found that the K-fiber signal intensities in CENP-C$^{\Delta M12BD}$ cells were significantly lower than those in CENP-C^{WT} cells, suggesting a reduction in K-fiber in CENP-C$^{\Delta M12BD}$ cells (Fig. 22A). The CENP-C$^{\Delta M12BD}$ cells were more sensitive to low-dose nocodazole treatment than the CENP-C^{WT} cells (Fig. 22B). This result further supported the reduction of K-fiber in CENP-C$^{\Delta M12BD}$ cells.

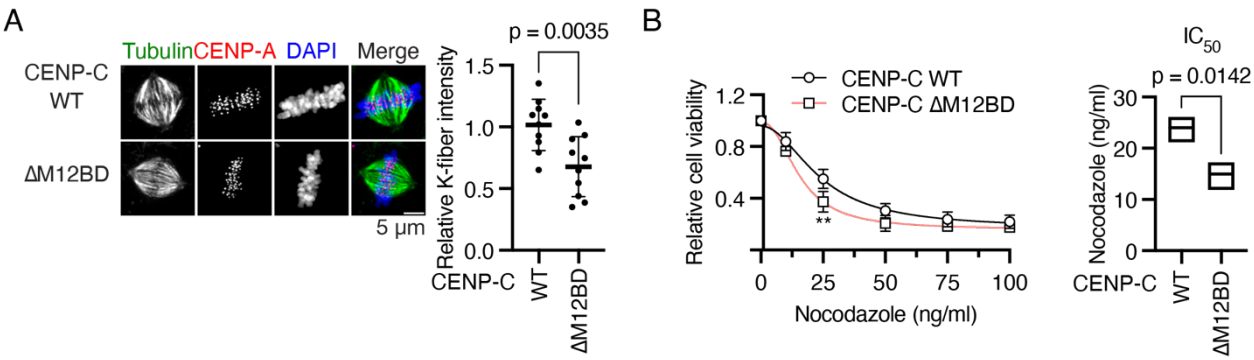

Figure.22 K-fiber reduction in CENP-C$^{\Delta M12BD}$ cells.

(A) K-fiber in CENP-C^{WT} or CENP-C$^{\Delta M12BD}$ cells. CENP-C^{WT} or CENP-C$^{\Delta M12BD}$ cells expressing mScarlet CENP-A were fixed after $CaCl_2$ treatment and stained with an anti-alpha-tubulin antibody. Scale bar, 5 μm. The mean tubulin signal intensities of the spindle in a cell were quantified as K-fiber signals (Mean and SD, two-tailed Student's t-test, CENP-C^{WT} cells: n = 10, CENP-C$^{\Delta M12BD}$ cells: n = 10).

(B) Cell viability of CENP-C^{WT} or CENP-C$^{\Delta M12BD}$ cells treated with various concentrations of nocodazole. Viable cells were measured three days after nocodazole addition. Three

independent experiments were performed (Mean and SD, two-way ANOVA with Šídák's multiple comparison test, **: p = 0.0022). IC_{50} indicates the average of concentration to reduce cell viability to 50% from three independent experiments (Mean and SD, two-tailed Student's t-test).

3.2.2 Ndc80C binding region deletion CENP-T causes K-fiber reduction

Given that the level of KNL1C was also reduced by disruption of CENP-C-Mis12C interaction (Fig. 19C) along with Ndc80C-K-fiber, it requires a different method or cell model could mimic the reduction of Ndc80C-K-fiber. The N-terminal of CENP-T contains two regions for Ndc80C binding besides one Ndc80C through Mis12C recruitment (Huis In 't Veld PJ et al., 2016; Takenoshita Y et al., 2022), suggesting the possibility of deletion of either Ndc80C binding region to mimic the reduction of K-fiber without disturbing KNL1C recruitment.

Firstly, construction of cell models which lack of either one Ndc80C binding region (Fig. 23), kindly was provided by Dr. Takenoshita. mScarlet-fused mutant human *CENP-T cDNAs*, devoid of either one of the two Ndc80C-binding sites (NBD-1: amino acids 6-31, NBD-2: amino acids 76-105) and full-length cDNA as wild type (WT) control, were introduced into the endogenous CENP-T locus (Figs. 23A-E, Fig. 24A, referred to as CENP-$T^{\Delta NBD-1}$ or CENP-$T^{\Delta NBD-2}$, and CENP-T^{WT}). Full-length human CENP-T fused with an auxin-inducible degron (AID)-tag was expressed from the AAVS1 locus. Upon induction of auxin (IAA), AID-tagged CENP-T underwent degradation, resulting in the exclusive expression of the mScarlet-fused CENP-T mutant or WT protein (Fig. 23F).

Subsequently, an examination was conducted to determine if the reduction of K-fibers in CENP-$C^{\Delta M12BD}$ cells without disturbing Mis12C-KNL1C recruitment. In cells expressing CENP-T ΔNBD-1 (CENP-$T^{\Delta NBD-1}$ cells) or ΔNBD-2 (CENP-$T^{\Delta NBD-2}$ cells), Ndc80C levels (Hec1) at the kinetochores were significantly lower than those in cells expressing full-length CENP-T (CENP-T^{WT} cells) (Fig. 24B). Importantly, the Mis12C (DSN1) and KNL1C (KNL1) levels at the kinetochores in CENP-$T^{\Delta NBD-1}$ and CENP-$T^{\Delta NBD-2}$ cells were

comparable to those in CENP-T^{WT} cells (Figs. 24C-D). As Ndc80C was reduced at the kinetochores, the K-fiber signal intensities in CENP-$T^{\Delta NBD-1}$ or CENP-$T^{\Delta NBD-2}$ cells were significantly lower than those in CENP-T^{WT} cells. Consistent with K-fiber reduction, CENP-$T^{\Delta NBD-1}$ and CENP-$T^{\Delta NBD-2}$ cells showed sensitivity to low-dose nocodazole (Fig. 24F).

Furthermore, CENP-T mutant cell models were used to determine the impact of K-fiber reduction on mitotic progression. Despite the reduced Ndc80C and associated K-fiber reduction, CENP-$T^{\Delta NBD-1}$ and CENP-$T^{\Delta NBD-2}$ cells showed neither significant mitotic delay nor increased chromosome segregation errors (Fig. 25).

These results suggest that the K-fiber reduction due to the decrease in Ndc80C is not the cause of mitotic defects in CENP-$C^{\Delta M12BD}$ cells.

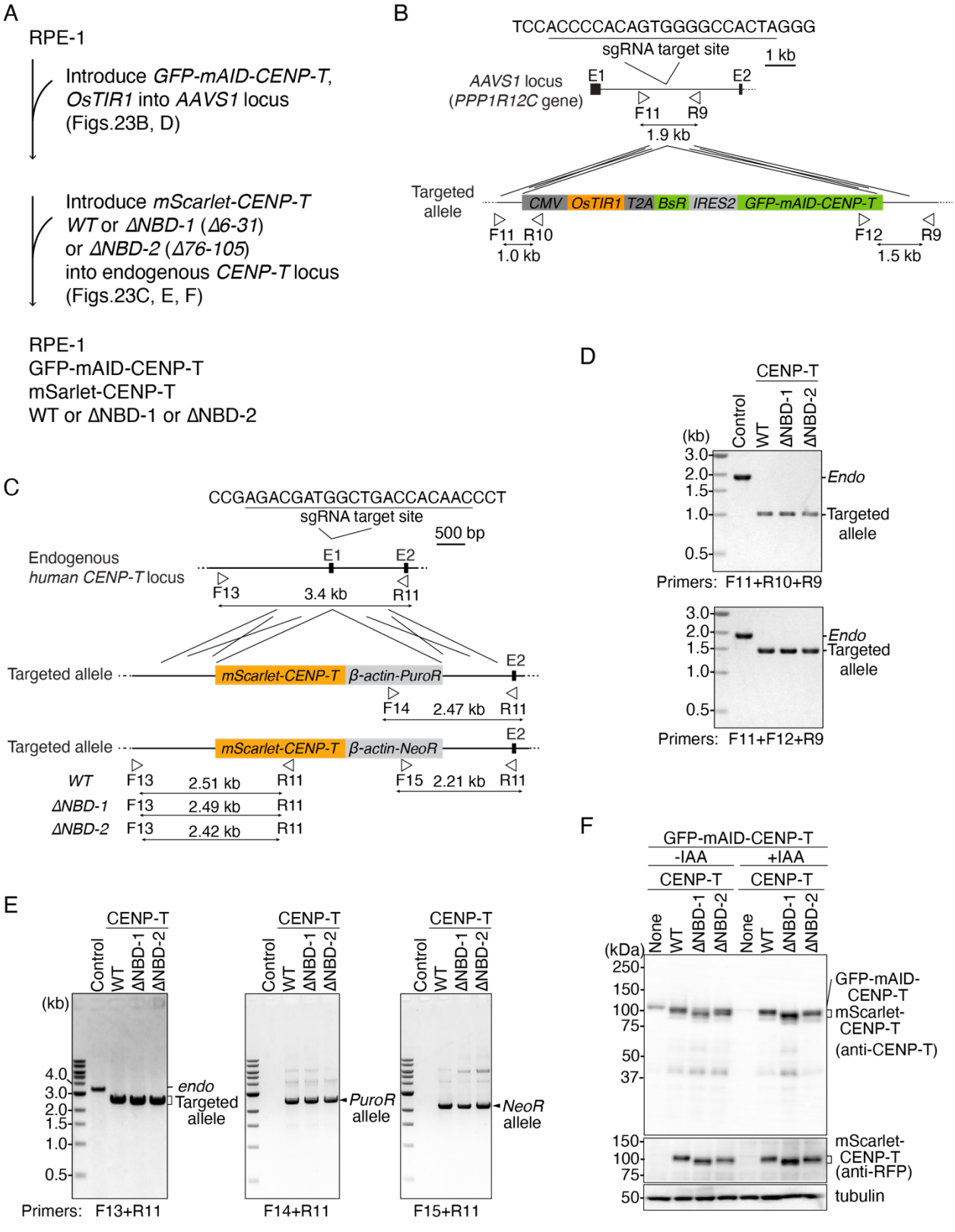
A
RPE-1
Introduce GFP-mAID-CENP-T, OsTIR1 into AAVS1 locus (Figs.23B, D)
Introduce mScarlet-CENP-T WT or ΔNBD-1 (Δ6-31) or ΔNBD-2 (Δ76-105) into endogenous CENP-T locus (Figs.23C, E, F)
RPE-1
GFP-mAID-CENP-T
mSarlet-CENP-T
WT or ΔNBD-1 or ΔNBD-2
B
TCCACCCCACAGTGGGGCCACTAGGG
sgRNA target site
1 kb
AAVS1 locus (PPP1R12C gene)
E1
E2
F11
R9
1.9 kb
Targeted allele
CMV OsTIR1 T2A BsR IRES2 GFP-mAID-CENP-T
F11 R10
1.0 kb
F12
R9
1.5 kb
C
CCGAGACGATGGCTGACCACAACCCT
sgRNA target site
500 bp
Endogenous human CENP-T locus
E1
E2
F13
3.4 kb
R11
Targeted allele
mScarlet-CENP-T β-actin-PuroR
E2
F14
2.47 kb
R11
Targeted allele
mScarlet-CENP-T β-actin-NeoR
E2
WT F13 2.51 kb R11
F15 2.21 kb R11
ΔNBD-1 F13 2.49 kb R11
ΔNBD-2 F13 2.42 kb R11
D
CENP-T
Control
WT
ΔNBD-1
ΔNBD-2
(kb)
3.0
2.0
1.5
1.0
0.5
Endo
Targeted allele
Primers: F11+R10+R9
Endo
Targeted allele
Primers: F11+F12+R9
E
CENP-T
Control
WT
ΔNBD-1
ΔNBD-2
(kb)
4.0
3.0
2.0
1.5
1.0
0.5
endo Targeted allele
PuroR allele
NeoR allele
Primers: F13+R11
F14+R11
F15+R11
F
GFP-mAID-CENP-T
-IAA
+IAA
CENP-T
None
WT
ΔNBD-1
ΔNBD-2
(kDa)
250
150
100
75
50
37
GFP-mAID-CENP-T
mScarlet-CENP-T
(anti-CENP-T)
mScarlet-CENP-T
(anti-RFP)
tubulin

Figure.23　Generation of CENP-T mutant RPE1 cell lines.

(A) Strategy to generate CENP-T^{WT}, CENP-T$^{\Delta NBD-1}$, or CENP-T$^{\Delta NBD-2}$ RPE1 cells (See also Figure 4). In the cells, mini auxin-inducible degron (mAID)-tagged human CENP-T was expressed together with OsTIR1. Since mAID-fused CENP-T is degraded upon IAA (Indole-3-acetic Acid) treatment, mScarlet-tagged CENP-T is only expressed CENP-T in CENP-T^{WT}, CENP-T$^{\Delta NBD-1}$, or CENP-T$^{\Delta NBD-2}$ RPE1 cells.

(B) Schematic representation of *GFP-mAID-CENP-T* and *OsTIR1* cDNA targeting into the *AAVS1* locus (*PPP1R12C* gene). To express GFP and mAID-fused human CENP-T and OsTIR1, the expression cassette was targeted into the intron1 by CRISPR/Cas9-mediated homologous recombination. Since the targeting construct has blasticidin resistance genes (*BsR*), targeted cells were selected using the *BsR* marker. The gRNA sequence and position of primers for genotyping are shown.

(C) Schematic representation of *mScarlet-CENP-T* cDNA targeting the endogenous *CENP-T* locus. To express mScarlet-tagged CENP-T wild-type (WT) or each of Ndc80C-binding domain mutants (ΔNBD-1: Δ6-31, ΔNBD-2: Δ76-105) under the control of the endogenous *CENP-T* promoter, *mScarlet-CENP-T WT*, Δ*NBD-1* or Δ*NBD-2* cDNA was targeted into the exon1 by CRISPR/Cas9-mediated homologous recombination. Since the targeting constructs have puromycin resistance genes (*PuroR*) or neomycin resistance genes (*NeoR*), targeted cells were selected using these selection markers. The gRNA sequence and position of primers for genotyping are shown.

(D) Genotyping PCR for *GFP-mAID-CENP-T/OsTIR1* expression cassette in CENP-T^{WT}, CENP-T$^{\Delta NBD-1}$, or CENP-T$^{\Delta NBD-2}$ RPE1 cells. The genotype in isolated single clones was examined using the primers shown in (B). Wild-type RPE-1 cells were used as a control.

(E) Genotyping PCR for targeted *mScarlet-CENP-T* in CENP-T^{WT}, CENP-T$^{\Delta NBD-1}$, or CENP-T$^{\Delta NBD-2}$ RPE1 cells. The genotype in isolated single clones was examined using the primers shown in (C). Wild-type RPE-1 cells were used as a control.

(F) CENP-T protein expression in CENP-T^{WT}, CENP-T$^{\Delta NBD-1}$, or CENP-T$^{\Delta NBD-2}$ RPE-1 cells. The cells were treated with or without IAA for one day and examined GFP-mAID-

CENP-T and mScarlet-CENP-T protein expression using an antibody against CENP-T or mScarlet (RFP). α-tubulin was probed as a loading control.

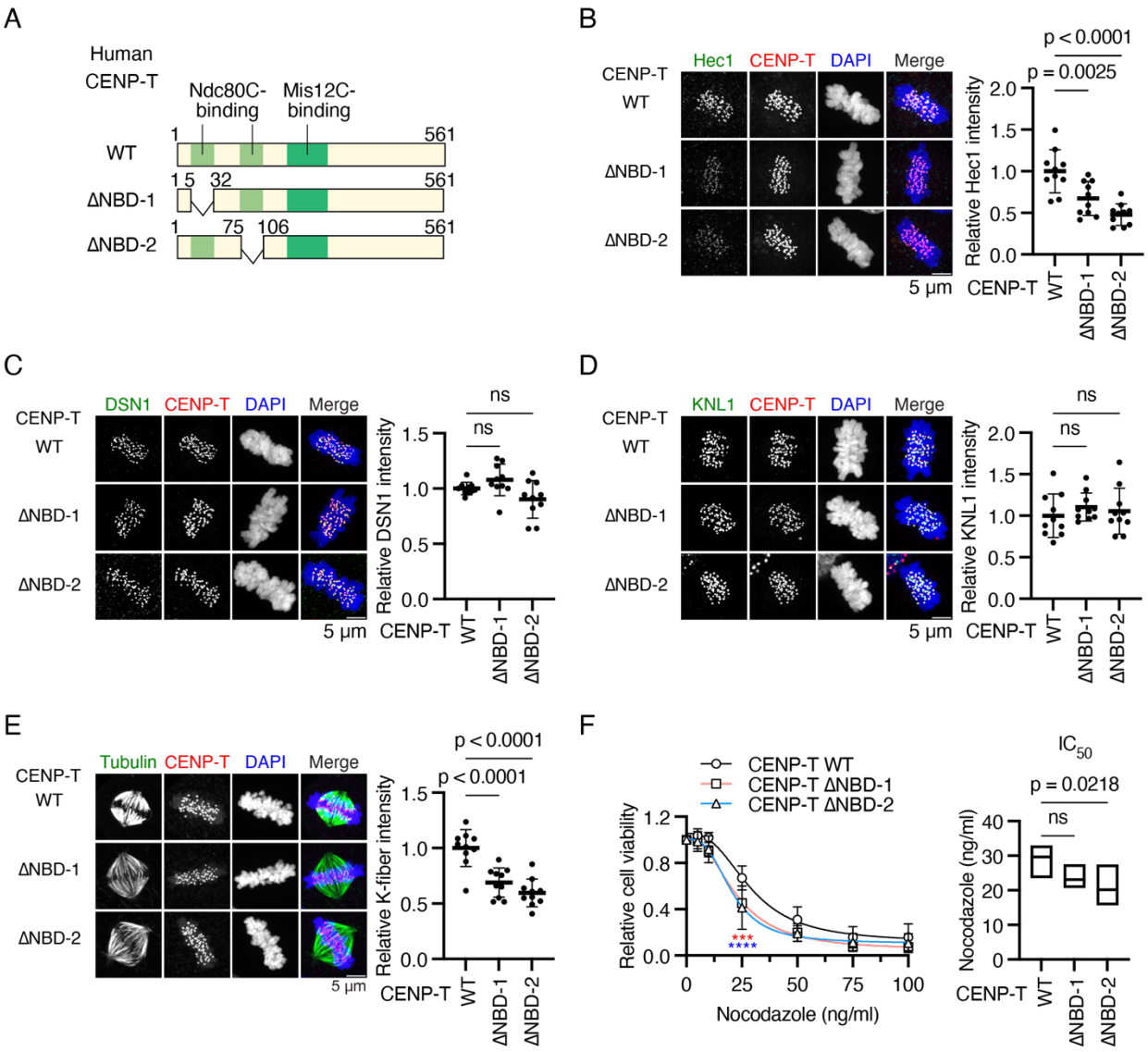

Figure.24 K-fiber reduction in CENP-T$^{\Delta NBD-1}$ or CENP-T$^{\Delta NBD-2}$ RPE-1 cells.

(A) Schematic representation of human CENP-T. human CENP-T wild-type (WT) has two Ndc80C binding regions (NBD-1 or -2: amino acids 6-31 or 76-105) and a Mis12-binding domain. Each NBD was deleted in CENP-T$^{\Delta NBD-1}$ or CENP-T$^{\Delta NBD-2}$, respectively.

mScarlet-fused CENP-T WT or each mutant was introduced into *CENP-T* locus in RPE-1 cells expressing OsTIR1 and GFP-mAID-CENP-T (CENP-T^{WT}, CENP-$T^{\Delta NBD-1}$, or CENP-$T^{\Delta NBD-2}$ cells, respectively).

(B) Hec1 localization in CENP-T^{WT}, CENP-$T^{\Delta NBD-1}$, or CENP-$T^{\Delta NBD-2}$ cells. Hec1, a subunit of Ndc80C, was stained with an antibody against Hec1 (green). mScarlet-CENP-T is a kinetochore marker (CENP-T, red). DNA was stained with DAPI (blue). Scale bar, 5 μm. Hec1 signal intensities at mitotic kinetochores were quantified (Mean and SD, one-way ANOVA with Dunnett's multiple comparison test, CENP-T^{WT} cells: n = 10, CENP-$T^{\Delta NBD-1}$ cells: n = 10, CENP-$T^{\Delta NBD-2}$ cells: n = 10).

(C) DSN1 localization in CENP-T^{WT}, CENP-$T^{\Delta NBD-1}$, or CENP-$T^{\Delta NBD-2}$ cells. DSN1, a subunit of Mis12C, was stained with an antibody against DSN1. DSN1 localization at mitotic kinetochores was examined and quantified as in (B). Scale bar, 5 μm. Mean and SD, one-way ANOVA with Dunnett's multiple comparison test, CENP-T^{WT} cells: n = 10, CENP-$T^{\Delta NBD-1}$ cells: n = 10, CENP-$T^{\Delta NBD-2}$ cells: n = 10.

(D) KNL1 localization in CENP-T^{WT}, CENP-$T^{\Delta NBD-1}$, or CENP-$T^{\Delta NBD-2}$ cells. KNL1, a subunit of KNL1C, was stained with an antibody against KNL1. KNL1 localization at mitotic kinetochores was examined and quantified as in (B). Scale bar, 5 μm. Mean and SD, one-way ANOVA with Dunnett's multiple comparison test, CENP-T^{WT} cells: n = 10, CENP-$T^{\Delta NBD-1}$ cells: n = 10, CENP-$T^{\Delta NBD-2}$ cells: n = 10.

(E) K-fiber in CENP-T^{WT}, CENP-$T^{\Delta NBD-1}$, or CENP-$T^{\Delta NBD-2}$ cells. CENP-T^{WT}, CENP-$T^{\Delta NBD-1}$, or CENP-$T^{\Delta NBD-2}$ cells were fixed after $CaCl_2$ treatment and stained with an anti-alpha-tubulin antibody. CENP-T fused with mScarlet is a kinetochore marker (CENP-T, red). Scale bar, 5 μm. The mean tubulin signal intensities of the spindle in a cell were quantified as K-fiber signals (Mean and SD, one-way ANOVA with Dunnett's multiple comparison test, CENP-T^{WT} cells: n = 10, CENP-$T^{\Delta NBD-1}$ cells: n = 10, CENP-$T^{\Delta NBD-2}$ cells: n = 10).

(F) Cell viability of CENP-T^{WT}, CENP-$T^{\Delta NBD-1}$, or CENP-$T^{\Delta NBD-2}$ cells treated with various concentrations of nocodazole. Viable cells were measured three days after nocodazole addition. Four independent experiments were performed (Mean and SD, two-way

ANOVA with Dunnett's multiple comparison test, ***: p = 0.0007, ****: p < 0.0001. Red: WT vs ΔNBD-1, Blue: WT vs ΔNBD-2). IC_{50} indicates the average of nocodazole concentration to reduce cell viability to 50% from four independent experiments (Mean and SD, one-way ANOVA with Dunnett's multiple comparison test).

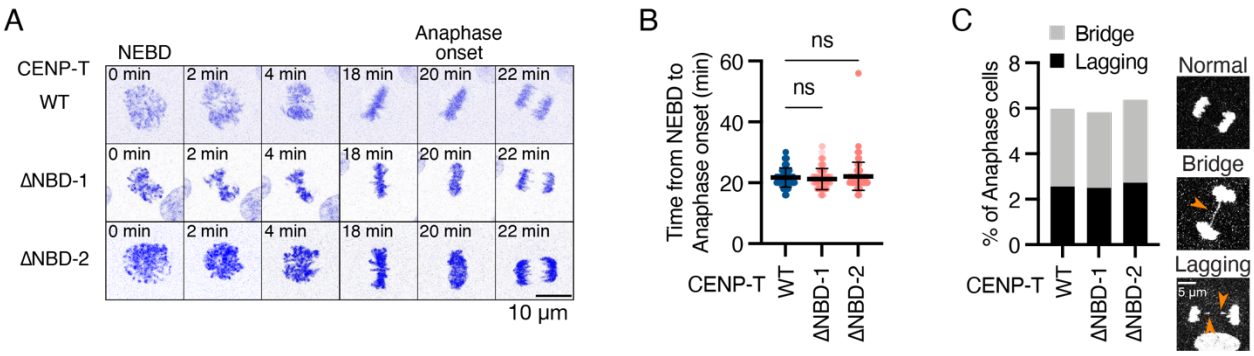

Figure.25 Mitotic progression in CENP-T$^{\Delta NBD-1}$ or CENP-T$^{\Delta NBD-2}$ RPE-1 cells.

(A) Representative time-lapse images of mitotic progression in CENP-T^{WT}, CENP-T$^{\Delta NBD-1}$, or CENP-T$^{\Delta NBD-2}$ cells. DNA was visualized with SPY505-DNA. Images were projected using maximum intensity projection and deconvoluted. Time is relative to nuclear envelope breakdown (NEBD). Scale bar, 10 μm.

(B) Mitotic duration from NEBD to anaphase onset in CENP-T^{WT}, CENP-T$^{\Delta NBD-1}$, or CENP-T$^{\Delta NBD-2}$ cells. The time-lapse images were analyzed to measure the time from NEBD to anaphase onset (Mean and SD, one-way ANOVA with Dunnett's multiple comparison test, CENP-T^{WT} cells: n = 117, CENP-T$^{\Delta NBD-1}$ cells: n = 120, CENP-T$^{\Delta NBD-2}$ cells: n = 110).

(C) Chromosome segregation errors in CENP-T^{WT}, CENP-T$^{\Delta NBD-1,}$ or CENP-T$^{\Delta NBD-2}$ cells. The lagging chromosomes and chromosome bridges during anaphase in the cells analyzed in (H) were scored. Representative images are shown. Scale bar 5 μm.

3.3 Discussion

To clarify the reduction effect of Ndc80/Hec1 and K-fiber on mitotic progression in CENP-C$^{\Delta M12BD}$ cells, I used the CENP-T$^{\Delta NBD-1}$ and CENP-T$^{\Delta NBD-2}$ cell models kindly provided by Dr. Takenoshita in my Lab. CENP-T can directly associate with Ndc80C at its N-terminal (Nishino T et al., 2013; Huis In 't Veld PJ et al., 2016). Immunostaining confirmed that CENP-T ΔNBD-1 and ΔNBD-2, which lack one binding domain of Ndc80/Hec1, did not disturb the recruitment of Mis12C and KNL1C. Deletion of NBD-2 reduced the signals of Hec1(~44%) more than NBD-1 (~30%). This may be because Ndc80C binding to the N-terminal of CENP-T relies on phosphorylation at T11 or T85 by CDK1, and NBD-2 has a higher affinity than NBD-1 (Huis In 't Veld PJ et al., 2016). Alternatively, the observed differences could be due to the limitations of immunostaining, which might not accurately reflect the precise signal levels.

Using time-lapse imaging, CENP-T$^{\Delta NBD-1}$ and CENP-T$^{\Delta NBD-2}$ did not show significant differences in the duration and frequency of anaphase errors compared to control cells under the same conditions. This suggests that partial K-fiber reduction through less Ndc80C recruitment did not affect mitotic progression, which contrasts with the observations in CENP-C$^{\Delta M12BD}$ cells. Therefore, it can be inferred that the interaction between Mis12C and CENP-C is crucial for accurate chromosome segregation. It also implyed that four Ndc80C binding region of CENP-C and CENP-T are not entirely occupied for attachment to microtubules, allowing for SAC silencing and the transition to anaphase. A quantitative analysis revealed that the ratio of CENP-C (KMN binding) to CENP-T to Ndc80C is 1:1:3 (Suzuki A et al., 2015), which can be explained by this result.

Notably, in our time-lapse imaging, CENP-T^{WT} showed a relatively higher incidence of segregation errors than CENP-C^{WT} cells. I suspect this is due to the toxicity of the DNA dye compared to using fluorescent protein markers for live cell imaging (GFP-H2A expression in CENP-C^{WT}). It has been reported that DNA dyes can cause DNA damage without affecting the duration of mitosis, which is consistent with my observations (Sen O et al., 2018). Previous reports indicate that reduction of K-fiber occupancy (35.5% reduction) with the depolymerizing drug BAL27862 delay anaphase onset slightly and

affect the segregation fidelity in RPE-1 cells without trigger the SAC neither Aurora B-dependent microtubule detachment (Dudka D et al., 2018). This may imply that microtubule dynamics are in the comparable level in CENP-T$^{\Delta NBD-1}$ or CENP-T$^{\Delta NBD-2}$ with CENP-T^{WT} cells, in which K-fiber decrease about 33% or 37% respectively, but the exerting force from kinetochore-microtubule attachment might be in a ‘delicate banlance’, since CENP-T$^{\Delta NBD-1}$ or CENP-T$^{\Delta NBD-2}$ was more sensitive to the nocodozole.

Neverthereless, further investigation into the molecular mechanisms underlying is required in CENP-C$^{\Delta M12BD}$ RPE-1 cells.

Chapter 4: The Mis12C Binding Domain of CENP-C Is Essential for Establishing Efficient Error Correction

4.1 Introduction

To ensure precise chromosome segregation, kinetochore proteins must assemble at the centromere and cooperate with surveillance systems, including Aurora B-mediated error correction (see in the general introduction section) (Fukagawa T et al., 1997; Tanaka K et al., 2009; McKinley KL et al., 2015; Nagpal H et al., 2016; Hara M et al., 2017; Banerjee A et al., 2020). Cells lacking the Mis12 binding region of CENP-C exhibit a high frequency of mis-segregations (2-fold in MEFs, 5-fold in RPE-1 cells) compared to control cells (Figs. 15D, 20C). However, a partial reduction of Ndc80C at metaphase did not contribute to significant mitotic defects (Fig. 25). This prompted me to investigate the error correction system during metaphase.

Kinetochore-microtubule (KT-MT) attachment errors, including monotelic, syntelic, or merotelic attachments, frequently occur during early prometaphase. Inefficient correction of these mal-orientations can result in lagging chromosomes (Ault JG et al., 1992; Cimini D et al., 2001, 2003, 2006; Compton DA. 2007). Aurora B kinase plays a crucial role in correcting KT-MT misattachments by phosphorylating the N-terminal region (about 80 amino acids) of Ndc80/Hec1, which destabilizes the KT-MT interaction (DeLuca JG et al., 2006, 2011; Cimini D et al., 2006; Zaytsev AV et al., 2014; Musacchio A. 2015). This process is known as an error correction. Through frequent turnover of errorneous and correctness, kinetochores on sister chromatids ultimately achieve amphitelic binding by attaching to the plus-ends of microtubules extending from opposite poles. Then, I examined how Aurora B reduction is related with mitotic defects in CENP-C$^{\Delta M12BD}$ cells.

4.2 Results

4.2.1 Aurora B localization to mitotic centromeres is diminished in CENP-C$^{\Delta M12BD}$ cells

To determine the cause of chromosome segregation errors and mitotic delay in CENP-C$^{\Delta M12BD}$ cells, I examined the regulatory mechanisms of kinetochore-microtubule attachment. Aurora B is a conserved mitotic kinase that phosphorylates kinetochore substrates, such as Hec1, facilitating the correction of erroneous kinetochore-microtubule attachment (Cheeseman IM et al., 2006; DeLuca JG et al., 2006, 2011; Liu D et al., 2009; Zaytsev AV et al., 2014; Long AF et al., 2017). As shown in Fig. 26, Aurora B was localized to the inner centromeric region between sister kinetochores in mitotic cells. I found that Aurora B levels were significantly reduced in CENP-C$^{\Delta M12BD}$ cells compared to those in CENP-C^{WT} cells (Fig. 26A). In contrast, the reduction of Aurora B at the centromeres was not observed in CENP-T$^{\Delta NBD-1}$ or CENP-T$^{\Delta NBD-2}$ cells (Fig. 26B), which underwent proper mitotic progression despite the reduction of Ndc80C levels at kinetochores (Figs. 24B, 25).

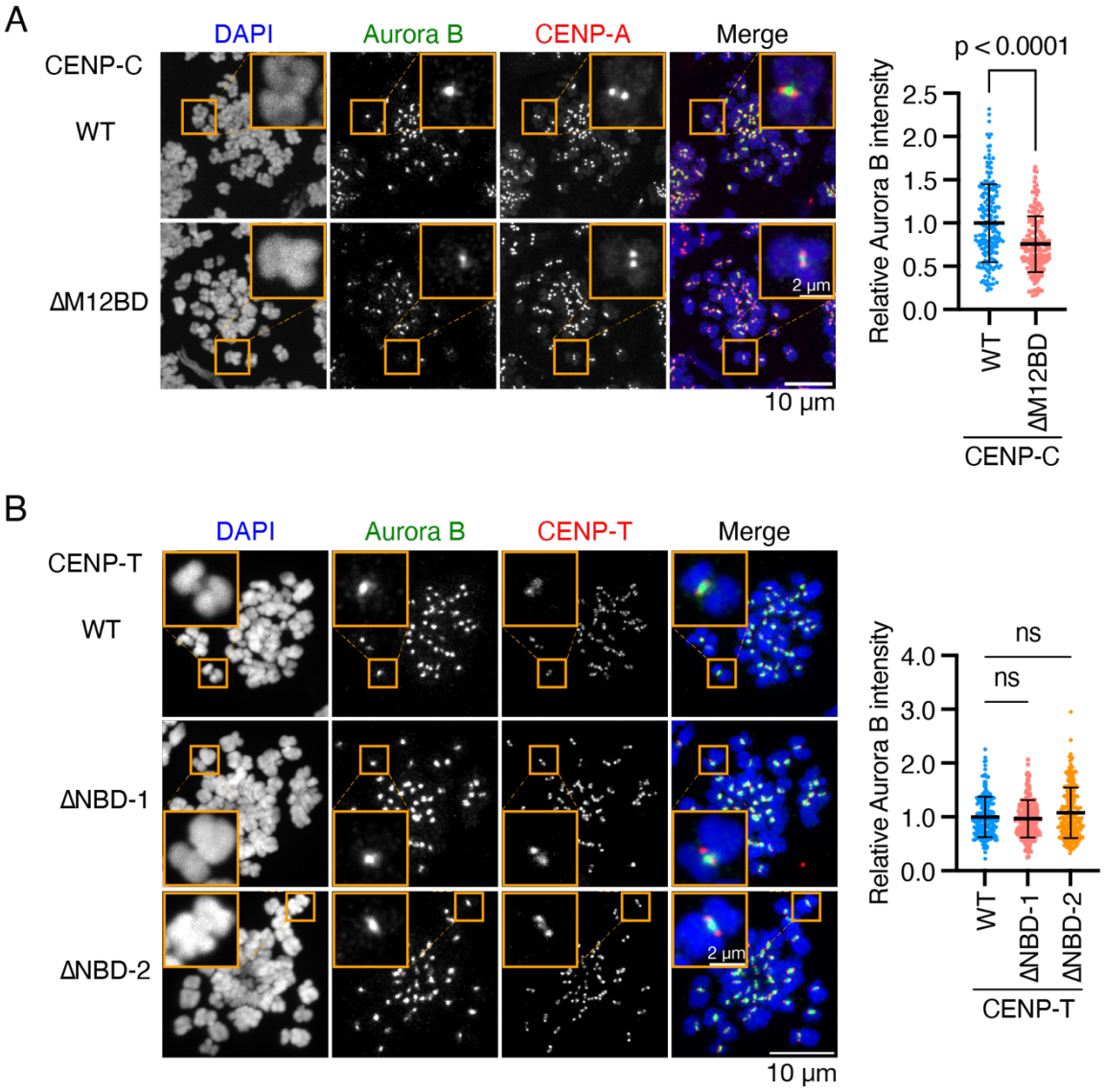

Figure.26 Aurora B recruitment reduction at centromeres in CENP-C$^{\Delta M12BD}$ cells.

(A) Aurora B localization in CENP-C^{WT} or CENP-C$^{\Delta M12BD}$ cells. Aurora B was stained with an antibody against Aurora B (green). mScarlet-CENP-A is a kinetochore marker (CENP-A, red). DNA was stained with DAPI (blue). Scale bar, 10 μm. The insets show an enlarged single chromosome (Scale bar, 2 μm). Aurora B signal intensities at inner centromeres were quantified (Mean and SD, two-tailed Student's t-test, CENP-C^{WT}: n = 188 centromeres from 5 cells, CENP-C$^{\Delta M12BD}$: n = 166 centromeres from 5 cells).

(B) Aurora B localization in CENP-T^{WT}, CENP-T$^{\Delta NBD-1}$, or CENP-T$^{\Delta NBD-2}$ cells. Aurora B and DNA were stained as in (A). mScarlet-CENP-T is a kinetochore marker (CENP-T,

red). Scale bar, 5 μm. The Aurora B signal intensities were quantified (Mean and SD, one-way ANOVA with Dunnett's multiple comparisons test, CENP-T^{WT}: n = 197 centromeres from 5 cells, CENP-$T^{\Delta NBD-1}$: n = 198 centromeres from 5 cells, CENP-$T^{\Delta NBD-2}$: n = 225 centromeres from 5 cells).

4.2.2 Bub1-H2AT120ph recruitment to mitotic centromeres is diminished in CENP-$C^{\Delta M12BD}$ cells

Centromeric localization of Aurora B is promoted by the phosphorylation of histone H3 at threonine 3 (H3T3ph) by Haspin and histone H2A at threonine 120 (H2AT120ph) by Bub1 (Watanabe Y., 2010; Wang F et al., 2011). To investigate how the CENP-C-Mis12C interaction is related to Aurora B localization, I examined the Bub1 level during mitotic progression, prophase, prometaphase, and metaphase. CENP-$C^{\Delta M12BD}$ cells showed less Bub1 localization at the kinetochores at each phase than did CENP-C^{WT} cells (Fig.27A). Since Bub1 localizes to kinetochores through KNL1 (Kiyomitsu T et al., 2007), the results aligned with the reduction of KNL1C, which binds to Mis12C (Dimitrova YN et al., 2016; Petrovic A et al., 2010, 2014) at kinetochores in CENP-$C^{\Delta M12BD}$ cells (Fig. 19C). Then I examined the phosphorylation of histones and found that H2AT120ph levels were significantly reduced in CENP-$C^{\Delta M12BD}$ cells (Fig. 27B); however, H3T3ph levels in CENP-$C^{\Delta M12BD}$ cells were comparable to those in CENP-C^{WT} cells (Fig. 28).

In contrast, Bub1, H2AT120ph, and H3T3ph levels in CENP-$T^{\Delta NBD-1}$ and CENP-$T^{\Delta NBD-2}$ cells, which showed neither mitotic defects nor Aurora B reduction, were comparable to those in CENP-T^{WT} cells (Fig. 29). The unaltered Bub1 and H2AT120ph levels were consistent with the finding that Mis12C and KNL1C levels at the centromeres in CENP-$T^{\Delta NBD-1}$ and CENP-$T^{\Delta NBD-2}$ cells were comparable to those in CENP-T^{WT} cells (Figs. 29B-C).

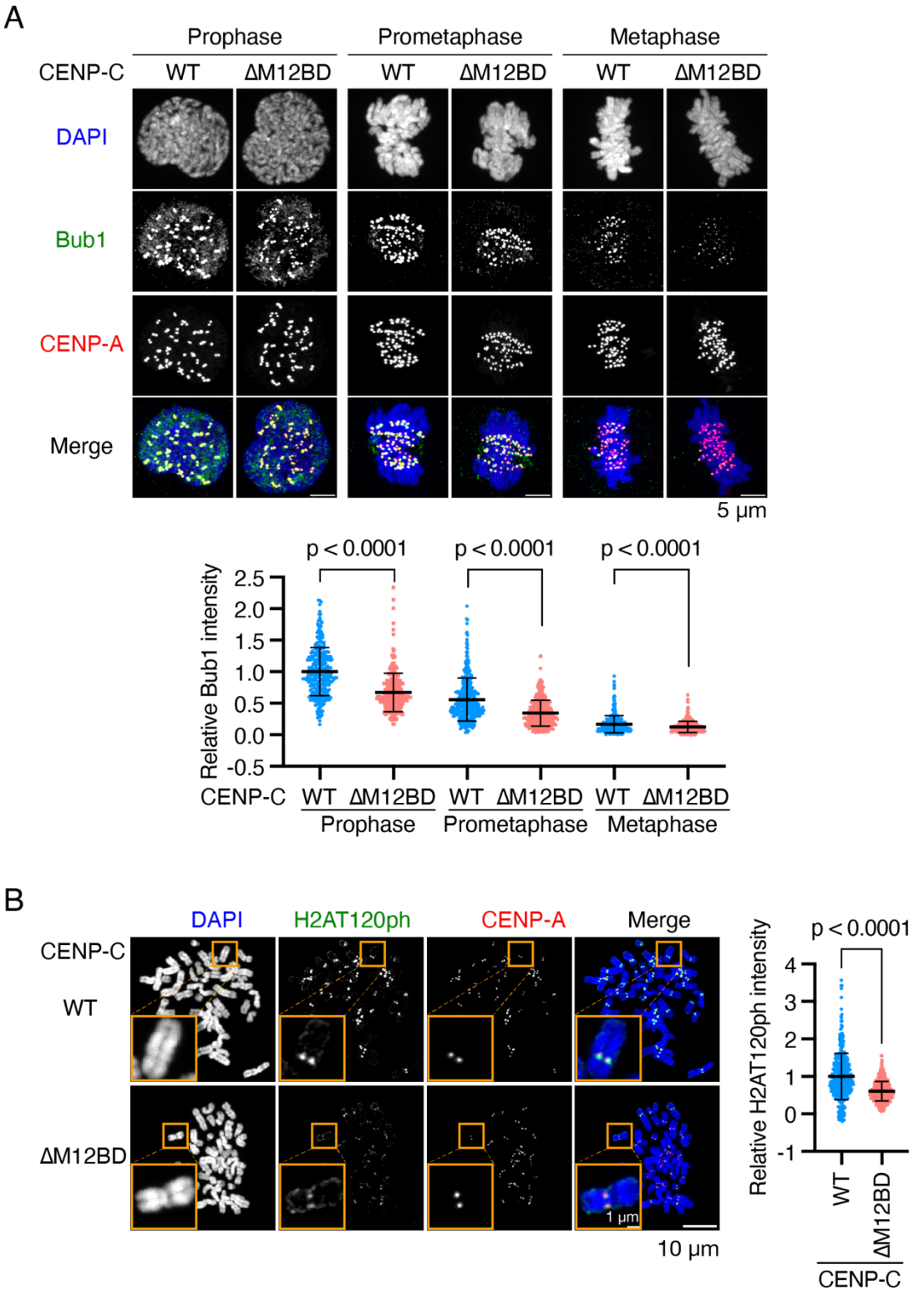

Figure.27 Bub1-H2AT120ph recruitment to mitotic centromeres is diminished in CENP-C$^{\Delta M12BD}$ RPE-1 cells.

(A) Bub1 localization in CENP-C^{WT} or CENP-C$^{\Delta M12BD}$ cells. Bub1 was stained with an antibody against Bub1 (green). mScarlet-CENP-A is a kinetochore marker (CENP-A, red). DNA was stained with DAPI (blue). Scale bar, 5 μm. Bub1 signal intensities at kinetochores were quantified (Mean and SD, two-tailed Student's t-test, CENP-C^{WT}: n = 318 kinetochores from 5 cells (prophase), n = 354 kinetochores from 5 cells (prometaphase), n = 440 kinetochores from 5 cells (metaphase); CENP-C$^{\Delta M12BD}$: n = 280 kinetochores from 5 cells (prophase), n = 423 kinetochores from 5 cells (prometaphase), n = 429 kinetochores from 5 cells (metaphase)).

(B) H2AT120ph localization in CENP-C^{WT} or CENP-C$^{\Delta M12BD}$ cells. H2AT120ph was stained with an antibody against H2AT120ph (green). mScarlet-CENP-A is a kinetochore marker (CENP-A, red). DNA was stained with DAPI (blue). Scale bar, 10 μm. The insets show an enlarged single chromosome (Scale bar, 1 μm). H2AT120ph signal intensities at kinetochore-proximal centromeres were quantified (Mean and SD, two-tailed Student's t-test, CENP-C^{WT}: n = 398 kinetochores from 5 cells, CENP-C$^{\Delta M12BD}$: n = 373 kinetochores from 5 cells).

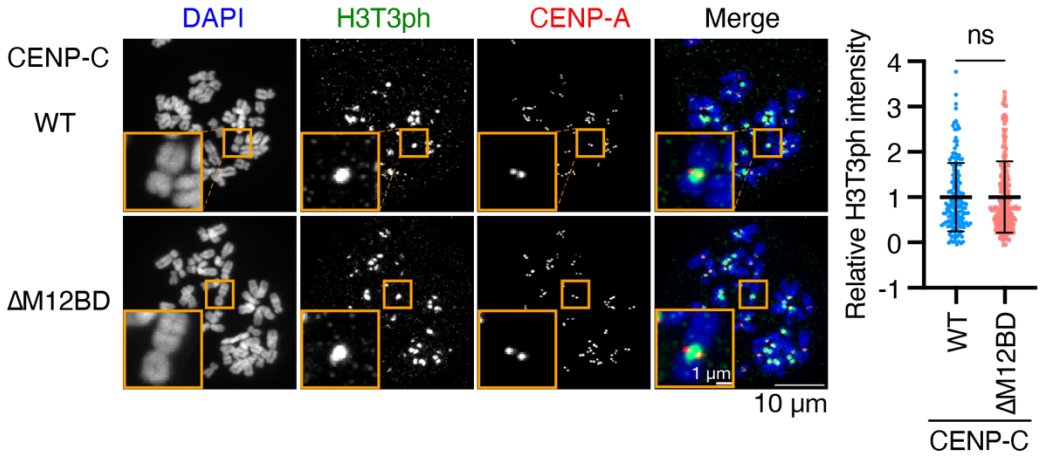

Figure.28 H3T3ph localization at centromeres in CENP-C$^{\Delta M12BD}$ RPE-1 cells.

H3T3ph was stained with an antibody against H3T3ph. H3T3ph localization at centromeres was examined and quantified as in (Fig. 26). Scale bar, 10 μm. The graph

displayed Mean and SD (Two-tailed Student's t-test, CENP-C^{WT}: n = 170 centromeres from 5 cells, CENP-C$^{\Delta M12BD}$: n = 204 centromeres from 5 cells).

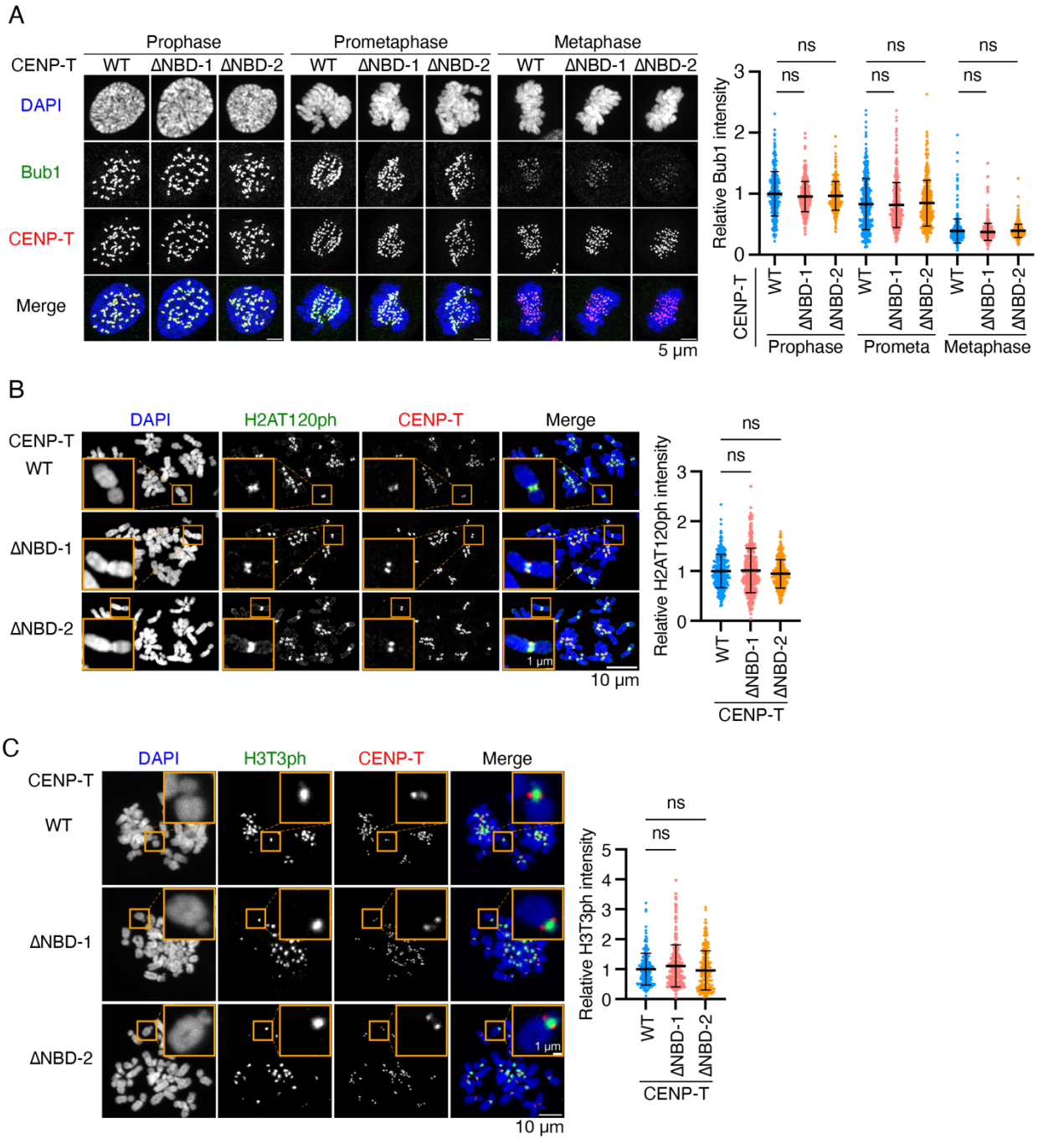

Figure.29　Bub1, H2AT120ph, and H3T3ph localization in CENP-T mutant RPE1 cell lines.

(A) Bub1 localization in CENP-T^{WT}, CENP-$T^{\Delta NBD-1}$, or CENP-$T^{\Delta NBD-2}$ RPE1 cells. Bub1 was stained with an antibody against Bub1 (green). mScarlet-CENP-T is a kinetochore marker (CENP-T, red). DNA was stained with DAPI (blue). Scale bar, 5 μm. Bub1 signal intensities at kinetochores were quantified. A representative result from two independent experiments is shown (Mean and SD, one-way ANOVA with Dunnett's multiple comparison test, CENP-T^{WT}: n = 427 kinetochores from 5 cells, CENP-$T^{\Delta NBD-1}$: n = 424 kinetochores from 5 cells, CENP-$T^{\Delta NBD-2}$: n = 423 kinetochores from 5 cells).

(B) H2AT120ph localization in CENP-T^{WT}, CENP-$T^{\Delta NBD-1}$, or CENP-$T^{\Delta NBD-2}$ RPE-1 cells. H2AT120ph was stained with an antibody against H2AT120ph (green). mScarlet-CENP-T is a kinetochore marker (CENP-T, red). DNA was stained with DAPI (blue). Scale bar, 10 μm. The insets show an enlarged single chromosome (Scale bar, 1 μm). H2AT120ph signal intensities at kinetochore-proximal centromeres were quantified. A representative result from three independent experiments is shown (Mean and SD, one-way ANOVA with Dunnett's multiple comparison test, CENP-T^{WT}: n = 316 kinetochores from 5 cells, CENP-$T^{\Delta NBD-1}$: n = 306 kinetochores from 5 cells, CENP-$T^{\Delta NBD-2}$: n = 325 kinetochores from 5 cells).

(C) H3T3ph localization in CENP-T^{WT}, CENP-$T^{\Delta NBD-1}$, or CENP-$T^{\Delta NBD-2}$ RPE1 cells. H3T3ph was stained with an antibody against H3T3ph. H3T3ph localization at centromeres was examined and quantified as in (A). Scale bar, 10 μm. A representative result from two independent experiments is shown (Mean and SD, one-way ANOVA with Dunnett's multiple comparison test, CENP-T^{WT}: n = 195 centromeres from 5 cells, CENP-$T^{\Delta NBD-1}$: n = 206 centromeres from 5 cells, CENP-$T^{\Delta NBD-2}$: n = 210 centromeres from 5 cells).

4.2.3 Chromosome osillation attenuated in CENP-C$^{\Delta M12BD}$ cells

To further evaluate the reduction of Aurora B activity at the centromeres in CENP-C$^{\Delta M12BD}$ cells, I examined metaphase chromosome oscillation, which is regulated by Aurora B through the phosphorylation of Hec1 (Zaytsev AV et al., 2014). CENP-C^{WT} or CENP-C$^{\Delta M12BD}$ cells were treated with MG132, a proteasome inhibitor, to arrest the cells at metaphase, and chromosome oscillations were observed by time-lapse imaging (Fig. 30 and Fig. 31A). The oscillation amplitude was assessed by quantifying the deviation from the average position (DAP) (Stumpff J et al., 2008) for tracked kinetochores labeled with mScarlet-CENP-A (Fig. 30 and Fig. 31A). The amplitude in CENP-C$^{\Delta M12BD}$ was significantly smaller than that in CENP-C^{WT} cells (Fig. 31A). Amplitude reduction was also observed in CENP-C^{WT} cells treated low-does (5 ng/ml) Nocodazole (Fig. 32).

In contrast, CENP-T^{NBD-1} and CENP-T^{NBD-2} cells did not show changes in the amplitude of oscillations compared to CENP-T^{WT} cells (Fig. 31B). These results suggest a reduction in Aurora B activity at the centromeres in CENP-C$^{\Delta M12BD}$ cells, but not in CENP-T^{NBD-1} and CENP-T^{NBD-2} cells.

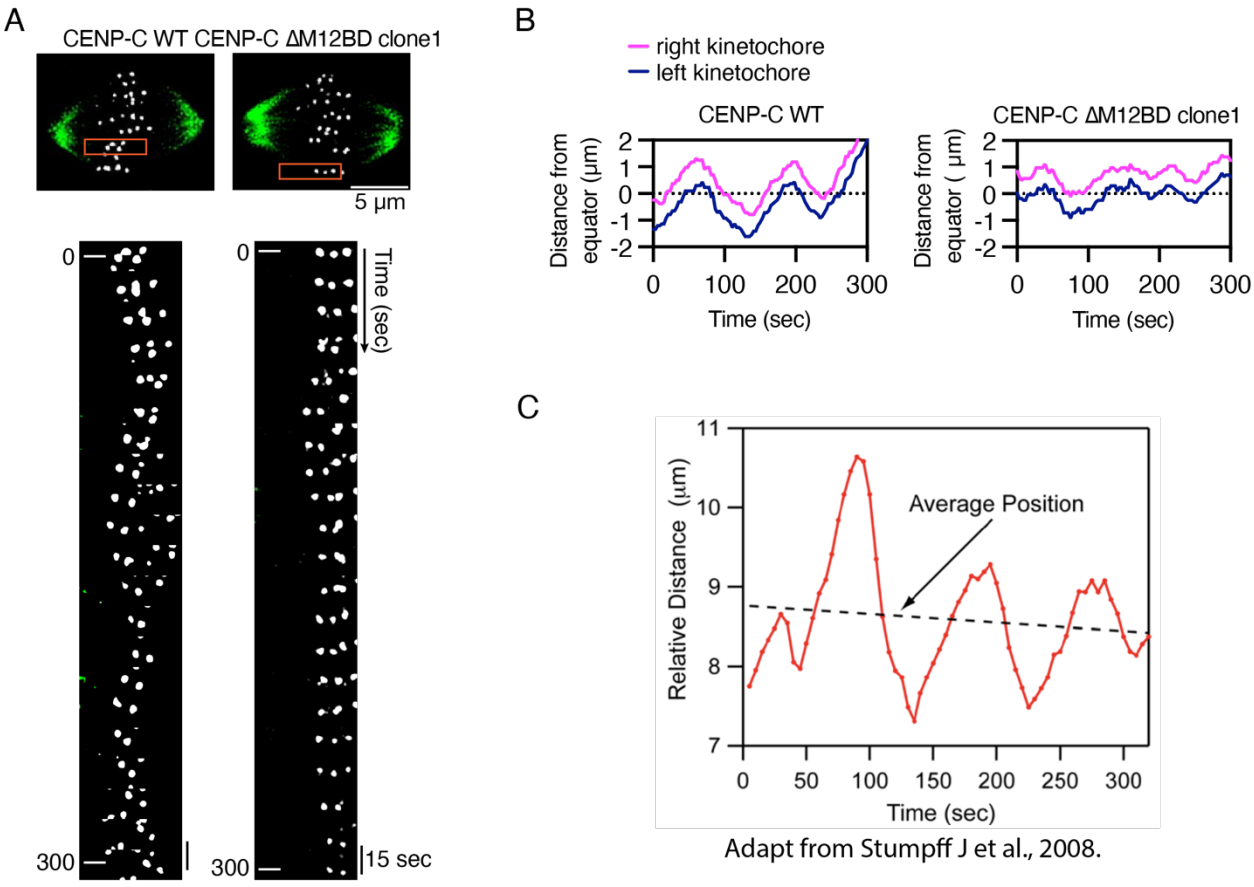

Figure.30 Quantifying chromosome amplitude in CENP-C$^{\Delta M12BD}$ cells.

(A) Chromosome oscillation in CENP-C^{WT} or CENP-C$^{\Delta M12BD}$ cells. Representative cell images are shown. mScarlet-CENP-A is a kinetochore marker (gray). The spindle was visualized with SiR-Tubulin (green). Scale bar, 5 μm. Kymographs represent the boxed kinetochore pairs at 15 sec intervals.

(B) Distance of sister kinetochores from the equator in CENP-C^{WT} or CENP-C$^{\Delta M12BD}$ cells. Representative trajectories for kinetochore pairs are shown.

(C) Deviation from average position (DAP) measurements. Measuring the extent of oscillatory movements is determined by the deviations from the average position of a kinetochore. This approach has the benefit of not depending on manually selecting directional changes, thus minimizing subjectivity. It remains applicable even in cases where turnarounds are not easily identifiable.The graph was adapt from Stumpff J et al., 2008.

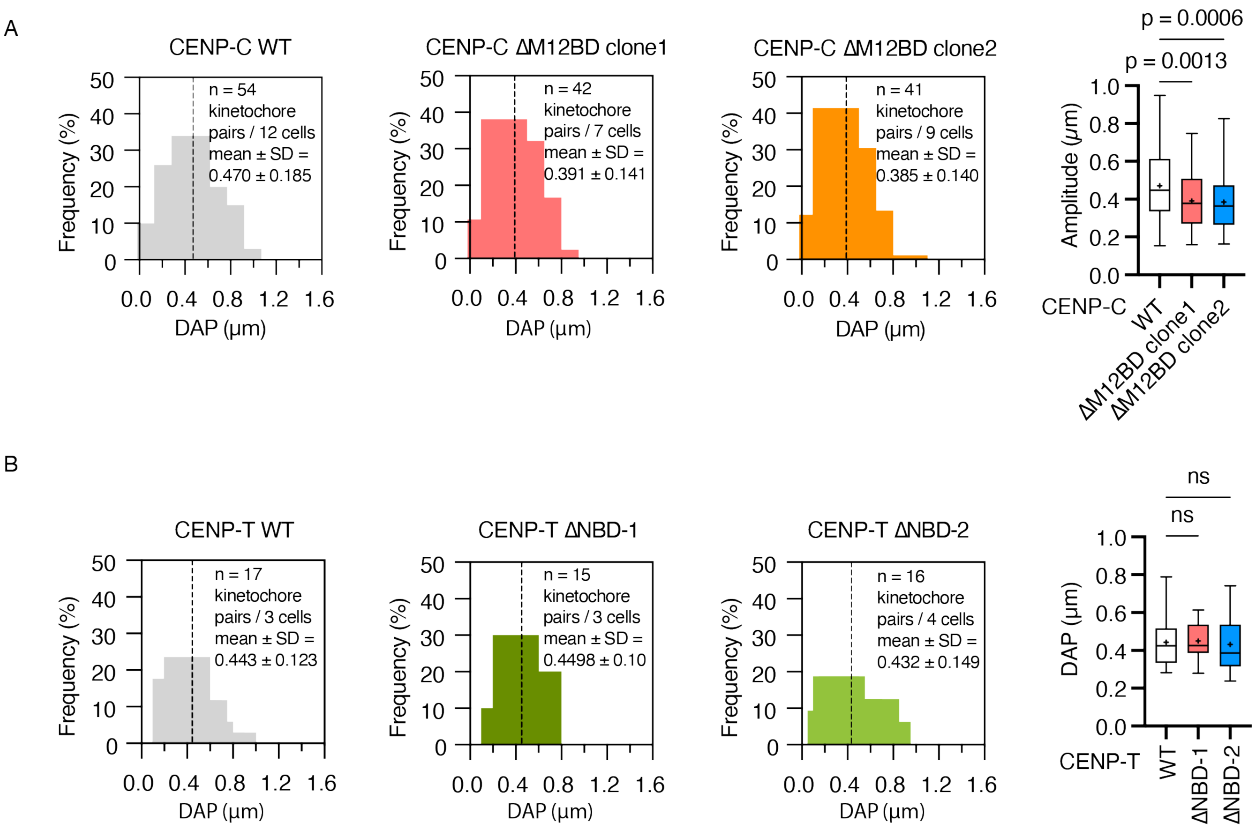

Figure.31 Chromosome osillation is attenuated in CENP-C$^{\Delta M12BD}$ cells.

(A) Frequency of DAP (the deviation from average position) values in CENP-C^{WT} or CENP-C$^{\Delta M12BD}$ cells. DAP is calculated by using trajectories of kinetochore pairs. 54 kinetochore pairs in 12 CENP-C^{WT} cells and 42 kinetochore pairs in 7 CENP-C$^{\Delta M12BD}$ cells were used for the quantification. The dashed lines indicate the mean. The graph displays the median and quantile with max and min (+ indicates mean) (One-way ANOVA with Dunnett's multiple comparison test, CENP-C^{WT} cells: n = 54 kinetochore pairs from 12 cells, CENP-C$^{\Delta M12BD}$ cells: n = 42 kinetochore pairs from 7 cells).

(B) Frequency of DAP values in CENP-T^{WT}, CENP-T$^{\Delta NBD-1}$, or CENP-T$^{\Delta NBD-2}$ cells. 17 kinetochore pairs in 3 CENP-T^{WT} cells, 15 kinetochore pairs in 3 CENP-T$^{\Delta NBD-1}$ cells, and 16 kinetochore pairs in 4 CENP-T$^{\Delta NBD-2}$ cells were used for the quantification. The dashed lines indicate the mean. The graph displays the median and quantile with max and min (+ indicates mean) (One-way ANOVA with Dunnett's multiple comparison test, CENP-T^{WT} cells: n = 17 kinetochore pairs from 3 cells, CENP-T$^{\Delta NBD-1}$ cells: n = 15

kinetochore pairs from 3 cells, CENP-T$^{\Delta NBD-2}$ cells: n = 16 kinetochore pairs from 4 cells).

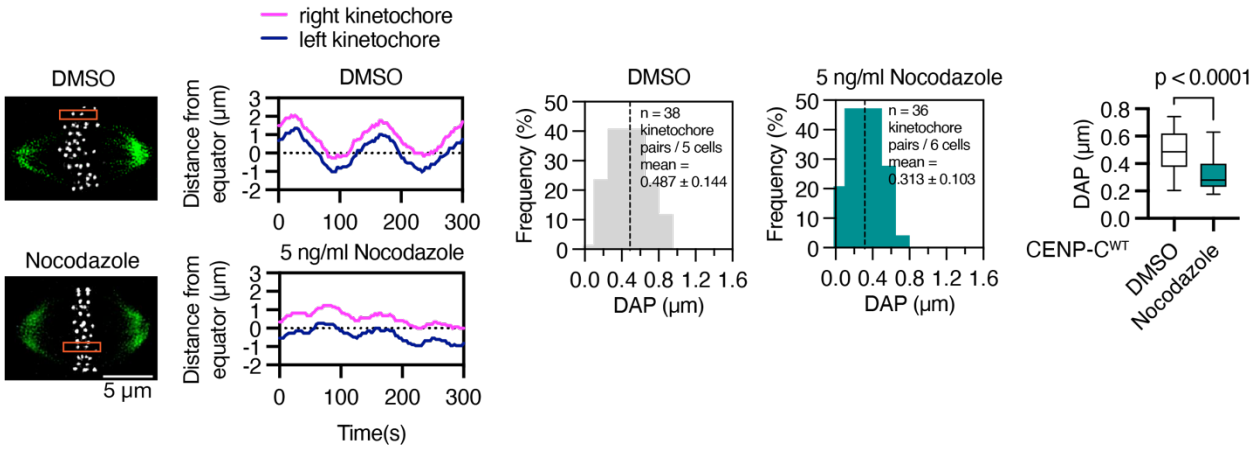

Figure.32 Chromosome oscillation is diminished in the presence of a depolymerization reagent. Quantification of DAP supplemented with 5 mg/ml nocodazole for 1 hour before imaging in CENP-C^{WT} RPE-1 cells. (Student's t-test, DMSO: n = 38 kinetochore pairs from 5 cells, nocodazole: n = 36 kinetochore pairs from 6 cells).

4.2.4 Error correction efficiency was reduced in CENP-C$^{\Delta M12BD}$ cells

As one of the key functions of Aurora B is mitotic error correction, which resolves erroneous kinetochore-microtubule attachments to facilitate the correct bipolar spindle microtubule attachment to the sister kinetochores (Dewar H et al., 2004; Lampson MA et al., 2004; Cimini D et al., 2006), I evaluated the error correction efficiency in CENP-C$^{\Delta M12BD}$ cells with low Aurora B levels at centromeres (Fig. 26A). RPE-1 cells were treated with monastrol, a reversible Eg5 inhibitor (Kapoor TM et al., 2000), to induce monopolar spindles with erroneous kinetochore-microtubule attachment. After release from monastrol, the cells were arrested at metaphase with MG132, and cells with unaligned chromosomes were scored (Lampson MA et al., 2004) (Figs. 33A-B). As a control for this error correction assay, I treated CENP-C^{WT} cells with AZD1152 (Yang J et

al., 2007), an Aurora B inhibitor, and confirmed an increase in cells with unaligned chromosomes 30 min after release (over 10% and 20% with 40 nM and 200 nM AZD1152, respectively), compared to the cells treated with DMSO (less than 10%) (Figs. 33A-B). This observation is consistent with previous reports, demonstrating that efficient error correction requires Aurora B (Lampson MA et al., 2004; Cimini D et al., 2006).

Next, I examined CENP-C$^{\Delta M12BD}$ cells and found that the cells with unaligned chromosomes (>2 unaligned) were significantly increased to ~20% 30 min after release from monastrol (Figs. 33A-B), and response the Aurora B inhibitor (Fig. 33B), suggesting that error correction was less efficient in CENP-C$^{\Delta M12BD}$ cells and that M12BD plays a role in mitotic error correction to facilitate bipolar attachment. In contrast, CENP-T$^{\Delta NBD-1}$ and CENP-T$^{\Delta NBD-2}$ cells exhibited error correction efficiencies equivalent to those in CENP-T^{WT} cells (Fig. 33C). This is consistent with the fact that the deletion of either NBD-1 or -2 did not alter the localization of centromeric Aurora B (Fig. 26B) In addition, the results implied that reduced K-fiber and Ndc80C levels did not affect error correction efficiency in this assay.

These results suggest that deletion of the M12BD of CENP-C diminishes error correction, possibly due to the reduction of Aurora B levels at centromeres, which is the primary cause of mitotic delay and chromosome segregation errors in CENP-C$^{\Delta M12BD}$ RPE-1 cells.

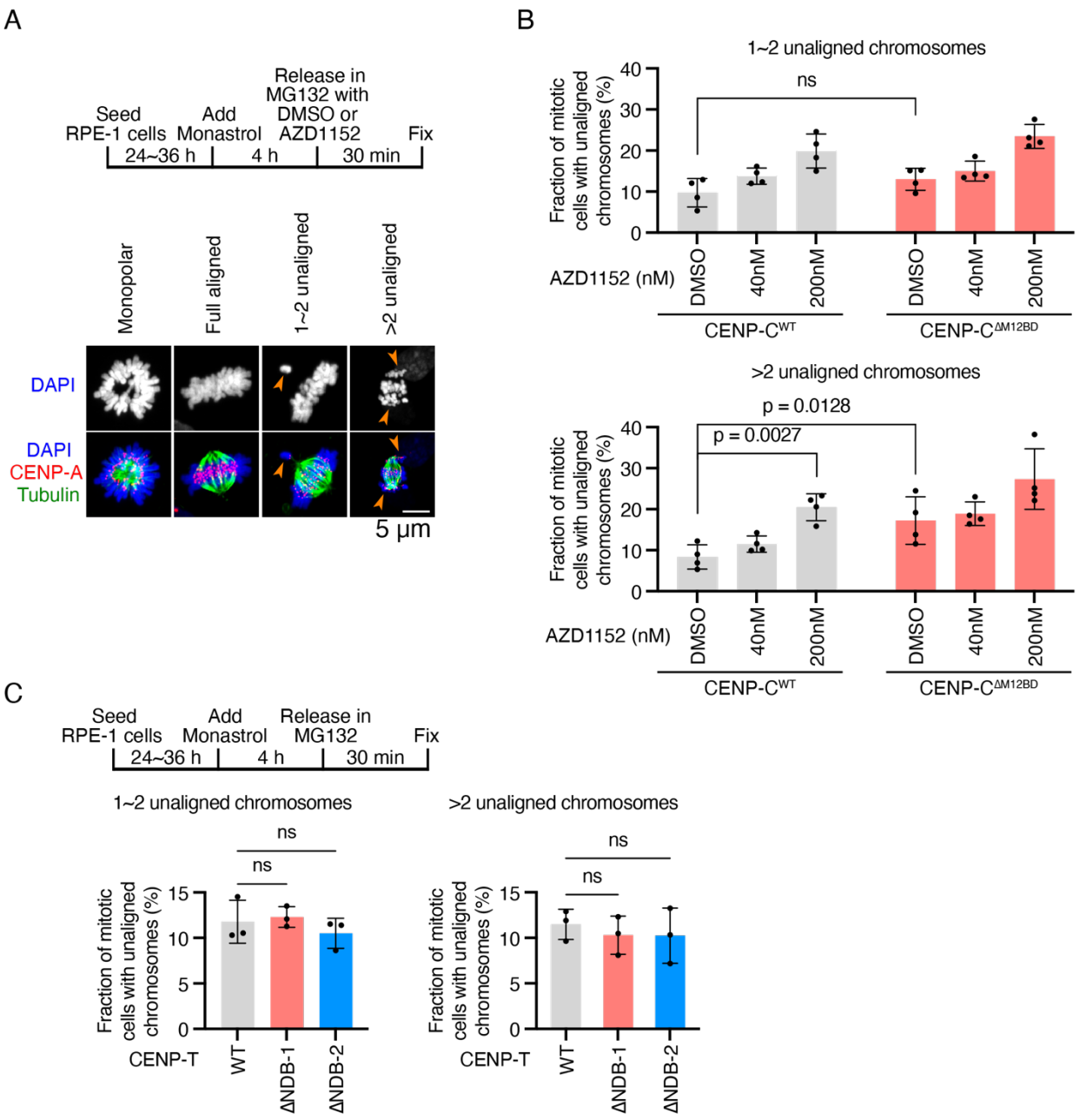

Figure.33 Deletion of Mis12C-binding domain of human CENP-C reduces kinetochore-microtubule error correction efficiency.

(A) Representative images of aligned or unaligned chromosomes. A monastrol-treated cell (monopolar), a cell with fully aligned chromosomes (fully aligned), and a cell with unaligned chromosomes (1~2 unaligned; > 2 unaligned). Arrows indicate unaligned chromosomes. Scale bar 5 μm. Mitotic cells with unaligned chromosomes were quantified.

(B) Error correction assay in CENP-C^{WT} or CENP-C$^{\Delta M12BD}$ cells. The cells were treated with monastrol for 4 h and then released and incubated in a medium with MG132 in the presence or absence of an Aurora B inhibitor (AZD1152 or DMSO) for 30 min. The cells were fixed, and microtubules (green) and DNA (blue) were stained with an antibody against alpha-tubulin and DAPI, respectively. mScarlet-CENP-A is a kinetochore marker (CENP-A, red). Four independent experiments were performed (Mean and SD, one-way ANOVA with Dunnett's multiple comparison test).

(C) Error correction assay in CENP-T^{WT}, CENP-T$^{\Delta NDB-1}$, or CENP-T$^{\Delta NDB-2}$ cells. The cells were treated with monastrol, released into a medium with MG132, and unaligned chromosomes were quantified as in (B). Three independent experiments were performed. (Mean and SD, one-way ANOVA with Dunnett's multiple comparison test).

4.3 Discussion

Deletion of the Mis12C binding region in CENP-C cells resulted in a significantly higher frequency of chromosomal mis-segregations, approximately five times in RPE-1 cells compared to control cells (Fig. 20C). This indicates a possible link to the defects of error correction system in cells with deletion of the Mis12C binding region in CENP-C. Error correction mechanisms are primarily mediated by Aurora B kinase (Cheeseman IM et al., 2006; DeLuca JG et al., 2006, 2011; Wimbish RT et al., 2020). To investigate the connection between the CENP-C-Mis12C interaction and Aurora B localization, I analyzed Aurora B signals in mitotic cells. Although the localization in CENP-C$^{\Delta M12BD}$ cells was unchanged within the inner-centromere, similar to CENP-C^{WT}, the signal intensity was notably reduced. Aurora B is indirectly recruited to the centromere via association with two phospho-histone markers, H2AT120ph and H3T3ph, which are substrates of Bub1 and Haspin, respectively (Watanabe Y, 2010; Wang F et al., 2011). In CENP-C$^{\Delta M12BD}$ cells, H2AT120ph levels associated with Bub1 were diminished, while H3T3ph levels remained unchanged. This reduction may be attributed to decreased KNL1C localization at kinetochores, which serve as docking sites for Bub1, whereas Haspin localization at cohesion was not affected. This inference was also confirmed as either Bub1-H2AT120ph-Aurora B or H3T3ph levels in CENP-T ΔNBD-1 or ΔNBD-2 cells were

comparable to those in WT cells. It is important to note that Bub1 is involved in recruiting spindle checkpoint components during early prometaphase. This suggests that a reduction in Bub1 may impact SAC functionality and requires further evaluation (Musacchio A, 2015; Lara-Gonzalez P et al., 2021).

To assess the extent of Aurora B reduction in CENP-C$^{\Delta M12BD}$ cells, I quantified the amplitude of chromosome oscillation and error correction efficiency. Alanine mutations at the phosphorylation sites of Hec1 (Hec1^{9A}) by Aurora B can stabilize kinetochore-microtubule attachments, leading to increased erroneous attachments (DeLuca KF et al., 2011). DAP was primarily attenuated due to changes in microtubule dynamics from Aurora B reduction rather than k-fiber reduction, although DAP could be alleviated by nocodazole treatment. Because the previous section discussing microtubule dynamics in CENP-T ΔNBD-1 or ΔNBD-2 cells may exhibit no significant changes. DAP was comparable in CENP-T ΔNBD-1 or ΔNBD-2 cells to WT cells, supporting this conclusion. The error correction capability demonstrated a notable impairment, nearly 2-fold the incidence of unaligned chromosomes (>2 unaligned chromosomes) in CENP-C$^{\Delta M12BD}$ cells after release from monastrol for 30min.

These results indicate that the prolonged duration at prometaphase and the elevated rate of mis-segregation are linked to the deficiency of Aurora B observed in cells lacking the mis12C-binding region of CENP-C. Moreover, particularly in mouse models, micronuclei formation resulting from mis-segregation could induce DNA damage and chromosome instability, consequently diminishing fitness in the environment and weakening resistance to cancer induction (Fig. 17).

The binding affinity between Mis12C and CENP-C is modulated through phosphorylation of DSN1 at S100 and S109 by Aurora B as reported (Petrovic A et al., 2010; Hara M et al., 2018), suggesting a positive regulatory feedback loop involving Aurora B via the CENP-C-Mis12C interaction.

Chapter 5: The Interaction of CENP-C-Mis12C Establish a Positive Regulation Loop of Aurora B

5.1 Introduction

Aurora B mediates the binding affinity of Mis12C and CENP-C through phosphorylation of the S100 and S109 residues of DSN1 (Petrovic A et al., 2010; Hara M et al., 2018). Along with previous results have shown that disruption of the CENP-C-Mis12C interaction contributes to the attenuation of Aurora B (Fig. 26A), suggesting a positive regulatory loop for Aurora B localization via the CENP-C-Mis12C interaction. Promoting the localization of Aurora B facilitates the bi-orientation of chromosomes. To confirm this positive regulatory loop, HeLa cells, which exhibit lower Aurora B activity compared to RPE-1 cells (Abe Y et al., 2016), could serve as a potential cell model for study. Enhancing the binding affinity might increase the correction capability through facilitate the localization of Aurora B at inner-centromere.

Deletion of the basic motif of DSN1, which contains S100 and S109, forces the binding of Mis12C to CENP-C (Petrovic A et al., 2016; Hara M et al., 2018). Using the DSN1$^{\Delta\text{Basic motif}}$ cell model (kindly provided by Mr. Miao in my Lab), I examined Aurora B levels and the error correction activity.

5.2 Results

5.2.1 Generation of DSN1$^{\Delta\text{Basic motif}}$ HeLa cells

The basic motif within DSN1 exerts an inhibitory effect on the binding of CENP-C to Mis12C, as previously reported (Petrovic A et al., 2016; Hara M et al., 2018). Removal of this basic motif from DSN1 is anticipated to enhance the recruitment of the KMN network to kinetochores and facilitate chromosome bio-orientation by enhancing Aurora B localization. To explore this proposed positive regulatory loop, a HeLa cell line expressing a DSN1 mutant lacking the basic motif from the endogenous *DSN1* locus was generated (referred to as DSN1$^{\Delta\text{Basic motif}}$ cells; Fig. 34) firstly. Additionally, cells

expressing wild-type (WT) DSN1 were generated as a control group (referred to as DSN1^{WT} cells).

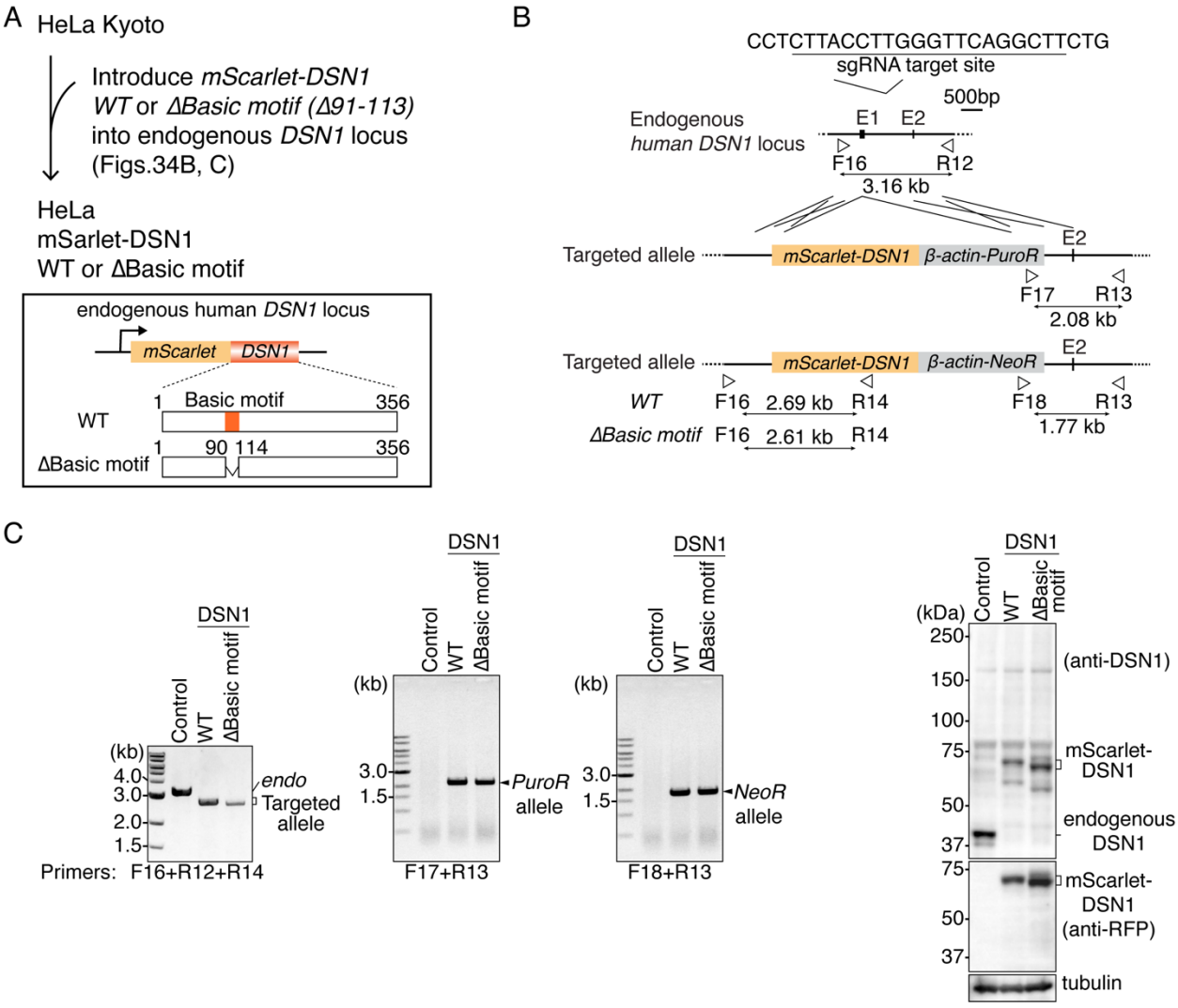

Figure.34 Construction of DSN1$^{\Delta Basic\ motif}$ HeLa cells.

(A) Strategy to generate DSN1^{WT} or DSN1$^{\Delta Basic\ motif}$ HeLa cells. (See also Figure 7A).

(B) Schematic representation of *mScarlet-DSN1* cDNA targeting the endogenous *DSN1* locus. To express mScarlet-tagged DSN1 wiled-type (WT) or a basic motif deletion mutant (ΔBasic motif: Δ91-113) under the control of the endogenous *DSN1* promoter, *mScarlet-DSN1 WT* or *ΔBasic motif,* cDNA was targeted into *DSN1 locus* by CRISPR/Cas9-mediated homologous recombination. Since the targeting constructs

have puromycin resistance genes (*PuroR*) or neomycin resistance genes (*NeoR*), targeted cells were selected using these selection markers. The gRNA sequence and position of primers for genotyping are shown.

(C) Genotyping PCR and immunoblotting for mScarlet-DSN1 in *mScarlet-DSN1*-introduced HeLa cells. The genotype in isolated single clones was examined using the primers shown in (B). In immunoblots, DSN1 was detected by an antibody against DSN1 or mScarlet (RFP), and α-tubulin was probed as a loading control.

The next, by immunostaining, Mis12C (DSN1) levels at kinetochores, as well as KNL1C (KNL1) and Ndc80C (Hec1) levels, were increased in DSN1$^{\Delta Basic\ motif}$ cells compared with those in DSN1^{WT} cells (Fig. 35), indicating that a stable CENP-C-Mis12C interaction occurred in Dsn1$^{\Delta Basic\ motif}$ cells.

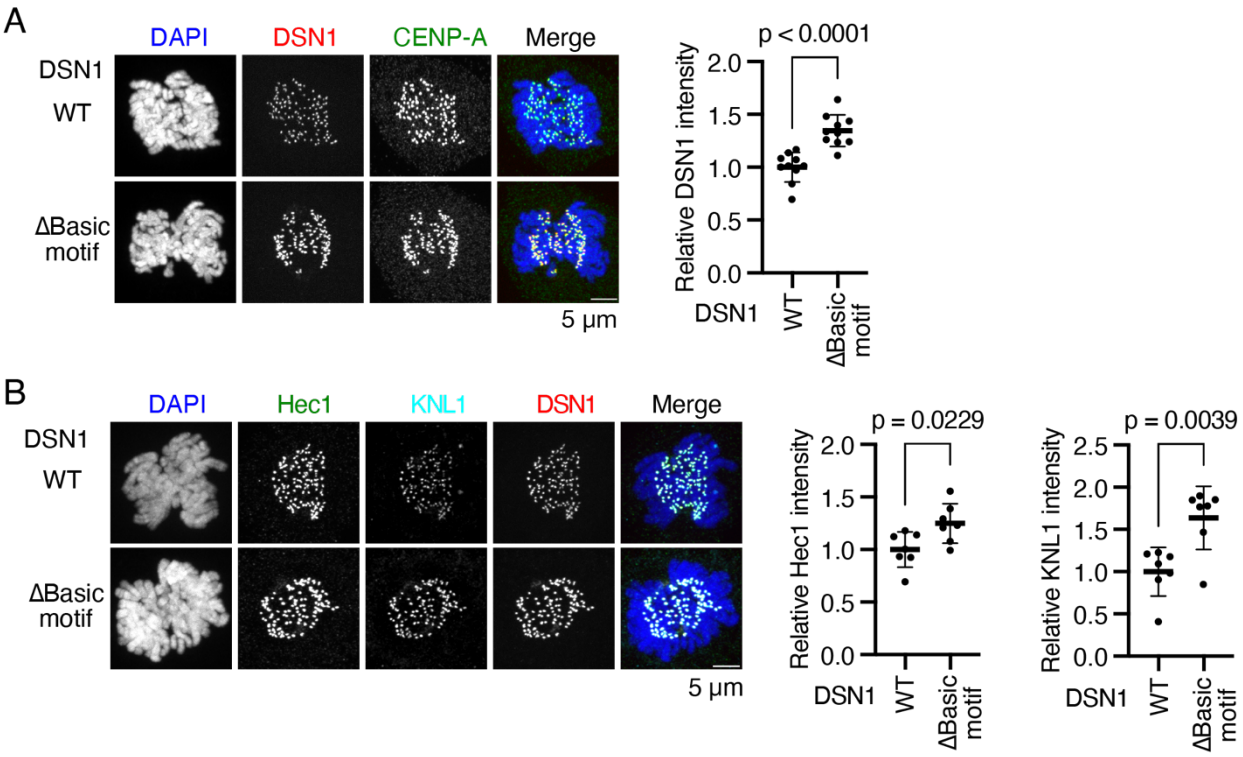

Figure.35 Phenotypes of DSN1$^{\Delta Basic\ motif}$ HeLa cells.

(A) DSN1 localization in DSN1^{WT} or DSN1$^{\Delta Basic\ motif}$ HeLa cells. DSN1, a subunit of the Mis12 complex, was stained with an antibody against DSN1 (red). DNA was stained with DAPI (blue). CENP-A was stained by an antibody against CENP-A as a kinetochore marker (green). Scale bar, 5 μm. DSN1 signal intensities at mitotic kinetochores were quantified (Mean and SD, two-tailed Student's t-test, DSN1^{WT}: n = 10 cells, DSN1$^{\Delta Basic\ motif}$: n = 10 cells).

(B) Hec1 and KNL1 localization in DSN1^{WT} or DSN1$^{\Delta Basic\ motif}$ HeLa cells. Hec1, a subunit of the Ndc80C (green), and KNL1, a subunit of the KNL1C (cyan), were stained with antibodies against Hec1 and KNL1, respectively. mScarlet-DSN1 is a kinetochore marker (DSN1, red). DNA was stained with DAPI (blue). Scale bar, 5 μm. Hec1 or KNL1 signal intensities at mitotic kinetochores were quantified. A representative result from two independent experiments is shown (Mean and SD, two-tailed Student's t-test, DSN1^{WT}: n = 7, DSN1$^{\Delta Basic\ motif}$: n = 7).

5.2.2 Increased the localization of Aurora B in DSN1$^{\Delta Basic\ motif}$ HeLa cells

HeLa cells, a cancer-derived cell line characterized by chromosomal instability and diminished Aurora B activity at mitotic centromeres (Fig. 36A) (Abe Y et al., 2016). It was hypothesized that enhancing Mis12C binding to CENP-C would aid in the localization of Aurora B levels through Bub1, which is known to localize at KNL1, considering the observed rise in kinetochore intensity of KNL1 (Fig. 35B). Upon immunostaining assessment, it was observed that both the signal intensity of Bub1 and its substrate, H2AT120ph, exhibited a significant increase when compared to the control cells (Fig. 36B-C). As anticipated, in chromosome spreads of DSN1$^{\Delta Basic\ motif}$ HeLa cells, Aurora B levels were elevated at inner-centromeres (Fig. 36C).

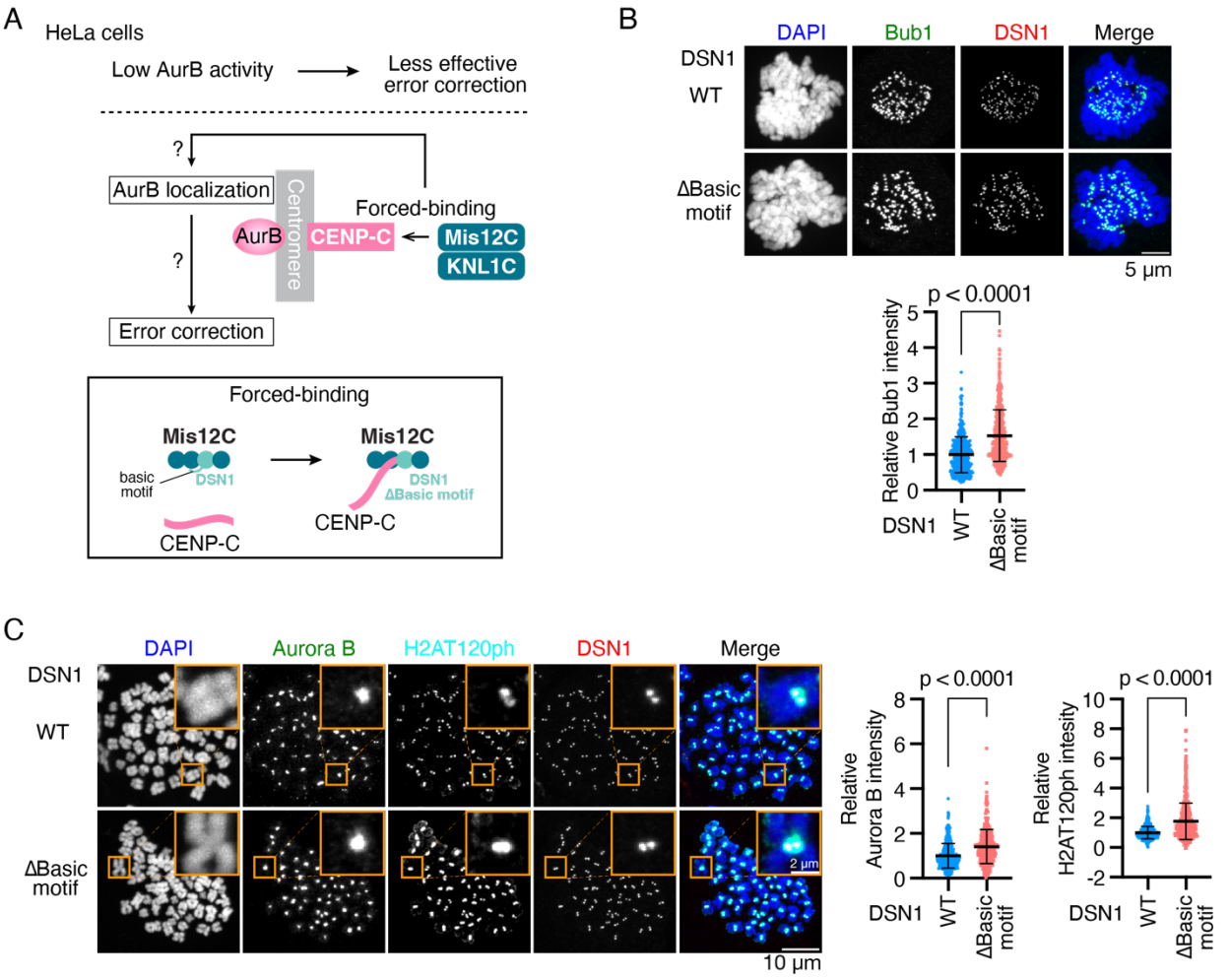

Figure.36 Bub1-H2AT120ph-Aurora B localization at centromeres in HeLa cells.

(A) Schematic representation for forced binding of Mis12C to CENP-C in HeLa cells. To validate the idea that the CENP-C-Mis12C interaction positively regulates Aurora B localization, we utilized HeLa cells in which Aurora B activity is low at centromeres, leading to chromosome instability. The CENP-C-Mis12C interaction was increased by expressing a DSN1 mutant lacking the basic motif (ΔBasic motif) in HeLa cells and examined the Aurora B levels and efficiency of kinetochore-microtubule error correction. Dsn1 is a subunit of Mis12C. The basic motif of DSN1 masks the CENP-C-binding surface of Mis12C, preventing the CENP-C-Mis12C interaction. The deletion of the basic motif increases the binding affinity between CENP-C and Mis12C (Petrovic A et al., 2016).

(B) Bub1 localization in DSN1^{WT} or DSN1$^{\Delta Basic\ motif}$ HeLa cells. Bub1 was stained with an antibody against Bub1 (green). DSN1 was stained as a kinetochore marker (red). DNA was stained with DAPI (blue). Scale bar, 5 μm. Bub1 signal intensities at kinetochores were quantified (Mean and SD, two-tailed Student's t-test, DSN1-C^{WT}: n = 523 kinetochores from 6 cells, DSN1$^{\Delta Basic\ motif}$: n = 501 kinetochores from 6 cells).

(C) Aurora B and H2AT120ph localization in DSN1^{WT} or DSN1$^{\Delta Basic\ motif}$ HeLa cells. Aurora B and H2AT120ph were stained with their antibodies (green and cyan). mScarlet-DSN1 is a kinetochore marker (DSN1, red). DNA was stained with DAPI (blue). Scale bar, 10 μm. The insets show an enlarged single chromosome (Scale bar, 2 μm). The signal intensities of Aurora B at centromeres and H2AT120ph at kinetochore-proximal centromeres were quantified (Mean and SD, two-tailed Student's t-test, DSN1-C^{WT}: n = 385 centromeres, 651 kinetochores from 6 cells for Aurora B, H2AT120ph, respectively, DSN1$^{\Delta Basic\ motif}$: n = 379 centromeres, 668 kinetochores from 6 cells for Aurora B, H2AT120ph, respectively).

5.2.3 Increased error correction efficiency in DSN1$^{\Delta Basic\ motif}$ HeLa cells

Forced binding of Mis12C to CENP-C markedly increased the centromeric localization of Aurora B, Bub1, and H2AT120ph in DSN1ΔBasic motif cells (Figs. 36B and C). To assess error correction, I conducted a monastrol washout assay on DSN1$^{\Delta Basic\ motif}$ HeLa cells and observed enhanced error correction efficiency (Fig. 37A). Cells were treated with 50 μM monastrol for 4 hours, followed by release into MG132 for 30 or 45 minutes (Fig. 37A). The proportion of cells with >2 unaligned chromosomes decreased by approximately 7.3% after 30 minutes of release from monastrol (Fig. 37A). DSN1^{WT} HeLa cells required 45 minutes to achieve approximately 90% bipolar attachment, whereas CENP-C^{WT} RPE-1 cells required only 30 minutes. Notably, at 45 minutes, DSN1$^{\Delta Basic\ motif}$ cells also showed reduced rates of cells with misaligned chromosomes. Quantification revealed no decrease in the frequency of cells with 1~2 unaligned

chromosomes in DSN1$^{\Delta basic\ motif}$ after 30 or 45 minutes of release (Fig. 37A). These results suggest that enforced binding of CENP-C to Mis12C promotes chromosome alignment at the mitotic plate.

In summary, the forced binding of Mis12C to CENP-C enhances centromeric localization of Aurora B and improves error correction efficiency in HeLa cells, supporting a positive regulatory loop between Aurora B recruitment and the CENP-C-Mis12C interaction.

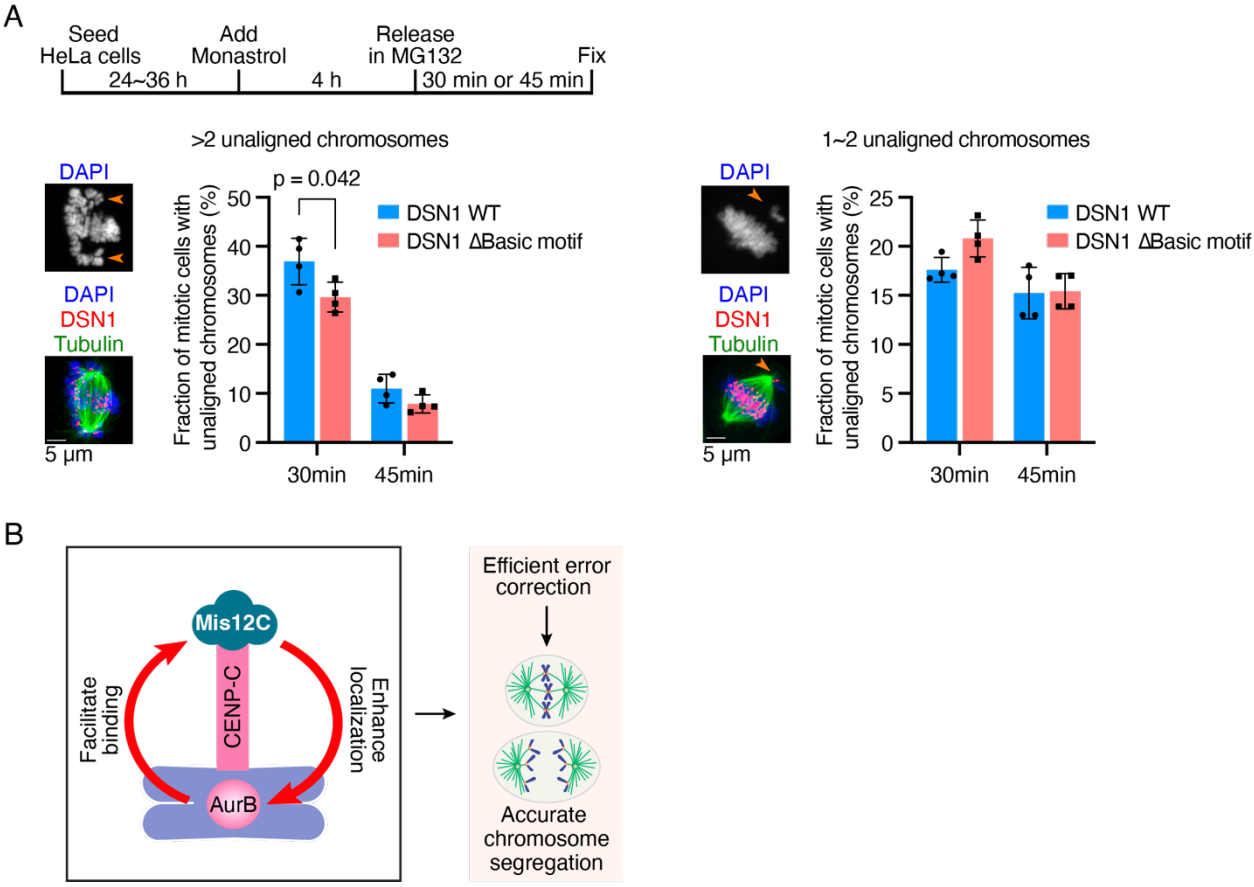

Figure.37 Increased error correction efficiency in DSN1$^{\Delta Basic\ motif}$ HeLa cells.

(A) Error correction assay in DSN1^{WT} or DSN1$^{\Delta Basic\ motif}$ HeLa cells. The cells were treated with monastrol for 4 h and then released and incubated in a medium with MG132 for 30 or 45 min. The cells were fixed, and microtubules (green) and DNA (blue) were stained with an antibody against alpha-tubulin and DAPI, respectively. mScarlet-DSN1 is a kinetochore marker (DSN1, red). Arrows indicate unaligned chromosomes.

Scale bar 5 μm. Mitotic cells with unaligned chromosomes were quantified. Four independent experiments were performed (Mean and SD, two-tailed Student's t-test).

(B) Model for a positive regulatory loop to facilitate Aurora B localization at the centromere through the CENP-C-Mis12C interaction. The regulatory system is required for efficient error correction of kinetochore-microtubule attachment, leading to accurate chromosome segregation.

5.3 Discussion

Aurora B is crucial for facilitating the binding of Mis12C to CENP-C and for mediating error correction during prometaphase (Klein UR et al., 2006; Carmena M et al., 2012; Kelly AE et al., 2010; DeLuca KF et al., 2011; Petrovic A et al., 2016; Hindriksen S et al., 2017; Hara M et al., 2018). A previous study has shown that Aurora B is enriched at unattached kinetochores and corresponds with an increased signal of its target, DSN1 S100 phosphorylation, in RPE-1 cells (Salimian KJ et al., 2011). However, a comprehensive model explaining the regulatory mechanisms of CCAN, KMN, and the error correction system is lacking. In this study, I focus on the interaction between CENP-C and Mis12C, providing insights into the regulatory mechanism of Aurora B, a key regulator for error correction.

Based on previous results and my study, I propose a positive feedback loop: at unaligned or mis-attached chromosomes, Aurora B phosphorylates DSN1 to promote the CENP-C-Mis12C interaction, which in turn enhances Aurora B localization at the centromere. Aurora B correct erroneous kinetochore-microtubule (KT-MT) attachments, through phosphorylate its substrate Ndc80/Hec1 as reported (Tanaka K et al., 2009; DeLuca KF et al., 2011; Banerjee A et al., 2020). When KT-MT achieves bi-orientation, the phosphorylation levels of substrates like DSN1 and Ndc80/Hec1 decrease (Salimian KJ et al., 2011; DeLuca KF et al., 2011), thereby alleviating the positive feedback loop of Aurora B at the centromere and allowing faithful chromosome segregation (Fig. 37B).

Additionally, as Bub1 also plays a role in spindle checkpoint assembly, the CENP-C-Mis12C interaction might take a part in spindle checkpoint functionality; however, this was not explored in the current study.

CENP-T also recruits Mis12C and KNL1C to the kinetochore in the presence of CDK1 or Aurora B (Huis In 't Veld PJ et al., 2016; Walstein K et al., 2021), suggesting that the CENP-T-Mis12C interaction may also be involved in the regulation of Aurora B enrichment at the centromere. However, the CENP-C-Mis12C interaction likely plays a dominant role in the positive feedback loop, as the binding of Mis12C to CENP-T primarily depends on CDK1 kinase activity. The residue S201 of CENP-T, a CDK1 phosphorylation site, when mutated to alanine, decreases Mis12C recruitment to CENP-T by ~80% (Huis In 't Veld PJ et al., 2016). Furthermore, CENP-C acts as the major scaffold for recruiting Mis12C during prometaphase, the phase responsible for error correction (Hara M et al., 2018). Nevertheless, further analyses are necessary to clarify whether the CENP-C-Mis12C and CENP-T-Mis12C interactions have distinct roles.

In addition, enforcing the binding of CENP-C-Mis12C improves error correction efficiency in DSN1$^{\Delta\text{Basic motif}}$ HeLa cells, but this efficiency is still lower than in RPE-1 cells. DSN1$^{\Delta\text{Basic motif}}$ HeLa cells achieve ~77% bipolar attachment in 45 minutes, while CENP-C^{WT} RPE-1 cells achieve ~82% in just 30 minutes after release from monastrol. It was known that full activation of Aurora B kinase requires binding of the heterochromatin protein HP1 at mitotic centromeres, and this regulatory mechanism is impaired in cancer cells (Abe Y et al., 2016). This indicates that effective error correction requires not only an adequate presence of Aurora B at the centromeres but also the maximum activity of Aurora B mediated by HP1.

Kinetochore protein assembly and error correction system are well studied currently, therefore there are possible other factors involved in the feedback loop of CENP-C-Mis12C and Aurora B recruitment. A deeper understanding of how these regulatory mechanisms are integrated will shed light on the dynamic regulatory systems of centromeres/kinetochores to ensure accurate chromosome segregation, potentially providing targets for cancer therapy.

Appendix: A Co-Effector of Mis12C Binding Domain of CENP-C

1.1 Introduction

To gain a deeper understanding of the factors involved in the CENP-C-Mis12C interaction, my colleague Miao Jiahang identified kinesin-8A (Kif18A) as a potential protein that is genetically related with the CENP-C-Mis12 interaction by a CRISPR screening. I'd like to further characterize the role of Kif18A in CENP-C$^{\Delta M12BD}$ cells to assess its significance.

Kif18A is a member of kinesin-8 motor family (Luboshits G et al., 2005; Messin LJ et al., 2014). Human Kif18A comprises several functional domains: a motor domain at the N-terminus, followed by a neck linker and coiled-coil region, and a nuclear localization motif at the C-terminus, as revealed by structural analysis (Peters C et al., 2010; Lin Y et al., 2020). Kif18A functions by moving along microtubules and accumulating at their plus-ends. It acts as a weak depolymerase at early prometaphase, thereby regulating microtubule dynamics and mediate chromosome congression, while stable the kinetochore-microtubule attachment by suppressing chromosome oscillation at the metaphase plate before anaphase transition (Mayr MI et al., 2007; Stumpff J et al., 2008; Varga V et al., 2009). Turnover of 'destablizing' to 'stablizing' fuction is still illusive, possibly depend on Kif18A position, cencentration, and the timing of cell cycle regulated by CDK1 and PP1 (Häfner J et al., 2014). Additionally, Kif18A directly interacts with CENP-E and BubR1, and knockdown of Kif18A leads to mitotic arrest in human cells (Huang Y et al., 2009). The multifaceted roles of Kif18A throughout the cell cycle have been extensively reviewed by Lin et al (Lin Y et al., 2020). Of particular interest, recent studies suggest that while Kif18A is dispensable for diploid somatic cells, it plays an essential role in cells exhibiting chromosome instability (Marquis C et al., 2021; Quinton RJ et al., 2021). Although numerous experiments have elucidated the role of Kif18A during mitosis, the underlying reasons for the specific dependence of chromosome instability (CIN) cancer cells on Kif18A for proliferation remain unclear. I

aim to assess the sensitivity of Kif18A in the CENP-C$^{\Delta M12BD}$ RPE-1 cell model and highlight the potential regulatory mechanisms involved.

1.2 Results

1.2.1 Kif18A loss is lethal for CENP-C$^{\Delta M12BD}$ RPE-1 cells

CIN cells characterized by frequently chromosome gain or loss, such as HeLa cells, with proliferation depend on Kif18A (Marquis C et al., 2021). Although CENP-C$^{\Delta M12BD}$ RPE-1 cells did not represent significant alterations in DNA content via flow cytometry analysis, micronuclei formation could induce DNA damage and subtle nucleotide changes or chromosomal translocations in progeny cells (Janssen A et al., 2011; Santaguida S et al., 2015). Consequently, I hypothesize that diploid cells undergoing aberrant cell division may also exhibit sensitivity to loss of Kif18A. To test this hypothesis, a viability assay was conducted in Kif18A knock-down CENP-C^{WT} or CENP-C$^{\Delta M12BD}$ cells. The results indicated that only CENP-C$^{\Delta M12BD}$ cells demonstrated sensitivity to Kif18A knock-down (Fig. 38A).

Furthermore, to evaluate the potential molecular mechanisms associated with sensitivity to Kif18A loss, Kif18A was knocked down in CENP-T ΔNBD-1 or ΔNBD-2 cells. In contrast to CENP-C$^{\Delta M12BD}$ cells, the viability of mutant CENP-T cells was equivalent to that of CENP-T WT cells (Fig. 38B). The viability quantification results in CENP-T cell lines suggest that Kif18A function may be linked to the CENP-C-Mis12C interaction-mediated Aurora B localization feedback loop or the Aurora B-mediated error correction system. This is because Aurora B is deficient in CENP-C$^{\Delta M12BD}$ cells but not in CENP-T$^{\Delta NBD-1}$ or CENP-T$^{\Delta NBD-2}$ cells, and its localization is positively regulated by the CENP-C-Mis12C interaction.

Additionally, mutant CENP-T cell lines did not exhibit abnormal cell division compared with control cells (Fig. 25), though relatively higher than CENP-C WT (Fig. 20C), possible because of DNA dye toxic (Sen O et al., 2018). Thus, the viability quantification result of CENP-T cell lines also confirmed the hypothesis.

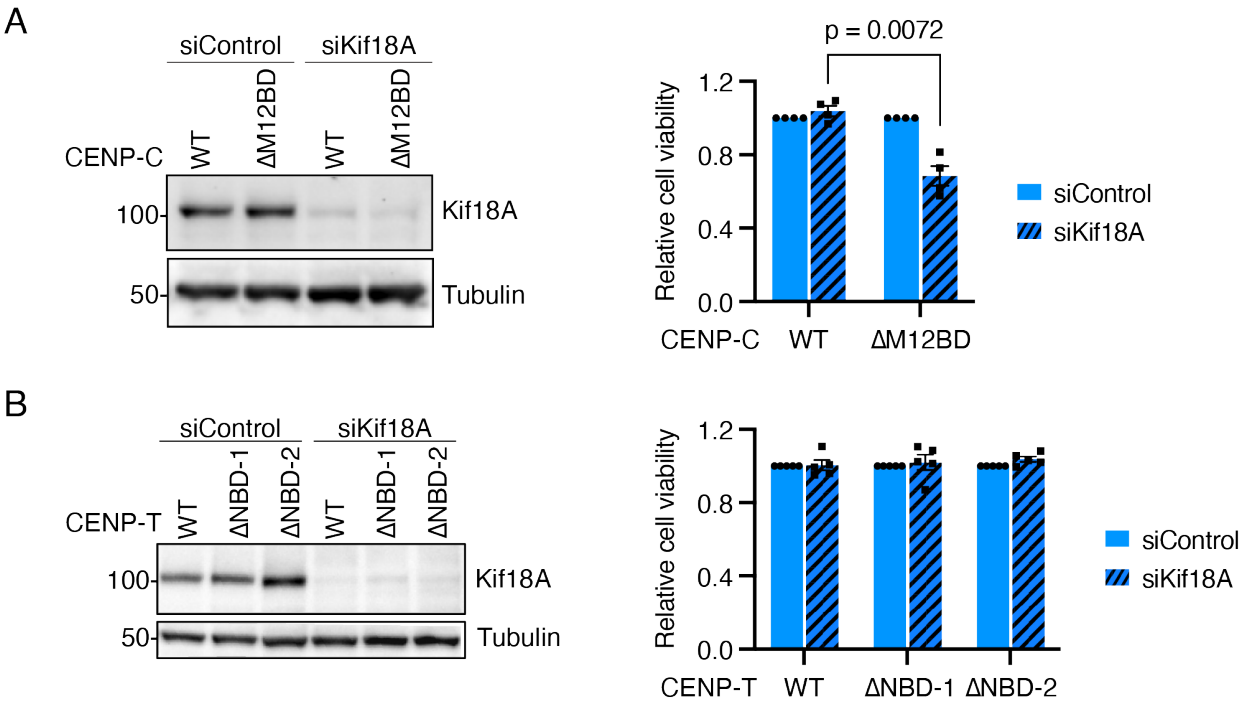

Figure.38 Viability of CENP-C$^{\Delta M12BD}$ RPE-1 cells was sensitive for Kif18A knock-down.

(A) Quantification of cell viability was conducted after transfection of control siRNA (siControl) or Kif18A siRNA (siKif18A) in CENP-C^{WT} or CENP-C$^{\Delta M12BD}$ cells for three days. Four independent experiments were performed (Right, Mean and SD, two-tailed Student's t-test). Protein level analysis by Immunoblot (Left). Kif18A was detected by an antibody against Kif18A, and α-tubulin was probed as a loading control.

(B) Quantification of cell viability was conducted after transfection of siControl or siKif18A in CENP-T^{WT}, CENP-T$^{\Delta NBD-1}$, or CENP-T$^{\Delta NBD-2}$ RPE-1 cells for three days. Five independent experiments were conducted (Right). Protein level analysis by Immunoblot (Left). Kif18A was detected by an antibody against Kif18A, and α-tubulin was probed as a loading control.

1.2.2 The combination of low-dose nocodazole and Kif18A knockdown synergistically reduces the viability of CENP-C$^{\Delta M12BD}$ RPE-1 cells

Kif18A plays a dual role in modulating microtubule dynamics throughout mitotic progression, influencing chromosome alignment by impeding microtubule polymerization during early prometaphase and restraining chromosome oscillation at the metaphase plate before the anaphase transition (Mayr MI et al., 2007; Stumpff J et al., 2008). To demonstrate the temporal involvement of Kif18A in CENP-C$^{\Delta M12BD}$ cells, supplementation with low-dose nocodazole, which exerted no discernible effect on cell viability (Fig. 39A). The administration of low-dose nocodazole (5 ng/ml) allowed chromosome alignment but dampened chromosome oscillation, as depicted in prior result (Fig. 32). Combining low-dose nocodazole with Kif18A knockdown resulted in a synergistically negative impact on the viability of CENP-C$^{\Delta M12BD}$ cells (Fig. 39A). This observation suggests that the absence of Kif18A leads to microtubule hyperstabilization, thereby impeding proper chromosome alignment in Kif18A-sensitive cells. Moreover, this effect was enhanced by dosage escalation (Fig. 38B).

A

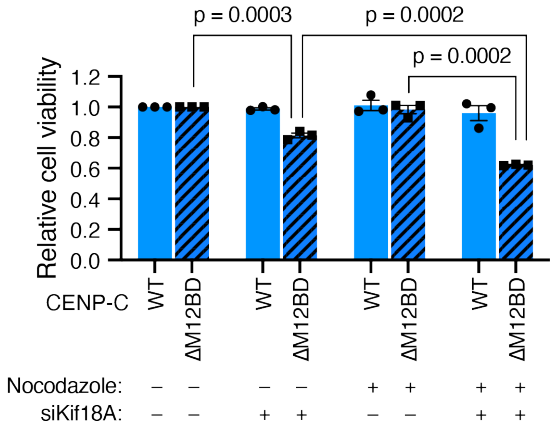

B

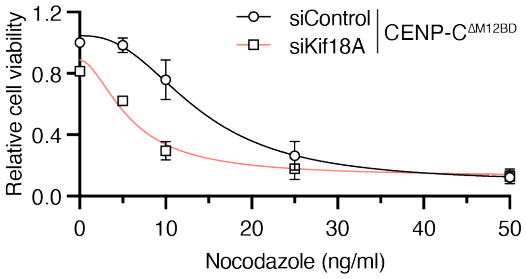

Figure.39 Viability assay for CENP-C$^{\Delta M12BD}$ cells with administration of nocodazole and siKif18A combination.

(A) Quantification of cell viability was conducted after transfection of siControl or siKif18A for three days with or without nocodazole in CENP-C^{WT} or CENP-C$^{\Delta M12BD}$ RPE-1 cells. The concentration of nocodazole was 0 ng/ml (DMSO, －) or 5 ng/ml (+) (upper lane). siControl (-) or siKif18A (+) (lower lane). Three independent experiments were performed for each group (Mean and SD, two-tailed Student's t-test).

(B) Quantification of cell viability was conducted in CENP-C$^{\Delta M12BD}$ cells after transfection with siControl or siKif18A for three days in the presence of nocodazole. Nocodazole concentration was 0, 5, 10, 25, 50 ng/ml. Three independent experiments were carried out for each group (Mean and SD).

1.2.3 Kif18A loss cause severe mitotic defects in CENP-C$^{\Delta M12BD}$ RPE-1 cells

Kif18A knockdown can reduce the turnover of microtubules at prometaphase, and also the SAC activation (Mayr MI et al., 2007; Janssen LME et al., 2018). Additionally, the previously observed result that reduced efficiency of Aurora B-mediated error correction in CENP-C$^{\Delta M12BD}$ cells, these facts likely accelerates the level of mitotic defects and contributes to the increased lethality associated with Kif18A depletion. Live-cell imaging analysis revealed that the loss of Kif18A extended the duration of mitosis in both CENP-C^{WT} and CENP-C$^{\Delta M12BD}$ cells, increasing from approximately 23 minutes and 27.8 minutes to about 30.5 minutes and 37 minutes, respectively (Fig. 40A-B). However, approximately 11.8% of CENP-C$^{\Delta M12BD}$ cells took from 1 to 2.3 hours to enter anaphase, compared to only around 3.1% of CENP-C^{WT} cells taking 1 to 1.2 hours (Fig. 40B). Furthermore, about 7.3% of CENP-C$^{\Delta M12BD}$ cells were arrested for over 3.3 hours

without exiting before imaging stopped (Fig. 40C). The loss of Kif18A in CENP-C$^{\Delta M12BD}$ results in a higher frequency of cell arrest for an extended duration.

Moreover, knockdown of Kif18A in CENP-C$^{\Delta M12BD}$ cells, compared to either siControl transfection or CENP-C^{WT} cells with Kif18A knockdown, showed significantly greater mitotic defects, including misaligned, lagging, and bridge chromosomes (Fig. 40C). Taken together with viability assay results, the prolonged mitotic duration and high frequency of segregation errors contribute to the lethality observed in CENP-C$^{\Delta M12BD}$ cells with Kif18A knockdown (Fig. 38A).

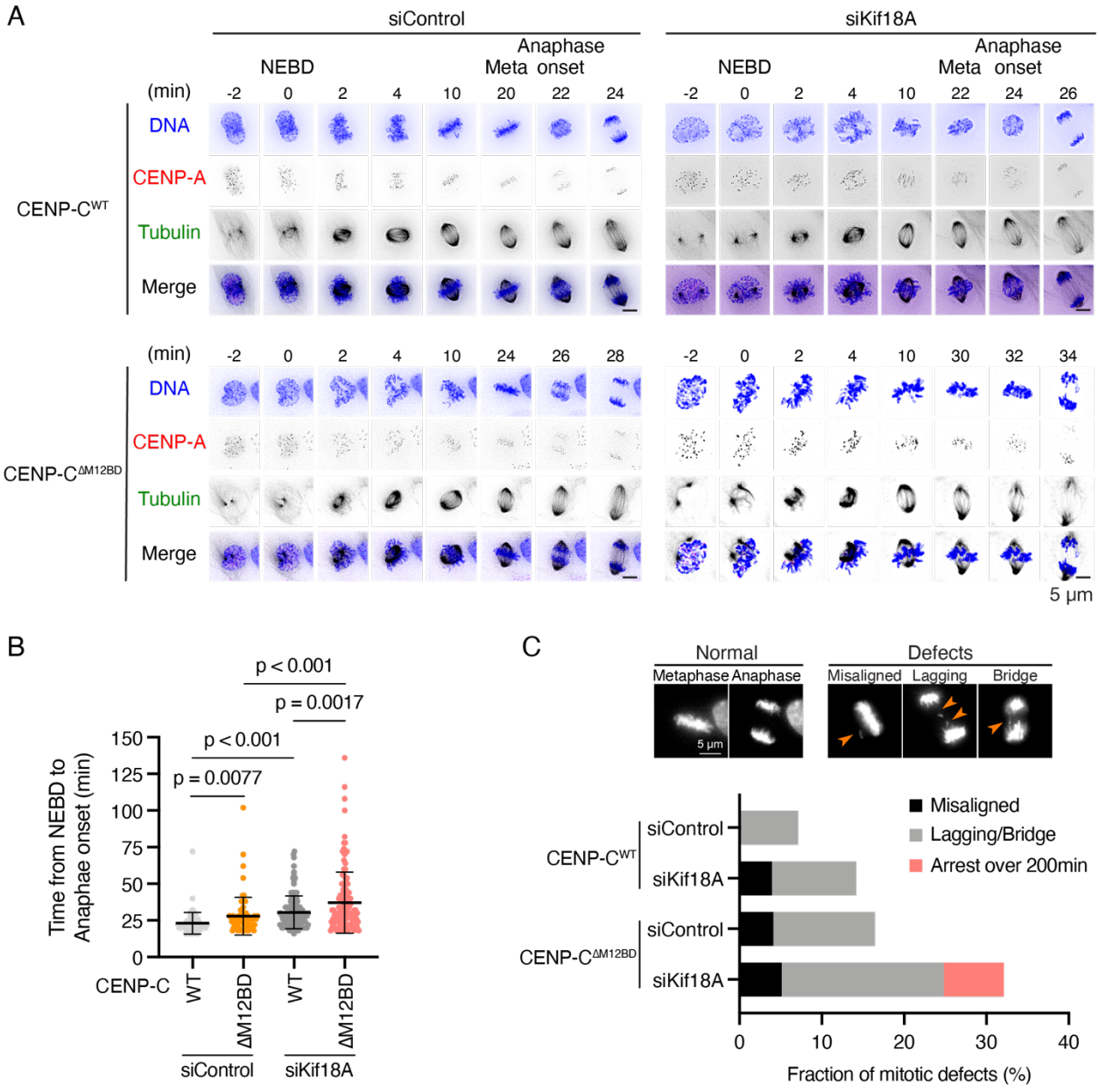

Figure.40 Knock-down Kif18A result in severe mitotic defects in CENP-C$^{\Delta M12BD}$ RPE-1 cells.

(A) Representative time-lapse images of mitotic progression in CENP-C^{WT} or CENP-C$^{\Delta M12BD}$ cells with siControl or siKif18A transfection. DNA was visualized with GFP-H2A. CENP-A was fused with mScarlet. Tubulin was stained by SirTubulin650. Images were projected using maximum intensity projection and deconvoluted. Time is relative to nuclear envelope breakdown (NEBD). Scale bar, 5 μm.

(B) Mitotic duration from NEBD to anaphase onset in CENP-C^{WT} or CENP-C$^{\Delta M12BD}$ cells with Kif18A knock-down. The time-lapse images were analyzed to measure the time from NEBD to anaphase onset. siControl or siKif18A transfection in CENP-C^{WT} or CENP-C$^{\Delta M12BD}$ cells were tested (Mean and SD, two-tailed Student's t-test, CENP-C^{WT} with siControl: n = 70, CENP-C^{WT} with siKif18A: n = 127, CENP-C$^{\Delta M12BD}$ with siControl: n = 73, CENP-C$^{\Delta M12BD}$ with siKif18A: n = 127).

(C) Frequency of mitotic defects in CENP-C^{WT} or CENP-C$^{\Delta M12BD}$ cells with Kif18A knock-dwon. The unaligned, lagging chromosomes and chromosome bridges during anaphase in the cells analyzed in (B) were scored. Representative images are shown. Scale bar 5 μm.

1.3 Discussion

Kif18A is considered a marker for CIN (chromosomal instability) cells because it is dispensable for chromosome-stable cells, such as normal diploid cells (Marquis C et al., 2021; Quinton RJ et al., 2021). This study suggests that Kif18A could also be an indicator for cells exhibiting abnormal chromosome segregation induced by dampened Aurora B activity. In RPE-1 cells, the interaction between CENP-C and Mis12C is required for the recruitment of Aurora B to the centromere. Disruption of this interaction

(CENP-C$^{\Delta M12BD}$) results in longer mitotic timing (Figs. 20A-B) and a remarkably increase in the incidence of chromosome segregation errors (Fig. 20C) compared to control cells (CENP-C^{WT}). Furthermore, a subset of CENP-C$^{\Delta M12BD}$ cells is lethal upon Kif18A loss through viability assay (Fig. 38A), possibly due to prolonged mitotic arrest, inefficient chromosome alignment, and an accelerated frequency of chromosome segregation errors (Fig. 40).

The molecular mechanism by which Kif18A is required for proliferation in CIN cells is still under investigation, given Kif18A multifaceted role during mitotic progression (Mayr MI et al., 2007; Stumpff J et al., 2008; Varga V et al., 2009). Kif18A mediates chromosome congression by acting as a depolymerase at early prometaphase. When positioned at the plus-end of microtubules, it stabilizes the kinetochore-microtubule attachment by attenuating chromosome oscillation. This dual role is possibly regulated by CDK1 and PP1 (Häfner J et al., 2014). CDK1 phosphorylates Kif18A at S674 and S684, facilitating its depolymerase-like activity, while PP1 antagonizes this role to promote the formation of a thin spindle plate. Additionally, Kif18A physically interacts with CENP-E and BubR1 to stabilize their complex; deletion of Kif18A can shorten the half-life of CENP-E, leading to misalligned chromosome (Huang Y et al., 2009). There is evidence showing that Kif18A knockdown promotes the recruitment of Mad1-Mad2 to the kinetochore, activating the spindle checkpoint at kinetochroes (Janssen LME et al., 2018). However, these pieces of evidence do not fully explain why CIN cells specifically require Kif18A for cell growth.

One possible reason is that the consequences of Kif18A loss crosslink inefficient error correction, reinforcing mitotic defects. Kif18A functions in early prometaphase, mediating chromosome congression via regulation of microtubule dynamics and CENP-E or other factors (Mayr MI et al., 2007; Huang Y et al., 2009; Häfner J et al., 2014). Its deletion leads to reduced turnover of microtubules, which may contribute to increased mal-oriented chromosomes. However, CENP-C$^{\Delta M12BD}$ RPE-1 cells display lower efficiency of correcting erroneous attachments, result in a high frequency of lagging chromosomes due to dampened Aurora B at the centromere. Along with the spindle assembly checkpoint activation at tension-absent or tension-low kinetochores induced

by Kif18A loss, this result in a longer duration (Janssen LME et al., 2018; Lin Y et al., 2020). Consequently, the degradation of cyclin B may enable cells 'escape' from prolonged arrest accompnied by mis-segregation, leading them to undergo apoptosis or death (Brito DA et al., 2006; Gascoigne KE et al., 2008; Hain KO et al., 2016). HeLa cells, characterized by CIN, also exhibit low activity and sensitivity to Kif18A loss (Abe Y et al., 2016; Marquis C et al., 2021), supporting this possibility. However, the molecular mechanisms possibly involved in this hypothesis require further elucidation.

The deletion of Kif18A in cells with robust Aurora B at centromeres, such as in CENP-T ΔNBD-1 or ΔNBD-2 cells, which lack one Ndc80C binding but retain Mis12C-KNL1C binding, did not exhibit significant lethality. One possibility is that Kif18A operates in a distinct pathway from the CENP-C-Mis12C-mediated Aurora B feedback loop but intersects with Aurora B-dependent error correction. Another possibility is that Kif18A may function in an unknown manner to cooperate with the interaction of CENP-C and Mis12C to regulate Aurora B localization, though the possibility of Kif18A participating in the CENP-T-Mis12C interaction cannot be excluded.

Kif18A, as a co-effector of Mis12C, remains enigmatic, but it is likely primarily involved with the Aurora B-error correction system and could serve as a marker for abnormal cell division.

Materials and Methods

Establishment of mutant mouse lines

Utilizing electroporation to introduce Cas9 protein and sgRNAs into 1-cell embryos (Hashimoto M et al., 2016) to delete the exon 2 to 4. Embryos were obtained from superovulated B6C3F1 females crossed to B6C3F1 males. Embryos were aligned in the 1-mm gap of a CUY501G1 electrode (Nepa Gene, Ichikawa, Japan) filled with 200 ng/μL of freshly prepared Guide-it TM Recombinant Cas9 (Electroporation-Ready, Cat#632641, Takara Bio, Japan), 100 ng/μl of each sgRNA in Opti-MEM I (Thermo Fisher Scientific). Electroporation was performed at 30 V (3 msec ON + 97 msec OFF) x 7 pluses using CUY21 EDIT electroporator (BEX, Tokyo, Japan). The embryos were then cultured in modified Whitten's medium (DR01032, PHC Japan) over night at 37°C under 5% of CO_2. The embryos that reached the 2-cell stage were transferred to the oviducts of pseudopregnant females. Cesarean sections were performed when pregnant females did not deliver naturally, and pups were raised with ICR foster mothers. After genotyping, mice with the deletion were crossed with C57BL/6 to F1 heterozygous mice.

Animal care and experiments were conducted in accordance with the Guidelines of Animal Experiment of the National Institutes of Natural Sciences and the Guide for the Care and Use of Laboratory Animals of the Ministry of Education, Culture, Sports, Science, and Technology of Japan. The experiments employed in this study were approved by the Institutional Animal Care and Use Committee of the National Institutes of Natural Sciences and by the Committee on the Ethics of Animal Experiments of Chiba Cancer Center.

gRNA synthesis

To delete exons 2 to 4 of the mouse *Cenpc1* (*Cenpc*) gene, we selected gRNA target sequences intron 1 and intron 4 using CRISPick (Doench JG et al., 2016; Sanson KR et

al., 2018). gRNAs were synthesized as previously described (Hashimoto M et al., 2016). We amplified DNA fragments containing T7 promotor, gRNA target sequence (intron 1: CCAACACTATAGCTGACAAG, intro 4: AAACTGATAGAGTACAGTGG), and gRNA scaffold sequence by PCR using primers shown in Table 1 and pX330 (Addgene plasmid #42230) (Cong L et al., 2013) as a template. After purification of the PCR products by ethanol precipitation, gRNAs were synthesized from the PCR products using MEGAshortscript T7 Transcription Kit (Thermo Fisher Scientific) and purified by phenol-chloroform-isoamyl alcohol extraction and isopropanol precipitation.

Establishment of mouse embryonic fibroblasts (MEFs)

Mouse embryonic fibroblasts were isolated from 14.5-day-old embryos of *Cenpc*$^{+/+}$, *Cenpc*$^{+/\Delta M12BD}$, and *Cenpc*$^{\Delta M12BD/\Delta M12BD}$ mice. Following the removal of the head and organs, the embryos were rinsed with PBS, minced, and subjected to digestion with trypsin-EDTA (0.05%) (Gibco) for 30 min at 37°C. Trypsin was quenched by adding DMEM with high glucose (Sigma-Aldrich) supplemented with 15% fetal bovine serum (FBS). Each digested embryo was then plated on a 100-mm-diameter dish and incubated in humidified air containing 5% CO_2 at 37°C. The passage number was documented for each batch of mouse embryonic fibroblasts and the first passage cells (P1) were cryopreserved in freeze cryopreservation medium (BAMBANKER, GC LYMPHOTEC) at -80°C.

Two-step skin carcinogenesis

Sixteen *Cenpc*$^{+/+}$, 22 *Cenpc*$^{+/\Delta M12BD}$, and 15 *Cenpc*$^{\Delta M12BD/\Delta M12BD}$ mice were subjected to the following protocol. At 8-10 weeks of age, the backs of the mice were shaved with an electric clipper. Two days later, 7,12-dimethylbenz(a)anthracene (DMBA) (Sigma), (25 μg per mouse in 200 μl acetone) was applied to the shaved dorsal back skin. Three days after the first DMBA treatment, 12-*O*-tetradecanoylphorbol-13-acetate (TAP) (Calbiochem), (10 μg per mouse in 200 μl acetone) was administered. After four rounds of DMBA/TPA treatment, the mice were further treated with TPA twice a week for 20

weeks. The number of papillomas was recorded from 8 to 20 weeks, and the development of squamous cell carcinoma was monitored for up to 36 weeks after TPA treatment.

Cell culture

Human hTERT-RPE-1 and HeLa Kyoto cell lines were maintained in a culture medium containing DMEM (Nacalai Tesque) supplemented with 10% fetal bovine serum (Sigma) and Penicillin-Streptomycin (100 µg/ml) (Thermo Fisher) and cultured at 37°C, 5% CO_2. For degradation of GFP-mAID-CENP-T (RPE-1 cKO-CENP-T) cells were treated with 500 µM of 3-Indole acetic acid (IAA; Wako).

For the analysis of MEFs, the P1 MEFs were thawed and subcultured in a culture medium containing DMEM (Nacalai Tesque) supplemented with 10% FBS (Sigma) and Penicillin-Streptomycin (100 µg/ml) (Thermo Fisher) at 37°C, 5% CO_2. They were then passed one more time (P2) and used for all downstream experiments.

Plasmid constructions for cell transfection

To express mScarlet-fused full-length CENP-A under the control of the CENP-A promoter in RPE-1 cells, the sequence of mScarlet-fused CENP-A followed by puromycin (PuroR) or neomycin resistance genes (NeoR) expression cassette driven by the beta-actin (ACTB) promoter was cloned into the pBluescript II SK (pBSK) with 5’ and 3’ homology arm fragments (approximately 1 kb each) surrounding the *CENP-A* start codon (pBSK_mScarlet-CENP-A) using In-Fusion Snap Assembly Master Mix (Takara Bio). To integrate the construct into the endogenous *CENP-A* locus, CRISPR/Cas9-mediated homologous recombination was utilized, employing pX330 (Addgene plasmid #42230) (Cong L et al., 2013) containing single-guide RNA (sgRNA) targeting a genomic sequence (GGGCCTCGGGCTTTCGGCTC) around the CENP-A start codon (pX330_sgCENP-A). sgRNA for CENP-A was designed using CRISPOR (Concordet JP et al., 2018).

To express GFP-fused full-length CENP-A under the control of CMV promoter in RPE-1 cells, the sequence of GFP-fused CENP-A followed by L-Histidinol resistance genes (HisD) expression cassette driven by the *ACTB* promoter was cloned into the pT2/HB (a gift from Perry Hackett, Addgene plasmid #26557) (pT2/HB_GFP-CENP-A). The GFP-fused CENP-A with HisD expression cassette was integrated into the genome using the Sleeping Beauty transposon system (Mates L et al., 2009).

To express GFP-fused histone H2A from the AAVS1 locus in RPE-1 cells, the sequence of GFP-fused H2A followed by the blasticidin S resistance gene (BsR) expression cassette driven by the ACTB promoter was cloned into the pBSK with 5' and 3' homology arm fragments of AAVS1 locus (approximately 1 kb each) (pBSK_GFP-H2A) using In-Fusion Snap Assembly Master Mix (Takara Bio). The construct was integrated into the endogenous AAVS1 locus by CRISPR/Cas9-mediated homologous recombination, employing pX330 (Addgene plasmid #42230) (Cong L et al., 2013) containing sgRNA targeting a genomic sequence (ACCCCACAGTGGGGCCACTA) within intron 1 of PPP1R112C (pX330_sgAAVS1). sgRNA for AAVS1 locus was designed using CRISPOR (Concordet JP et al., 2018).

To express Flag-tagged full-length human CENP-C (CENP-CWT) or ∆Mis12C-binding domain (M12BD: aa1-75) under the control of the endogenous CENP-C promoter in RPE-1 cells, the cDNA of Flag-tagged human CENP-C WT or ∆M12BD followed by the zeocin (*ZeoR*) or *HisD* expression cassette driven by the *ACTB* promoter was cloned into the pBSK with 5' and 3' homology arm fragments (approximately 1 kb each) surrounding the *CENP-C* start codon (pBSK_FLAG-CENP-C^{WT} or FLAG-CENP-$C^{\Delta M12BD}$) using In-Fusion Snap Assembly Master Mix (Takara Bio). The constructs were integrated into the endogenous *CENP-C* locus by CRISPR/Cas9-mediated homologous recombination, employing pX330 (Addgene plasmid #42230) (Cong L et al., 2013) containing sgRNA targeting a genomic sequence (GGCCGGAACATGGCTGCGTC) around the *CENP-C* start codon (pX330_sgCENP-C). sgRNA for *CENP-C* was designed using CRISPOR (Concordet JP et al., 2018).

To express OsTIR1-T2A-BsR and GFP-mAID-fused human CENP-T simultaneously under control of the CMV promoter, *CENP-T* cDNA was cloned into the pAID1.2-NEGFP

(Nishimura K et al., 2009; Nishimura K et al., 2017; Nishimura K et al., 2020) (pAID1.2-CMV-NGFP-CENP-T, which includes CMV promoter-OsTIR1-T2A-BsR-IRES2-GFP-mAID-CENP-T). To express OsTIR1-T2A-BsR and GFP-mAID-fused CENP-T simultaneously under the control of the CMV promoter from the *AAVS1* locus in RPE-1 cells, the sequence of CMV promoter OsTIR1-T2A-BsR-IRES2-GFP-mAID-CENP-T was cloned into the pBSK with 5' and 3' homology arm fragments of *AAVS1* locus (approximately 1 kb each) (pBSK_AAVS1_OsTIR1_GFP-mAID-CENP-T). The construct was integrated into the endogenous *AAVS1* locus in RPE-1 cells by CRISPR/Cas9-mediated homologous recombination by using pX330_sgAAVS1.

Mutant CENP-T cDNAs (ΔNBD-1 (Ndc80C-binding domain 1: aa6-31), ΔNBD-2 (Ndc80C-binding domain 2: aa76-105), CENP-T$^{\Delta NBD-1}$ and CENP-T$^{\Delta NBD-2}$, respectively) were generated using PCR and In-Fusion Snap Assembly Master Mix (Takara Bio). To express the mScarlet-fused full-length CENP-T (CENP-T^{WT}), CENP-T$^{\Delta NBD-1}$, or CENP-T$^{\Delta NBD-2}$ under the control of the endogenous *CENP-T* promoter in RPE-1 cells, the cDNA of *mScarlet*-fused *CENP-T WT*, *ΔNBD-1*, or *ΔNBD-2* followed by *NeoR* or *PuroR* expression cassette driven by the *ACTB* promoter was cloned into the pBSK with 5' and 3' homology arm fragments (approximately 1 kb each) surrounding the *CENP-T* start codon (pBSK_mScarlet-CENP-T^{WT}, CENP-T$^{\Delta NBD-1}$, or CENP-T$^{\Delta NBD-2}$). Each construct was integrated into the endogenous *CENP-T* locus in RPE-1 cells by CRISPR/Cas9-mediated homologous recombination, employing pX330 (Addgene plasmid #42230) (Cong L et al., 2013) containing sgRNA targeting a genomic sequence (AGACGATGGCTGACCACAAC) around the *CENP-T* start codon (pX330_sgCENP-T). sgRNA for *CENP-T* was designed using CRISPOR (Concordet JP et al., 2018).

To express mScarlet-fused full-length DSN1 (DSN1^{WT}) or ΔBasic motif (aa91-113) mutant under the control of the endogenous *DSN1* promoter in HeLa cells, the cDNA of *mScarlet*-fused *DSN1 WT* or *ΔBasic motif* followed by *NeoR* and *PuroR* expression cassette driven by the *ACTB* promoter was cloned into the pBSK with 5' and 3' homology arm fragments (approximately 1 kb each) surrounding the *DSN1* start codon (pBSK_mScarlet-DSN1^{WT} or DSN1$^{\Delta Basic\ motif}$) using In-Fusion Snap Assembly Master Mix (Takara Bio). Each construct was integrated into the endogenous *DSN1* locus in HeLa

cells by CRISPR/Cas9-mediated homologous recombination, employing pX330 (Addgene plasmid #42230) (Cong L et al., 2013) containing sgRNA targeting a genomic sequence (CTTACCTTGGGTTCAGGCTT) around the *DSN1* start codon (pX330_sgDSN1). sgRNA for DSN1 was designed using CRISPOR (Concordet JP et al., 2018).

To express mouse CENP-C protein (aa1-405) in *E. coli*, *mouse CENP-C* (aa1-405) cDNA was cloned into pET30b (Merck) or pGEX6p-1 (Cytiva).

Generation of cell lines

To establish RPE-1 cell lines expressing mScarlet-fused CENP-A under the control of the endogenous *CENP-A* promoter, the RPE-1 cells were co-transfected with pBSK_mScarlet-CENP-A and pX330_sgCENP-A using Neon Transfection System (Thermo Fisher) with 6 pulses (1400 V, 5 msec), as previously described (Takenoshita Y et al., 2022). Transfected cells were then subjected to selection in a medium containing 2 mg/ml puromycin (Takara Bio) and 500 μg/ml G418 (Sigma) to isolate single-cell clones (RPE-1 mScarlet-CENP-A cells).

To generate RPE-1 mScarlet-CENP-A cells expressing GFP-fused H2A from the *AAVS1* locus under the control of the CMV promoter, RPE-1 mScarlet-CENP-A cells were co-transfected with pBSK_GFP-H2A and pX330_sgAAVS using Neon Transfection System (Thermo Fisher) with 6 pulses (1400 V, 5 msec). Transfected cells were selected in a medium containing 1 mg/ml Blasticidin S hydrochloride (Kaken Pharmaceutical) to isolate single-cell clones (RPE-1 mScarlet-CENP-A GFP-H2A cells)

To establish RPE-1 mScarlet-CENP-A GFP-H2A cells expressing either CENP-C WT or ΔM12BD under the control of the endogenous *CENP-C* promoter, RPE-1 mScarlet-CENP-A GFP-H2A cells were co-transfected with pBSK_FLAG-CENP-C^{WT} or CENP-$C^{\Delta M12BD}$ and pX330_sgCENP-C using Neon Transfection System (Thermo Fisher) with 6 pulses (1400 V, 5 msec). Transfected cells were selected in a medium containing 10 ng/ml Zeocin (Invitrogen) and 1.5 mg/ml L-Histidinol dihydrochloride (Sigma) to isolate

single-cell clones (RPE-1 mScarlet-CENP-A GFP-H2A Flag-CENP-C^{WT} or CENP-C$^{\Delta M12BD}$ cells).

To generate an inducible CENP-T protein degradation system using the AID system in RPE-1 cells, the CENP-T AID system expression cassette (CMV promoter OsTIR1-T2A-BsR-IRES2-GFP-mAID-CENP-T) was integrated into the *AAVS1* locus. RPE-1 cells were co-transfected with pBSK_AAVS1_OsTIR1_GFP-mAID-CENP-T and pX330_sgAAVS1 using Neon Transfection System (Thermo Fisher) with 6 pulses (1400 V, 5 msec). Transfected cells were selected in a medium containing 1 mg/ml Blasticidin S hydrochloride (Kaken Pharmaceutical) to isolate single-cell clones (RPE-1 cKO-CENP-T cells).

To generate RPE-1 cKO-CENP-T cells (GFP-mAID-CENP-T) expressing either CENP-T WT, ΔNBD-1, or ΔNBD-2, RPE-1 cKO-CENP-T cells were co-transfected with pBSK_mScarlet-CENP-T^{WT}, CENP-T$^{\Delta NBD-1}$, or CENP-T$^{\Delta NBD-2}$, and pX330_sgCENP-T using Neon Transfection System (Thermo Fisher) with 6 pulses (1400 V, 5 msec). Transfected cells were selected in a medium containing 2 mg/ml puromycin (Takara Bio) and 500 μg/ml G418 (Sigma) to isolate single-cell clones (RPE-1 cKO-CENP-T mScarlet-CENP-T^{WT}, CENP-T$^{\Delta NDB-1}$, or CENP-T$^{\Delta NDB-2}$ cells). To express GFP-CENP-A in RPE-1 cKO-CENP-T mScarlet-CENP-T^{WT}, CENP-T$^{\Delta NBD-1}$, or CENP-T$^{\Delta NBD-2}$ cells, we utilized the Sleeping Beauty transposon system (Mates L et al., 2009). The cells were transfected with pT2/HB_GFP-CENP-A and pCMV(CAT)T7-SB100 (Addgene plasmid #34879) (Mates L et al., 2009) selected in a medium containing 1.5 mg/ml L-Histidinol dihydrochloride (Sigma) to isolate single-cell clones (RPE-1 cKO-CENP-T GFP-CENP-A mScarlet-CENP-T^{WT}, CENP-T$^{\Delta NBD-1}$, or CENP-T$^{\Delta NBD-2}$).

To establish HeLa cells expressing mScarlet-fused DSN1 WT or ΔBasic motif under the control of the endogenous *DSN1* promoter, HeLa cells were co-transfected with pBSK_mScarlet-DSN1^{WT} or DSN1$^{\Delta Basic\ motif}$, and pX330_sgDSN1 using Neon Transfection System (Thermo Fisher) with 6 pulses (1400 V, 5 msec). Transfected cells were selected in a medium containing 2 mg/ml puromycin (Takara Bio) and 2 mg/ml G418 (Sigma) to isolate single-cell clones (HeLa mScarlet-DSN1^{WT} or DSN1$^{\Delta Basic\ motif}$ cells).

Cell counting

To count the number of RPE-1 cells or MEFs, the culture medium was aspirated and then the cells were washed with PBS. Subsequently, 2.5 g/liter of Trypsin and 1 mmol/liter EDTA solution (Nacalai Tesque) was added and incubated for 3 to 5 minutes at room temperature (RT). Trypsin was quenched by adding the culture medium. The cells were suspended by pipetting several times and then mixed with an equal volume of 0.4 wt/vol% Trypan Blue Solution (Wako). The living cells were counted using Countess II (Thermo Fisher).

Genotyping

To extract genomic DNA from MEFs, RPE-1 cells, or HeLa cells, the cells were collected after trypsinization, and washed with PBS as described previously (Takenoshita Y et al., 2022). The collected cells were resuspended in 0.2 mg/ml Proteinase K (Sigma) in PBST (0.1% Tween 20 (Nacalai tesque) in PBS) and then incubated for 90 min at 55°C followed by heating for 15 min at 96°C. The integration of target constructs was confirmed by PCR using primers listed in Table 1.

Anti-mouse CENP-C antibody generation

Mouse CENP-C aa1-405 fused with 6 × His was expressed in *E. coli* Rosetta2(DE3) transformed with pET30b-mouse CENP-$C^{1\text{-}405}$ and affinity-purified. The purified protein was injected into rabbits to raise antisera (Wako). For affinity purification of mouse CENP-C antibody, GST-fused mouse CENP-C aa1-405 was expressed in E. coli Rosetta2(DE3) transformed with pGEX6P-1-mouse CENP-$C^{1\text{-}405}$ and affinity-purified. GST- CENP-$C^{1\text{-}405}$ was conjugated with CNBr Sepharose 4B (Cytiva) and incubated with the antiserum for 1 h at RT. After a wash with 50 mM Tris-HCl pH7.5, 150 mM NaCl, the antibodies were eluted by 200 mM Glycin-HCl pH2.0, 150 mM NaCl and immediately neutralized with 1/20 vol. of 1 M Tris. The affinity-purified antibodies were

concentrated and then buffer-exchanged to 50 mM Tris-HCl pH7.5, 150 mM NaCl with Amicon Ultra-0.5 ml (Merk).

Immunoblotting

RPE-1 cells, MEFs, or HeLa cells were collected after trypsinization, washed with PBS, and suspended in 1x Laemmli Sample Buffer (LSB: 62.5 mM Tris (Trizma base, Sigma)-HCl, pH6.8, 2% SDS (Nacalai tesque), 10% Glycerol (Nacalai tesque), 50 mM DTT (Nacalai tesque), bromophenol blue (Wako)) to a final concentration of $1x10^4$ cells/μl. The lysate was sonicated and heated for 5 min at 96°C. Subsequently, the lysate was separated by 5-20% SDS-PAGE (SuperSepAce, Wako) and transferred onto a PVDF membrane (Immobilon-P, Merck). After washing in TBST (0.1% Tween 20 in TBS (50 mM Tris-HCl pH7.5, 150 mM NaCl)) for 15 min, the membrane was incubated with primary antibodies overnight at 4°C. Following a 15 min wash with TBST, the membrane was incubated with secondary antibodies for 1 h at RT. After another 15 min wash with TBST, the membrane was incubated with ECL Prime Western Blotting Detection Reagent (Cytiva) for 5 min. The signal was detected and visualized using a ChemiDoc Touch imaging system (Bio-Rad) and the image was processed using Image Lab (Bio-Rad) and Photoshop 2019 (Adobe).

To detect CENP-C signals in RPE-1 CENP-C^{WT} or CENP-$C^{\Delta M12BD}$ cell lines, harvested cells were suspended in TMS buffer (20 mM Tris-HCl, pH8.0, 5 mM $MgCl_2$, 250 mM sucrose, 0.5% NP-40, 10% glycerol) for 10 min on ice. The cells were spun down at 17,000 x*g* for 15 min at 4°C. The pellet was collected and washed with TKS buffer (20 mM Tris-HCl, pH8.0, 200 mM KCl, 250 mM sucrose, 1% Triton X-100, 10% glycerol, 1 mM DTT). The precipitate was suspended in lysis buffer (50 mM NH_2PO_4, 50 mM Na_2HPO_4, 0.3 M NaCl, 0.1% NP-40, 1 mM DTT). Following sonication, the lysate was diluted in 2 x LSB and heated for 5 min at 96°C. The proteins were detected as above.

The primary antibodies used in this study were rabbit anti-mouse CENP-C (1:5000), Guinea pig anti-human CENP-C (1:10,000) (Ando S et al., 2002), mouse anti-human CENP-A (1:3000) (Ando S et al., 2002), rabbit anti-human DSN1 (1:5000) (a gift from

Iain Cheeseman, Whitehead Institute, MIT) (Kline SL et al., 2006), rat anti-RFP (1:1000) (Chromotek), rat anti-human CENP-T (1:1000) (a gift from Kinya Yoda, Nagoya University, Nagoya, Japan), rat anti-histone H3 (1:5000) (a gift from Hiroshi Kimura, Tokyo Tech, Tokyo, Japan) (Nozawa RS et al., 2010), and mouse anti-α-tubulin (1:10,000) (Sigma). The secondary antibodies were HRP-conjugated anti-rabbit IgG (1:10,000) (Jackson ImmunoResearch), HRP-conjugated anti-guinea pig IgG (1:10,000) (Sigma), HRP-conjugated anti-mouse IgG (1:10,000) (Jackson ImmunoResearch), and HRP-conjugated anti-rat IgG (1:10,000) (Jackson ImmunoResearch). All antibodies were diluted in Signal Enhancer Hikari (Nacalai tesque) to enhance signal sensitivity and specificity.

Immunofluorescence staining and image acquisition

For the analysis of DSN1, KNL1, CENP-A, and Bub1, RPE-1 or HeLa cells were seeded onto 35 mm glass-bottom culture dishes (MatTek) for 24 to 36 hours. The samples were fixed with 4% paraformaldehyde (PFA; Electron Microscopy Sciences) in PHEM buffer (60 mM PIPES, 25 mM HEPES, 10 mM EGTA, 2 mM MgCl2, pH6.8) for 10 min at RT. The cells were permeabilized with 0.5% Triton X-100 in PBS for 10 min at RT, followed by blocking with antibody dilution buffer (Abdil, 3% BSA, 0.1% Triton X-100, 0.1% NaAzide in TBS) for 5 to 10 min at RT. The samples were then incubated with primary antibodies for 1 h at 37°C or overnight at 4°C. After washing the samples with PBST (0.1% Triton X-100 in PBS) three times for 5 min each, they were incubated with secondary antibodies for 1 h at RT. Subsequently, the samples were washed in PBST three times for 5 min each, followed by staining DNA in 0.1 μg/ml DAPI (Roche) in PBS for 10 min at RT. After washing with PBS once, cells were mounted with VECTASHIELD Mounting Medium (Vector Laboratories).

For the analysis of K-fiber, RPE-1 cells were seeded onto 35 mm glass-bottom culture dishes (MatTek) for 24 to 36 h, and supplemented with MG132 (50 μM) for 1 h. After rinsing the cells with culture medium, the cells were incubated with $CaCl_2$ buffer (1 mM $MgCl_2$, 1 mM $CaCl_2$, 0.5% Triton X-100, 100 mM Pipes, adjusted to pH 6.8) for 1 min at 37°C. The cells were then fixed in 1% glutaraldehyde (Nacalai Tesque) in PHEM for 10

min at 37°C. To quench the reaction, 0.1 g/ml sodium tetrahydridoborate (Nacalai Tesque) in PHEM was added and incubated for 20 min at RT. The cells were permeabilized with 0.5% Triton X-100 in PBS for 10 min and blocked with Abdil for 5 to 10 min at RT. The cells were incubated with primary antibody for 1 h at 37°C, followed by the aforementioned protocol for secondary antibody staining and counterstaining with DAPI.

For α-tubulin staining in error correction assay, RPE-1 or HeLa cells were seeded onto 35 mm glass-bottom culture dishes (MatTek) for 24 to 36 h. The cells were then fixed and permeabilized with 3.2% PFA, 0.5% Triton X-100, 1% glutaraldehyde in PHEM for 10 min at RT, followed by blocking with Abdil for 5 to 10 min at RT. Subsequently, the cells were incubated with primary antibodies for 1 h at 37°C. The secondary antibody staining and counterstaining with DAPI were performed as above.

For micronuclei analysis, MEFs or RPE-1 cells were seeded onto 35 mm glass-bottom culture dishes (MatTek) and cultured for two days. The cells were then fixed and permeabilized with a solution containing 4% PFA and 0.5% Triton X-100 in PHEM buffer for 10 minutes at RT. Nuclei were stained with DAPI as above.

For the analysis of Aurora B, H3T3ph, and H2AT120ph, chromosome spread samples were used. The cells were cultured with 100 ng/ml nocodazole (Sigma) for 2 to 4 h at 37°C. To spread and swell chromosomes, the method was modified from the protocol described previously (Moran EC et al., 2021). After shaking off and collecting the mitotic-arrested cells, they were suspended in a hypotonic buffer (75 mM KCl (Nacalai Tesque): 0.8% sodium citrate (Nacalai Tesque): water at 1:1:1) with 1x cOmplete EDTA-free proteinase inhibitor (Roche) on ice. The suspended cells were cytospun onto coverslips using the Cytospin III Cytocentrifuge and fixed in 2% PFA in PBS for 20 min. The cells were blocked in 1% BSA in PBS for 10 min at RT, followed by incubation with primary antibody for 1 h at 37°C or overnight at 4°C. Subsequently, the above protocol for secondary antibody staining and counterstaining with DAPI was performed.

Primary antibodies used were diluted in Abdil, except for Aurora B (diluted in 1% BSA/PBS). The primary antibodies included rabbit anti-human Hec1 (1:5000) (Abcam, ab3613), mouse anti-human CENP-A (1:250) (Ando S et al., 2002), mouse anti-human

Aurora B (1:500) (BD Bioscience, 611082), rabbit anti-human DSN1 (1:2000) (a gift from Iain Cheeseman, Whitehead Institute, MIT) (Kline SL et al., 2006), rabbit anti-human KNL1 (1:2000) (a gift from Iain Cheeseman, Whitehead Institute, MIT) (Cheeseman IM et al., 2008), mouse anti-human Bub1 (1:400) (MAB3610, Millipore), rabbit anti-H2AT120ph (1:1000) (ActiveMotif), mouse anti-H3T3ph (1:3000) (Kimura H et al., 2008), FITC-conjugated mouse anti-α-tubulin (1:1000) (Sigma, F2168), and mouse anti-α-tubulin (1:5000) (Sigma). Secondary antibodies used in immunofluorescence staining were FITC-conjugated goat anti-mouse IgG (1:1000) (Jackson ImmunoResearch), FITC-conjugated goat anti-rabbit IgG (1:1000) (Jackson ImmunoResearch), Alexa647-conjugated goat anti-mouse IgG (1:1000) (Jackson ImmunoResearch), and Alexa647-conjugated goat anti-rabbit IgG (1:1000) (Jackson ImmunoResearch).

Immunofluorescence images were captured with a spinning disk confocal unit CSU-W1 or CSU-W1-SoRa (Yokogawa) controlled with NIS-elements (v5.42.01, Nikon) with an objective lens (Nikon; PlanApo VC 60×/1.40 or Lambda 100×/1.45 NA) and an Orca-Fusion BT (Hamamatsu Photonics) sCMOS camera. The images were acquired with Z-stacks at intervals of 0.2 or 0.3-μm. Maximum intensity projections (MIPs) of the Z-stack were generated using Fiji software (Schindelin J et al., 2012) for display and analysis. These images were processed using Fiji and Photoshop 2019 (Adobe).

Live cell imaging

For analyzing CENP-C^{WT} or CENP-C$^{\Delta M12BD}$ RPE-1 cells, cells plated onto 35 mm glass-bottom dishes (MatTek) were switched to phenol red-free culture medium (phenol red-free DMEM (Nakalai Tesque), supplemented with 20% fetal bovine serum, 25 mM HEPES, 2 mM L-glutamine) and sealed with mineral oil (Sigma). Images were captured every 2 min with DeltaVision Elite imaging system (GE healthcare) equipped with a PlanApo N OSC 60×/1.40 NA oil immersion objective lens (Olympus) and a CoolSNAP HQ2 CCD camera (Photometrics) controlled with built-in SoftWoRx software (version 5.5) in a temperature-controlled room at 37°C. A Z-series of 7 sections with 2-μm increments was acquired. The Z-series was then projected using MIP for analysis by

SoftWoRx. For analyzing CENP-T^{WT}, CENP-$T^{\Delta NBD-1}$, or CENP-$T^{\Delta NBD-2}$ RPE-1 cells, the cells plated onto 35 mm glass-bottom dishes supplemented with IAA (500 μM) for two days were switched to phenol red-free culture medium supplemented with IAA (500 μM) and SPY505-DNA (1:1000) (Spirochrome) for 4 to 6 h before imaging. For analyzing *Cenpc*$^{+/+}$, *Cenpc*$^{+/\Delta M12BD}$, or *Cenpc*$^{\Delta M12BD/\Delta M12BD}$ MEFs, the cells plated onto 35 mm glass-bottom dishes were switched to phenol red-free culture medium supplemented with SPY650-DNA (1:3000) (Spirochrome) for 4 to 6 h before imaging.

Images were captured every 2 min with CSU-W1-SoRa system described above at 37°C under 5% CO_2 condition. Z-series of 7 sections were taken at intervals of 2-μm. Acquired time-lapse images were projected by MIP and processed using Fiji and Photoshop 2019 (Adobe).

For chromosome oscillation analysis, cells were treated with SiRTubulin (1:5000) (Spirochrome) for 4 to 6 h and then supplemented with MG132 (5 μM) for 2 h. Images were filmed every 3 sec for 5 min, Z-series of 5 or 7 sections in 0.5-μm increments. The deviation from the average position (DAP) was determined according to the previously described method (Stumpff J et al., 2008; Iemura K et al., 2015). In brief, the Z-stack images were deconvolved using plug-in function of NIS-element (Richardson-Lucy method) and then projected by MIP for quantification. Individual kinetochores were tracked by Manual Tracking (plug-in of Fiji, http://rsb.info.nih.gov/ij/plugins/track/track.html) after aligning the cell movement using the StackReg (plug-in of Fiji) (Thevenaz P et al., 1998). The obtained data were analyzed in Microsoft Excel.

Flow cytometry

MEFs were collected after trypsinization. The harvested cells were washed twice with ice-cold 1% BSA/PBS, fixed with ice-cold 70% ethanol, and stored at -20°C. The fixed cells were washed again with 1% BSA/PBS and incubated with 20 μg/ml propidium iodide (Sigma) in 1% BSA/PBS for 20 min at RT, followed by overnight incubation at 4°C. The stained cells were then subjected to flow cytometry analysis using a BD FACS

Canto II Flow Cytometer and analyzed with BD FACSDiva 9.0 Software (BD Biosciences).

Cell viability assay

RPE-1 cells were seeded onto opaque-walled tissue culture plates with a clear bottom (Corning) at a density of 2500 cells per well and incubated for 12 h. The cells were treated with nocodazole at indicated concentrations for 3 days, with each concentration tested in triplicate. After treatment, RealTime-Glo reagents (RealTime-Glo MT Cell Viability Assay, Promega) were added to the cells and incubated for 1 h at 37°C. Luminescence was measured using a GloMax Discover System Microplate Reader (Promega). IC_{50} values were determined using GraphPad Prism 9.5.1 (GraphPad).

Chromosome counting

For chromosome number counting, using chromosome spread samples. MEFs were supplemented with 100 ng/ml nocodazole for 4~5h, after wash three times by culture medium, shake off and collect mitotic cells. Cell pellet was suspend in hypotonic buffer like above described (75 mM KCl (Nacalai Tesque): 0.8% sodium citrate (Nacalai Tesque): water at 1:1:1)) for 5~10 min. Then washed by fixative solution (3 methanol : 1 acetic acid) for three times. At last, the cells in fixative solution was droped onto the surface of glass slides with 3~4 drops. Let it air dry and then supply with 1mg/ml DAPI solution on the surface for 10 min. Remove the liquid and drop the VECTASHIELD Mounting Medium (Vector Laboratories), covering by coverslip.

siRNA transfection

For transfection in a 6-well tissue culture plate (Corning), prepare a duplex of 10 pmol siRNA and 3 µl transfection reagent (Lipofectamine RNAiMAX, Invitrogen) in 250 µl Opti-MEM (Invitrogen) per well. Transfer the duplex into one well, then add 7.5×10^4 to 8×10^4 cells. Incubate for 3 days before conducting subsequent experiments. For

transfection in a 96-well tissue culture plate (Corning), prepare a duplex of 0.5 pmol siRNA and 3 µl transfection reagent in 20 µl Opti-MEM for one well. Transfer the duplex into one well, then add 1250 cells per well. Incubate for 3 days, or for 12 hours followed by supplementation with nocodazole at indicated concentrations for an additional 3 days for the viability assay. The control siRNA (siControl) is a non-targeting pool (Dharmacon, ON-TARGETplus Non-targeting Pool), whereas the Kif18A siRNA pool (siKif18A) targets four independent sequences of the human Kif18A transcripts (UAAAUUACCCGAACAAGAA, GAAAGUAGUAGUUCGUGUA, CAAAAUCCGUCUACAGUAA, GGAUAUAAUUGCACAGUAC) (Dharmacon, ON-TARGETplus SMARTpool siRNA).

Error correction assay

RPE-1 or HeLa cells were plated and incubated on 35 mm glass-bottom culture dishes (MatTek) for 24 to 36 h. Subsequently, the cells were treated with 50 µM monastrol (Selleckchem) for 4 h, followed by washing with culture medium four times. The cells were then supplemented with MG132 (5 µM) (Sigma) for indicated timing and fixed (3.2% PFA, 0.5% Triton X-100, 1% glutaraldehyde in PHEM at RT for 10 min) immediately. Following fixation and permeabilization, staining was performed using antibodies and DAPI as aforementioned protocol.

Quantification and Statistical Analysis

The fluorescence signal intensities of DSN1, KNL1, Hec1, Bub1, and mScarlet-DSN1 on kinetochores were quantified using Imaris (Bitplane). The fluorescence signal intensities of Aurora B and H3T3ph within the inner centromere regions were measured using Fiji. The signal intensities were quantified by subtracting background signals in a 15-pixel circular region of chromosome adjacent to the inner centromere region from the signals in a 15-pixel circular region of the inner centromere region. The fluorescence signal intensities of H2AT120ph within the kinetochore-proximal centromere region were measured using Fiji. The signal intensities were quantified by subtracting background

signals in a chromosomal region from the signals in a 10-pixel circular region circular area centered on the kinetochore. For quantification of the k-fiber signal intensities, to select the spindle area in a cell thresholding is applied to the tubulin signals (MIP) using Fiji. The mean signal intensities in the selected area are measured. The value is subtracted by the mean background signal intensities adjacent to the spindle area and quantified as the averaged k-fiber signals. Data processing was carried out using Microsoft Excel and GraphPad Prism 9.5.1 (GraphPad), and p-values were calculated using two-tailed Student's t-test or one-way or two-way ANOVA test followed by multiple comparison tests. Each experiment was repeated four times (Figure 24F), three times (Figures 15F, 19C, 19D, 22A, 22B, 24B, 24E, 26A, 26B, 27A, 27B, 29B, 35A), or twice (Figures 19B, 24C, 24D, 28, 29A, 29C, 35B, 36B, 36C), and representative data of replicates were presented.

Table 1 Sequence information of primers and gRNAs

Primer	Sequence
F1	CATCGATGGGTGTAAGATGGAATCTCAGAG
F2	GCCAATTATAGTCAATCATCAAGCAAAAAGG
F3	ACGTCGAGTGCCCGAAGGAC
F4	TGGAATTACTGGATCATCTGG
F5	AGGACATAGCGTTGGCTACC
F6	TGAGCTCTACTGGCTTCTGC
F7	ACGATTGAAGAACTCATTCCAC
F8	ATTGGCCTTCATAGTTGACAGCATTTG
F9	TGACCGAGATCGGCGAGCAG
F10	TGACCGTACAGGAACTGTCG
F11	TGCCGTCTCTCTCCTGAGTC
F12	GCCACTATGTGAAACTCTTTAGC
F13	TCAACCAGTGAAAAATACGGAGG
F14	GGCTCGGCTTCACCGTCACC
F15	GGCTACCCGTGATATTGCTGAAG
F16	CAGGTAGAAGGACAGATATGTGC
F17	ACCGAGCTGCAAGAACTCTTCCTCACG
F18	TCCATCATGGCTGATGCAATGC

R1	CGGCAATATCTTCTGTGGTAGTTCTTTAGATGATC
R2	TCTGTGTAGCCCTGGCTATCACTCTGTAG
R3	CTAGGGTGAACGAGAATTCAGC
R4	GAACCGCATGAACTCCTTG
R5	TATTGGCGTTACTATGGGAACATAC
R6	AAGGCAGCCTGGTAGACAGG
R7	GTGGCTTCACTTGGTTCTACAACA
R8	CTTAAACAGATATGTAAATCACCAAAG
R9	TACCCCGAAGAGTGAGTTTGC
R10	GAAAGTCCCTATTGGCGTTAC
R11	CAGCAGACCTGGAGCCAGGGTTGTG
R12	CCACTTGGAAATAGGACGATACCTT
R13	GTCACCCAGGATAGATTGAGTGG
R14	AAGAGCTGATCCCAAGTCTG
CenpC1_gRNA_intron1	TTAATACGACTCACTATAGGCCAACACTATAGCTGACAAGGTTTTAGAGCTAGAAATAGCAAGTTAAAAT
CenpC1_gRNA_intron4	TTAATACGACTCACTATAGGAAACTGATAGAGTACAGTGGGTTTTAGAGCTAGAAATAGCAAGTTAAAAT
gRNA common Rv	AAAAGCACCGACTCGGTGCCACTTTT

References

Paweletz N. Walther Flemming: pioneer of mitosis research. Nat Rev Mol Cell Biol. 2001 Jan;2(1):72-5. doi: 10.1038/35048077

O'Connor C, Miko I. Developing the chromosome theory. Nature Education 1(1):44. 2008.

Darlington CD. The external mechanics of the chromosomes. Proc R Soc Lond 121:264–319. 1936. https://doi.org/10.1098/rspb.1936.0064

Hara M, Fukagawa T. Critical Foundation of the Kinetochore: The Constitutive Centromere-Associated Network (CCAN). Prog Mol Subcell Biol. 2017;56:29-57. doi: 10.1007/978-3-319-58592-5_2

Clarke L, Carbon J. Genomic substitutions of centromeres in Saccharomyces cerevisiae. Nature. 1983 Sep 1-7;305(5929):23-8. doi: 10.1038/305023a0

Moroi Y, Peebles C, Fritzler MJ, Steigerwald J, Tan EM. Autoantibody to centromere (kinetochore) in scleroderma sera. Proc Natl Acad Sci U S A. 1980 Mar;77(3):1627-31. doi: 10.1073/pnas.77.3.1627

Carbon J, Clarke L. Structural and functional analysis of a yeast centromere (CEN3). J Cell Sci Suppl. 1984;1:43-58. doi: 10.1242/jcs.1984.supplement_1.4

McKinley KL, Cheeseman IM. The molecular basis for centromere identity and function. Nat Rev Mol Cell Biol. 2016 Jan;17(1):16-29. doi: 10.1038/nrm.2015.5. Epub 2015 Nov 25

Fukagawa T, Earnshaw WC. The centromere: chromatin foundation for the kinetochore machinery. Dev Cell. 2014 Sep 8;30(5):496-508. doi: 10.1016/j.devcel.2014.08.016

Sundararajan K, Straight AF. Centromere Identity and the Regulation of Chromosome Segregation. Front Cell Dev Biol. 2022 Jun 2;10:914249. doi: 10.3389/fcell.2022.914249

Sullivan KF. A solid foundation: functional specialization of centromeric chromatin. Curr Opin Genet Dev. 2001 Apr;11(2):182-8. doi: 10.1016/s0959-437x(00)00177-5

Sullivan KF, Hechenberger M, Masri K. J Cell Biol. 1994 Nov;127(3):581-92. doi: 10.1083/jcb.127.3.581

Ariyoshi M, Makino F, Watanabe R, Nakagawa R, Kato T, Namba K, Arimura Y, Fujita R, Kurumizaka H, Okumura EI, Hara M, Fukagawa T. Cryo-EM structure of the CENP-A

nucleosome in complex with phosphorylated CENP-C. EMBO J. 2021 Mar 1;40(5):e105671. doi: 10.15252/embj.2020105671

Tian T, Li X, Liu Y, Wang C, Liu X, Bi G, Zhang X, Yao X, Zhou ZH, Zang J. Molecular basis for CENP-N recognition of CENP-A nucleosome on the human kinetochore. Cell Res. 2018 Mar;28(3):374-378. doi: 10.1038/cr.2018.13

Régnier V, Vagnarelli P, Fukagawa T, Zerjal T, Burns E, Trouche D, Earnshaw W, Brown W. CENP-A is required for accurate chromosome segregation and sustained kinetochore association of BubR1. Mol Cell Biol. 2005 May;25(10):3967-81. doi: 10.1128/MCB.25.10.3967-3981.2005

Shrestha RL, Ahn GS, Staples MI, Sathyan KM, Karpova TS, Foltz DR, Basrai MA. Mislocalization of centromeric histone H3 variant CENP-A contributes to chromosomal instability (CIN) in human cells. Oncotarget. 2017 Jul 18;8(29):46781-46800. doi: 10.18632/oncotarget.18108

Warburton PE, Cooke CA, Bourassa S, Vafa O, Sullivan BA, Stetten G, Gimelli G, Warburton D, Tyler-Smith C, Sullivan KF, Poirier GG, Earnshaw WC. Immunolocalization of CENP-A suggests a distinct nucleosome structure at the inner kinetochore plate of active centromeres. Curr Biol. 1997 Nov 1;7(11):901-4. doi: 10.1016/s0960-9822(06)00382-4

Hori T, Shang WH, Takeuchi K, Fukagawa T. The CCAN recruits CENP-A to the centromere and forms the structural core for kinetochore assembly. J Cell Biol. 2013 Jan 7;200(1):45-60. doi: 10.1083/jcb.201210106

Fukagawa T, Brown WR. Efficient conditional mutation of the vertebrate CENP-C gene. Hum Mol Genet. 1997 Dec;6(13):2301-8. doi: 10.1093/hmg/6.13.2301

Earnshaw WC, Rothfield N. Identification of a family of human centromere proteins using autoimmune sera from patients with scleroderma. Chromosoma. 1985;91(3-4):313-21. doi: 10.1007/BF00328227

Musacchio A, Desai A. A Molecular View of Kinetochore Assembly and Function. Biology (Basel). 2017 Jan 24;6(1):5. doi: 10.3390/biology6010005

Hughes-Schrader S., Ris H. The diffuse spindle attachment of coccids, verified by the mitotic behavior of induced chromosome fragments. J. Exp. Zool. 1941;87:429–456. doi: 10.1002/jez.1400870306

Drinnenberg IA, deYoung D, Henikoff S, Malik HS. Recurrent loss of CenH3 is associated with independent transitions to holocentricity in insects. Elife. 2014 Sep 23;3:e03676. doi: 10.7554/eLife.03676

Cuacos M, H Franklin FC, Heckmann S. Atypical centromeres in plants-what they can tell us. Front Plant Sci. 2015 Oct 26;6:913. doi: 10.3389/fpls.2015.00913

Cheeseman IM. The kinetochore. Cold Spring Harb Perspect Biol. 2014 Jul 1;6(7):a015826. doi: 10.1101/cshperspect.a015826

Nagpal H, Fukagawa T. Kinetochore assembly and function through the cell cycle. Chromosoma. 2016 Sep;125(4):645-59. doi: 10.1007/s00412-016-0608-3

DeLuca JG, Musacchio A. Structural organization of the kinetochore-microtubule interface. Curr Opin Cell Biol. 2012 Feb;24(1):48-56. doi: 10.1016/j.ceb.2011.11.003

Cheeseman IM, Desai A. Molecular architecture of the kinetochore-microtubule interface. Nat Rev Mol Cell Biol. 2008 Jan;9(1):33-46. doi: 10.1038/nrm2310

McEwen BF, Hsieh CE, Mattheyses AL, Rieder CL. A new look at kinetochore structure in vertebrate somatic cells using high-pressure freezing and freeze substitution. Chromosoma. 1998 Dec;107(6-7):366-75. doi: 10.1007/s004120050320

McKinley KL, Sekulic N, Guo LY, Tsinman T, Black BE, Cheeseman IM. The CENP-L-N Complex Forms a Critical Node in an Integrated Meshwork of Interactions at the Centromere-Kinetochore Interface. Mol Cell. 2015 Dec 17;60(6):886-98. doi: 10.1016/j.molcel.2015.10.027

Pentakota S, Zhou K, Smith C, Maffini S, Petrovic A, Morgan GP, Weir JR, Vetter IR, Musacchio A, Luger K. Decoding the centromeric nucleosome through CENP-N. Elife. 2017 Dec 27;6:e33442. doi: 10.7554/eLife.33442

Przewloka MR, Venkei Z, Bolanos-Garcia VM, Debski J, Dadlez M, Glover DM. CENP-C is a structural platform for kinetochore assembly. Curr Biol. 2011 Mar 8;21(5):399-405. doi: 10.1016/j.cub.2011.02.005

Screpanti E, De Antoni A, Alushin GM, Petrovic A, Melis T, Nogales E, Musacchio A. Direct binding of Cenp-C to the Mis12 complex joins the inner and outer kinetochore. Curr Biol. 2011 Mar 8;21(5):391-8. doi: 10.1016/j.cub.2010.12.039

Carroll CW, Milks KJ, Straight AF. Dual recognition of CENP-A nucleosomes is required for centromere assembly. J Cell Biol. 2010 Jun 28;189(7):1143-55. doi: 10.1083/jcb.201001013

Kato H, Jiang J, Zhou BR, Rozendaal M, Feng H, Ghirlando R, Xiao TS, Straight AF, Bai Y. A conserved mechanism for centromeric nucleosome recognition by centromere protein CENP-C. Science. 2013 May 31;340(6136):1110-3. doi: 10.1126/science.1235532

Kwon MS, Hori T, Okada M, Fukagawa T. CENP-C is involved in chromosome segregation, mitotic checkpoint function, and kinetochore assembly. Mol Biol Cell. 2007 Jun;18(6):2155-68. doi: 10.1091/mbc.e07-01-0045

Watanabe R, Hara M, Okumura EI, Hervé S, Fachinetti D, Ariyoshi M, Fukagawa T. CDK1-mediated CENP-C phosphorylation modulates CENP-A binding and mitotic kinetochore localization. J Cell Biol. 2019 Dec 2;218(12):4042-4062. doi: 10.1083/jcb.201907006

Hara M, Ariyoshi M, Sano T, Nozawa RS, Shinkai S, Onami S, Jansen I, Hirota T, Fukagawa T. Centromere/kinetochore is assembled through CENP-C oligomerization. Mol Cell. 2023 Jul 6;83(13):2188-2205.e13. doi: 10.1016/j.molcel.2023.05.023

Hara M, Ariyoshi M, Okumura EI, Hori T, Fukagawa T. Publisher Correction: Multiple phosphorylations control recruitment of the KMN network onto kinetochores. Nat Cell Biol. 2018 Dec;20(12):1434. doi: 10.1038/s41556-018-0252-7

Hori T, Amano M, Suzuki A, Backer CB, Welburn JP, Dong Y, McEwen BF, Shang WH, Suzuki E, Okawa K, Cheeseman IM, Fukagawa T. CCAN makes multiple contacts with centromeric DNA to provide distinct pathways to the outer kinetochore. Cell. 2008a Dec 12;135(6):1039-52. doi: 10.1016/j.cell.2008.10.019

Nishino T, Takeuchi K, Gascoigne KE, Suzuki A, Hori T, Oyama T, Morikawa K, Cheeseman IM, Fukagawa T. CENP-T-W-S-X forms a unique centromeric chromatin structure with a histone-like fold. Cell. 2012 Feb 3;148(3):487-501. doi: 10.1016/j.cell.2011.11.061

Takeuchi K, Nishino T, Mayanagi K, Horikoshi N, Osakabe A, Tachiwana H, Hori T, Kurumizaka H, Fukagawa T. The centromeric nucleosome-like CENP-T-W-S-X complex induces positive supercoils into DNA. Nucleic Acids Res. 2014 Feb;42(3):1644-55. doi: 10.1093/nar/gkt1124

Nishino T, Rago F, Hori T, Tomii K, Cheeseman IM, Fukagawa T. CENP-T provides a structural platform for outer kinetochore assembly. EMBO J. 2013 Feb 6;32(3):424-36. doi: 10.1038/emboj.2012.348

Fukagawa T, Mikami Y, Nishihashi A, Regnier V, Haraguchi T, Hiraoka Y, Sugata N, Todokoro K, Brown W, Ikemura T. CENP-H, a constitutive centromere component, is required for centromere targeting of CENP-C in vertebrate cells. EMBO J. 2001 Aug 15;20(16):4603-17. doi: 10.1093/emboj/20.16.4603

Nagpal H, Hori T, Furukawa A, Sugase K, Osakabe A, Kurumizaka H, Fukagawa T. Dynamic changes in CCAN organization through CENP-C during cell-cycle progression. Mol Biol Cell. 2015 Nov 1;26(21):3768-76. doi: 10.1091/mbc.E15-07-0531

Huis In 't Veld PJ, Jeganathan S, Petrovic A, Singh P, John J, Krenn V, Weissmann F, Bange T, Musacchio A. Molecular basis of outer kinetochore assembly on CENP-T. Elife. 2016 Dec 24;5:e21007. doi: 10.7554/eLife.21007

Krenn V, Overlack K, Primorac I, van Gerwen S, Musacchio A. KI motifs of human Knl1 enhance assembly of comprehensive spindle checkpoint complexes around MELT repeats. Curr Biol. 2014 Jan 6;24(1):29-39. doi: 10.1016/j.cub.2013.11.046

Dimitrova YN, Jenni S, Valverde R, Khin Y, Harrison SC. Structure of the MIND Complex Defines a Regulatory Focus for Yeast Kinetochore Assembly. Cell. 2016 Nov 3;167(4):1014-1027.e12. doi: 10.1016/j.cell.2016.10.011

Kim S, Yu H. Multiple assembly mechanisms anchor the KMN spindle checkpoint platform at human mitotic kinetochores. J Cell Biol. 2015 Jan 19;208(2):181-96. doi: 10.1083/jcb.201407074

Welburn JP, Vleugel M, Liu D, Yates JR 3rd, Lampson MA, Fukagawa T, Cheeseman IM. Aurora B phosphorylates spatially distinct targets to differentially regulate the kinetochore-microtubule interface. Mol Cell. 2010 May 14;38(3):383-92. doi: 10.1016/j.molcel.2010.02.034

Takenoshita Y, Hara M, Fukagawa T. Recruitment of two Ndc80 complexes via the CENP-T pathway is sufficient for kinetochore functions. Nat Commun. 2022 Feb 14;13(1):851. doi: 10.1038/s41467-022-28403-8

Nishihashi A, Haraguchi T, Hiraoka Y, Ikemura T, Regnier V, Dodson H, Earnshaw WC, Fukagawa T. CENP-I is essential for centromere function in vertebrate cells. Dev Cell. 2002 Apr;2(4):463-76. doi: 10.1016/s1534-5807(02)00144-2

Sugata N, Munekata E, Todokoro K. Characterization of a novel kinetochore protein, CENP-H. J Biol Chem. 1999 Sep 24;274(39):27343-6. doi: 10.1074/jbc.274.39.27343

Saitoh S, Takahashi K, Yanagida M. Mis6, a fission yeast inner centromere protein, acts during G1/S and forms specialized chromatin required for equal segregation. Cell. 1997 Jul 11;90(1):131-43. doi: 10.1016/s0092-8674(00)80320-7

Okada M, Cheeseman IM, Hori T, Okawa K, McLeod IX, Yates JR 3rd, Desai A, Fukagawa T. The CENP-H-I complex is required for the efficient incorporation of newly synthesized CENP-A into centromeres. Nat Cell Biol. 2006 May;8(5):446-57. doi: 10.1038/ncb1396

Foltz DR, Jansen LE, Black BE, Bailey AO, Yates JR 3rd, Cleveland DW. The human CENP-A centromeric nucleosome-associated complex. Nat Cell Biol. 2006 May;8(5):458-69. doi: 10.1038/ncb1397

Basilico F, Maffini S, Weir JR, Prumbaum D, Rojas AM, Zimniak T, De Antoni A, Jeganathan S, Voss B, van Gerwen S, Krenn V, Massimiliano L, Valencia A, Vetter IR, Herzog F, Raunser S, Pasqualato S, Musacchio A. The pseudo GTPase CENP-M drives human kinetochore assembly. Elife. 2014 Jul 8;3: e02978. doi: 10.7554/eLife.02978

Carroll CW, Silva MC, Godek KM, Jansen LE, Straight AF. Centromere assembly requires the direct recognition of CENP-A nucleosomes by CENP-N. Nat Cell Biol. 2009 Jul;11(7):896-902. doi: 10.1038/ncb1899

Fang J, Liu Y, Wei Y, Deng W, Yu Z, Huang L, Teng Y, Yao T, You Q, Ruan H, Chen P, Xu RM, Li G. Structural transitions of centromeric chromatin regulate the cell cycle-dependent recruitment of CENP-N. Genes Dev. 2015 May 15;29(10):1058-73. doi: 10.1101/gad.259432.115

Pesenti ME, Prumbaum D, Auckland P, Smith CM, Faesen AC, Petrovic A, Erent M, Maffini S, Pentakota S, Weir JR, Lin YC, Raunser S, McAinsh AD, Musacchio A. Reconstitution of a 26-Subunit Human Kinetochore Reveals Cooperative Microtubule Binding by CENP-OPQUR and NDC80. Mol Cell. 2018 Sep 20;71(6):923-939.e10. doi: 10.1016/j.molcel.2018.07.038

Liu R, Dou Z, Tian T, Gao X, Chen L, Yuan X, Wang C, Hao J, Gui P, Mullen M, Aikhionbare F, Niu L, Bi G, Zou P, Zhang X, Fu C, Yao X, Zang J, Liu X. Dynamic phosphorylation of CENP-N by CDK1 guides accurate chromosome segregation in mitosis. J Mol Cell Biol. 2023 Nov 27;15(6): mjad041. doi: 10.1093/jmcb/mjad041

Hori T, Okada M, Maenaka K, Fukagawa T. CENP-O class proteins form a stable complex and are required for proper kinetochore function. Mol Biol Cell. 2008 Mar;19(3):843-54. doi: 10.1091/mbc.e07-06-0556

Pesenti ME, Weir JR, Musacchio A. Progress in the structural and functional characterization of kinetochores. Curr Opin Struct Biol. 2016 Apr;37:152-63. doi: 10.1016/j.sbi.2016.03.003

Varma D, Salmon ED. The KMN protein network--chief conductors of the kinetochore orchestra. J Cell Sci. 2012 Dec 15;125(Pt 24):5927-36. doi: 10.1242/jcs.093724

Ariyoshi M, Fukagawa T. An updated view of the kinetochore architecture. Trends Genet. 2023 Dec;39(12):941-953. doi: 10.1016/j.tig.2023.09.003

Wei RR, Sorger PK, Harrison SC. Molecular organization of the Ndc80 complex, an essential kinetochore component[J]. Proceedings of the National Academy of Sciences, 2005, 102(15): 5363-5367. Doi: 10.1073/pnas.050116810

Ciferri C, Pasqualato S, Screpanti E, Varetti G, Santaguida S, Dos Reis G, Maiolica A, Polka J, De Luca JG, De Wulf P, Salek M, Rappsilber J, Moores CA, Salmon ED,

Musacchio A. Implications for kinetochore-microtubule attachment from the structure of an engineered Ndc80 complex. Cell. 2008 May 2;133(3):427-39. doi: 10.1016/j.cell.2008.03.020

Maure JF, Komoto S, Oku Y, Mino A, Pasqualato S, Natsume K, Clayton L, Musacchio A, Tanaka TU. The Ndc80 loop region facilitates formation of kinetochore attachment to the dynamic microtubule plus end. Curr Biol. 2011 Feb 8;21(3):207-13. doi: 10.1016/j.cub.2010.12.050

Petrovic A, Mosalaganti S, Keller J, Mattiuzzo M, Overlack K, Krenn V, De Antoni A, Wohlgemuth S, Cecatiello V, Pasqualato S, Raunser S, Musacchio A. Modular assembly of RWD domains on the Mis12 complex underlies outer kinetochore organization. Mol Cell. 2014 Feb 20;53(4):591-605. doi: 10.1016/j.molcel.2014.01.019

Petrovic A, Pasqualato S, Dube P, Krenn V, Santaguida S, Cittaro D, Monzani S, Massimiliano L, Keller J, Tarricone A, Maiolica A, Stark H, Musacchio A. The MIS12 complex is a protein interaction hub for outer kinetochore assembly. J Cell Biol. 2010 Sep 6;190(5):835-52. doi: 10.1083/jcb.201002070

Polley S, Raisch T, Ghetti S, Körner M, Terbeck M, Gräter F, Raunser S, Aponte-Santamaría C, Vetter IR, Musacchio A. Structure of the human KMN complex and implications for regulation of its assembly. Nat Struct Mol Biol. 2024 Mar 8. doi: 10.1038/s41594-024-01230-9

Yatskevich S, Yang J, Bellini D, Zhang Z, Barford D. Structure of the human outer kinetochore KMN network complex. Nat Struct Mol Biol. 2024 Mar 8. doi: 10.1038/s41594-024-01249-y

Akiyoshi B, Nelson CR, Biggins S. The aurora B kinase promotes inner and outer kinetochore interactions in budding yeast. Genetics. 2013 Jul;194(3):785-9. doi: 10.1534/genetics.113.150839

Welburn JP, Vleugel M, Liu D, Yates JR 3rd, Lampson MA, Fukagawa T, Cheeseman IM. Aurora B phosphorylates spatially distinct targets to differentially regulate the kinetochore-microtubule interface. Mol Cell. 2010 May 14;38(3):383-92. doi: 10.1016/j.molcel

Kiyomitsu T, Obuse C, Yanagida M. Human Blinkin/AF15q14 is required for chromosome alignment and the mitotic checkpoint through direct interaction with Bub1 and BubR1. Dev Cell. 2007 Nov;13(5):663-676. doi: 10.1016/j.devcel.2007.09.005

Cheeseman IM, Chappie JS, Wilson-Kubalek EM, Desai A. The conserved KMN network constitutes the core microtubule-binding site of the kinetochore. Cell. 2006 Dec 1;127(5):983-97. doi: 10.1016/j.cell.2006.09.039

Karess R. Rod-Zw10-Zwilch: a key player in the spindle checkpoint. Trends Cell Biol. 2005 Jul;15(7):386-92. doi: 10.1016/j.tcb.2005.05.003

Varma D, Wan X, Cheerambathur D, Gassmann R, Suzuki A, Lawrimore J, Desai A, Salmon ED. Spindle assembly checkpoint proteins are positioned close to core microtubule attachment sites at kinetochores. J Cell Biol. 2013 Sep 2;202(5):735-46. doi: 10.1083/jcb.201304197

Kiyomitsu T, Murakami H, Yanagida M. Protein interaction domain mapping of human kinetochore protein Blinkin reveals a consensus motif for binding of spindle assembly checkpoint proteins Bub1 and BubR1. Mol Cell Biol. 2011 Mar;31(5):998-1011. doi: 10.1128/MCB.00815-10

Bolanos-Garcia VM, Lischetti T, Matak-Vinković D, Cota E, Simpson PJ, Chirgadze DY, Spring DR, Robinson CV, Nilsson J, Blundell TL. Structure of a Blinkin-BUBR1 complex reveals an interaction crucial for kinetochore-mitotic checkpoint regulation via an unanticipated binding Site. Structure. 2011 Nov 9;19(11):1691-700. doi: 10.1016/j.str.2011.09.017

Chen Y, Riley DJ, Chen PL, Lee WH. HEC, a novel nuclear protein rich in leucine heptad repeats specifically involved in mitosis. Mol Cell Biol. 1997 Oct;17(10):6049-56. doi: 10.1128/MCB.17.10.6049

Osborne MA, Schlenstedt G, Jinks T, Silver PA. Nuf2, a spindle pole body-associated protein required for nuclear division in yeast. J Cell Biol. 1994 May;125(4):853-66. doi: 10.1083/jcb.125.4.853

Wigge PA, Kilmartin JV. The Ndc80p complex from Saccharomyces cerevisiae contains conserved centromere components and has a function in chromosome segregation. J Cell Biol. 2001 Jan 22;152(2):349-60. doi: 10.1083/jcb.152.2.349

Wei RR, Schnell JR, Larsen NA, Sorger PK, Chou JJ, Harrison SC. Structure of a central component of the yeast kinetochore: the Spc24p/Spc25p globular domain. Structure. 2006 Jun;14(6):1003-9. doi: 10.1016/j.str.2006.04.007

Tooley J, Stukenberg PT. The Ndc80 complex: integrating the kinetochore's many movements. Chromosome Res. 2011 Apr;19(3):377-91. doi: 10.1007/s10577-010-9180-5

Miller SA, Johnson ML, Stukenberg PT. Kinetochore attachments require an interaction between unstructured tails on microtubules and Ndc80(Hec1). Curr Biol. 2008 Nov 25;18(22):1785-91. doi: 10.1016/j.cub.2008.11.007

DeLuca JG, Gall WE, Ciferri C, Cimini D, Musacchio A, Salmon ED. Kinetochore microtubule dynamics and attachment stability are regulated by Hec1. Cell. 2006 Dec 1;127(5):969-82. doi: 10.1016/j.cell.2006.09.047

O'Toole ET, Winey M, McIntosh JR. High-voltage electron tomography of spindle pole bodies and early mitotic spindles in the yeast Saccharomyces cerevisiae. Mol Biol Cell. 1999 Jun;10(6):2017-31. doi: 10.1091/mbc.10.6.2017

Indjeian VB, Murray AW. Budding yeast mitotic chromosomes have an intrinsic bias to biorient on the spindle. Curr Biol. 2007 Nov 6;17(21):1837-46. doi: 10.1016/j.cub.2007.09.056

Tanaka TU. Chromosome bi-orientation on the mitotic spindle. Philos Trans R Soc Lond B Biol Sci. 2005 Mar 29;360(1455):581-9. doi: 10.1098/rstb.2004.1612

Ault JG, Rieder CL. Chromosome mal-orientation and reorientation during mitosis. Cell Motil Cytoskeleton. 1992;22(3):155-9. doi: 10.1002/cm.970220302

Cimini D, Moree B, Canman JC, Salmon ED. Merotelic kinetochore orientation occurs frequently during early mitosis in mammalian tissue cells and error correction is achieved by two different mechanisms. J Cell Sci. 2003 Oct 15;116(Pt 20):4213-25. doi: 10.1242/jcs.00716

Compton DA. Chromosome orientation. J Cell Biol. 2007 Oct 22;179(2):179-81. doi: 10.1083/jcb.200709152

Gregan J, Polakova S, Zhang L, Tolić-Nørrelykke IM, Cimini D. Merotelic kinetochore attachment: causes and effects. Trends Cell Biol. 2011 Jun;21(6):374-81. doi: 10.1016/j.tcb.2011.01.003

Ricke RM, van Deursen JM. Correction of microtubule-kinetochore attachment errors: mechanisms and role in tumor suppression. Semin Cell Dev Biol. 2011 Aug;22(6):559-65. doi: 10.1016/j.semcdb.2011.03.007

Dudka D, Noatynska A, Smith CA, Liaudet N, McAinsh AD, Meraldi P. Complete microtubule-kinetochore occupancy favours the segregation of merotelic attachments. Nat Commun. 2018 May 23;9(1):2042. doi: 10.1038/s41467-018-04427-x

Cimini D, Howell B, Maddox P, Khodjakov A, Degrassi F, Salmon ED. Merotelic kinetochore orientation is a major mechanism of aneuploidy in mitotic mammalian tissue cells. J Cell Biol. 2001 Apr 30;153(3):517-27. doi: 10.1083/jcb.153.3.517

Torres EM, Williams BR, Amon A. Aneuploidy: cells losing their balance. Genetics. 2008 Jun;179(2):737-46. doi: 10.1534/genetics.108.090878

Tanaka K, Hirota T. Chromosome segregation machinery and cancer. Cancer Sci. 2009 Jul;100(7):1158-65. doi: 10.1111/j.1349-7006.2009.01178.x

Banerjee A, Adames N, Peccoud J, Tyson JJ. A stochastic model for error correction of kinetochore-microtubule attachments in budding yeast. PLoS One. 2020 Aug 6;15(8):e0236293. doi: 10.1371/journal.pone.0236293

Musacchio A. The Molecular Biology of Spindle Assembly Checkpoint Signaling Dynamics. Curr Biol. 2015 Oct 19;25(20):R1002-18. doi: 10.1016/j.cub.2015.08.051

Vleugel M, Hoogendoorn E, Snel B, Kops GJ. Evolution and function of the mitotic checkpoint. Dev Cell. 2012 Aug 14;23(2):239-50. doi: 10.1016/j.devcel.2012.06.013

Musacchio A, Salmon ED. The spindle-assembly checkpoint in space and time. Nat Rev Mol Cell Biol. 2007 May;8(5):379-93. doi: 10.1038/nrm2163

Lara-Gonzalez P, Pines J, Desai A. Spindle assembly checkpoint activation and silencing at kinetochores. Semin Cell Dev Biol. 2021 Sep;117:86-98. doi: 10.1016/j.semcdb.2021.06.009

Hartwell LH, Weinert TA. Checkpoints: controls that ensure the order of cell cycle events. Science. 1989 Nov 3;246(4930):629-34. doi: 10.1126/science.2683079

Hoyt MA, Totis L, Roberts BT. S. cerevisiae genes required for cell cycle arrest in response to loss of microtubule function. Cell. 1991 Aug 9;66(3):507-17. doi: 10.1016/0092-8674(81)90014-3

Li R, Murray AW. Feedback control of mitosis in budding yeast. Cell. 1991 Aug 9;66(3):519-31. doi: 10.1016/0092-8674(81)90015-5

Weiss E, Winey M. The Saccharomyces cerevisiae spindle pole body duplication gene MPS1 is part of a mitotic checkpoint. J Cell Biol. 1996 Jan;132(1-2):111-23. doi: 10.1083/jcb.132.1.111

Hwang LH, Lau LF, Smith DL, Mistrot CA, Hardwick KG, Hwang ES, Amon A, Murray AW. Budding yeast Cdc20: a target of the spindle checkpoint. Science. 1998 Feb 13;279(5353):1041-4. doi: 10.1126/science.279.5353.1041

Sudakin V, Chan GK, Yen TJ. Checkpoint inhibition of the APC/C in HeLa cells is mediated by a complex of BUBR1, BUB3, CDC20, and MAD2. J Cell Biol. 2001 Sep 3;154(5):925-36. doi: 10.1083/jcb.200102093

Fraschini R, Beretta A, Sironi L, Musacchio A, Lucchini G, Piatti S. Bub3 interaction with Mad2, Mad3 and Cdc20 is mediated by WD40 repeats and does not require intact kinetochores. EMBO J. 2001 Dec 3;20(23):6648-59. doi: 10.1093/emboj/20.23.6648

Schrock MS, Stromberg BR, Scarberry L, Summers MK. APC/C ubiquitin ligase: Functions and mechanisms in tumorigenesis. Semin Cancer Biol. 2020 Dec;67(Pt 2):80-91. doi: 10.1016/j.semcancer.2020.03.001

Parker LL, Piwnica-Worms H. Inactivation of the p34cdc2-cyclin B complex by the human WEE1 tyrosine kinase. Science. 1992 Sep 25;257(5078):1955-7. doi: 10.1126/science.1384126

Mueller PR, Coleman TR, Kumagai A, Dunphy WG. Myt1: a membrane-associated inhibitory kinase that phosphorylates Cdc2 on both threonine-14 and tyrosine-15. Science. 1995 Oct 6;270(5233):86-90. doi: 10.1126/science.270.5233.86

Boutros R, Dozier C, Ducommun B. The when and wheres of CDC25 phosphatases. Curr Opin Cell Biol. 2006 Apr;18(2):185-91. doi: 10.1016/j.ceb.2006.02.003

Gavet O, Pines J. Progressive activation of CyclinB1-Cdk1 coordinates entry to mitosis. Dev Cell. 2010 Apr 20;18(4):533-43. doi: 10.1016/j.devcel.2010.02.013

Kraft C, Herzog F, Gieffers C, Mechtler K, Hagting A, Pines J, Peters JM. Mitotic regulation of the human anaphase-promoting complex by phosphorylation. EMBO J. 2003 Dec 15;22(24):6598-609. doi: 10.1093/emboj/cdg627

Fujimitsu K, Grimaldi M, Yamano H. Cyclin-dependent kinase 1-dependent activation of APC/C ubiquitin ligase. Science. 2016 May 27;352(6289):1121-4. doi: 10.1126/science.aad3925

Zhang S, Chang L, Alfieri C, Zhang Z, Yang J, Maslen S, Skehel M, Barford D. Molecular mechanism of APC/C activation by mitotic phosphorylation. Nature. 2016 May 12;533(7602):260-264. doi: 10.1038/nature17973

Morin V, Prieto S, Melines S, Hem S, Rossignol M, Lorca T, Espeut J, Morin N, Abrieu A. CDK-dependent potentiation of MPS1 kinase activity is essential to the mitotic checkpoint. Curr Biol. 2012 Feb 21;22(4):289-95. doi: 10.1016/j.cub.2011.12.048

Qi W, Tang Z, Yu H. Phosphorylation- and polo-box-dependent binding of Plk1 to Bub1 is required for the kinetochore localization of Plk1. Mol Biol Cell. 2006 Aug;17(8):3705-16. doi: 10.1091/mbc.e06-03-0240

Wong OK, Fang G. Plx1 is the 3F3/2 kinase responsible for targeting spindle checkpoint proteins to kinetochores. J Cell Biol. 2005 Aug 29;170(5):709-19. doi: 10.1083/jcb.200502163

Elowe S, Hümmer S, Uldschmid A, Li X, Nigg EA. Tension-sensitive Plk1 phosphorylation on BubR1 regulates the stability of kinetochore microtubule interactions. Genes Dev. 2007 Sep 1;21(17):2205-19. doi: 10.1101/gad.436007

von Schubert C, Cubizolles F, Bracher JM, Sliedrecht T, Kops GJPL, Nigg EA. Plk1 and Mps1 Cooperatively Regulate the Spindle Assembly Checkpoint in Human Cells. Cell Rep. 2015 Jul 7;12(1):66-78. doi: 10.1016/j.celrep.2015.06.007

Chao WC, Kulkarni K, Zhang Z, Kong EH, Barford D. Structure of the mitotic checkpoint complex. Nature. 2012 Mar 21;484(7393):208-13. doi: 10.1038/nature10896

Liu ST, Zhang H. The mitotic checkpoint complex (MCC): looking back and forth after 15 years. AIMS Mol Sci. 2016;3(4):597-634. doi: 10.3934/molsci.2016.4.597

Wilson L, Panda D, Jordan MA. Modulation of microtubule dynamics by drugs: a paradigm for the actions of cellular regulators. Cell Struct Funct. 1999 Oct;24(5):329-35. doi: 10.1247/csf.24.329

Sarli V, Huemmer S, Sunder-Plassmann N, Mayer TU, Giannis A. Synthesis and biological evaluation of novel EG5 inhibitors. Chembiochem. 2005 Nov;6(11):2005-13. doi: 10.1002/cbic.200500168

Bunning AR, Gupta ML Jr. The importance of microtubule-dependent tension in accurate chromosome segregation. Front Cell Dev Biol. 2023 Jan 23;11:1096333. doi: 10.3389/fcell.2023.1096333

Overlack K, Primorac I, Vleugel M, Krenn V, Maffini S, Hoffmann I, Kops GJ, Musacchio A. A molecular basis for the differential roles of Bub1 and BubR1 in the spindle assembly checkpoint. Elife. 2015 Jan 22;4:e05269. doi: 10.7554/eLife.05269

Di Fiore B, Davey NE, Hagting A, Izawa D, Mansfeld J, Gibson TJ, Pines J. The ABBA motif binds APC/C activators and is shared by APC/C substrates and regulators. Dev Cell. 2015 Feb 9;32(3):358-372. doi: 10.1016/j.devcel.2015.01.003

Santaguida S, Tighe A, D'Alise AM, Taylor SS, Musacchio A. Dissecting the role of MPS1 in chromosome biorientation and the spindle checkpoint through the small molecule inhibitor reversine. J Cell Biol. 2010 Jul 12;190(1):73-87. doi: 10.1083/jcb.201001036

Cunha-Silva S, Osswald M, Goemann J, Barbosa J, Santos LM, Resende P, Bange T, Ferrás C, Sunkel CE, Conde C. Mps1-mediated release of Mad1 from nuclear pores ensures the fidelity of chromosome segregation. J Cell Biol. 2020 Mar 2;219(3):e201906039. doi: 10.1083/jcb.201906039

Karess R. Rod-Zw10-Zwilch: a key player in the spindle checkpoint. Trends Cell Biol. 2005 Jul;15(7):386-92. doi: 10.1016/j.tcb.2005.05.003

Dou Z, Prifti DK, Gui P, Liu X, Elowe S, Yao X. Recent Progress on the Localization of the Spindle Assembly Checkpoint Machinery to Kinetochores. Cells. 2019 Mar 23;8(3):278. doi: 10.3390/cells8030278

Lara-Gonzalez P, Kim T, Oegema K, Corbett K, Desai A. A tripartite mechanism catalyzes Mad2-Cdc20 assembly at unattached kinetochores. Science. 2021 Jan 1;371(6524):64-67. doi: 10.1126/science.abc1424

Brito DA, Rieder CL. Mitotic checkpoint slippage in humans occurs via cyclin B destruction in the presence of an active checkpoint. Curr Biol. 2006 Jun 20;16(12):1194-200. doi: 10.1016/j.cub.2006.04.043

Gascoigne KE, Taylor SS. Cancer cells display profound intra- and interline variation following prolonged exposure to antimitotic drugs. Cancer Cell. 2008 Aug 12;14(2):111-22. doi: 10.1016/j.ccr.2008.07.002

Rudner AD, Murray AW. Phosphorylation by Cdc28 activates the Cdc20-dependent activity of the anaphase-promoting complex. J Cell Biol. 2000 Jun 26;149(7):1377-90. doi: 10.1083/jcb.149.7.1377

Ballister ER, Riegman M, Lampson MA. Recruitment of Mad1 to metaphase kinetochores is sufficient to reactivate the mitotic checkpoint. J Cell Biol. 2014 Mar 17;204(6):901-8. doi: 10.1083/jcb.201311113

Heinrich S, Sewart K, Windecker H, Langegger M, Schmidt N, Hustedt N, Hauf S. Mad1 contribution to spindle assembly checkpoint signalling goes beyond presenting Mad2 at kinetochores. EMBO Rep. 2014 Mar;15(3):291-8. doi: 10.1002/embr.201338114

Pines J. Mitosis: a matter of getting rid of the right protein at the right time. Trends Cell Biol. 2006 Jan;16(1):55-63. doi: 10.1016/j.tcb.2005.11.006

Hagting A, Den Elzen N, Vodermaier HC, Waizenegger IC, Peters JM, Pines J. Human securin proteolysis is controlled by the spindle checkpoint and reveals when the APC/C switches from activation by Cdc20 to Cdh1. J Cell Biol. 2002 Jun 24;157(7):1125-37. doi: 10.1083/jcb.200111001

Reddy SK, Rape M, Margansky WA, Kirschner MW. Ubiquitination by the anaphase-promoting complex drives spindle checkpoint inactivation. Nature. 2007 Apr 19;446(7138):921-5. doi: 10.1038/nature05734

Jia L, Li B, Warrington RT, Hao X, Wang S, Yu H. Defining pathways of spindle checkpoint silencing: functional redundancy between Cdc20 ubiquitination and p31(comet). Mol Biol Cell. 2011 Nov;22(22):4227-35. doi: 10.1091/mbc.E11-05-0389

Jia L, Kim S, Yu H. Tracking spindle checkpoint signals from kinetochores to APC/C. Trends Biochem Sci. 2013 Jun;38(6):302-11. doi: 10.1016/j.tibs.2013.03.004

McLean JR, Chaix D, Ohi MD, Gould KL. State of the APC/C: organization, function, and structure. Crit Rev Biochem Mol Biol. 2011 Apr;46(2):118-36. doi: 10.3109/10409238.2010.541420

Miniowitz-Shemtov S, Eytan E, Kaisari S, Sitry-Shevah D, Hershko A. Mode of interaction of TRIP13 AAA-ATPase with the Mad2-binding protein p31comet and with mitotic checkpoint complexes. Proc Natl Acad Sci U S A. 2015 Sep 15;112(37):11536-40. doi: 10.1073/pnas.1515358112

Herman JA, Miller MP, Biggins S. chTOG is a conserved mitotic error correction factor. Elife. 2020 Dec 30;9:e61773. doi: 10.7554/eLife.61773

Spittle C, Charrasse S, Larroque C, Cassimeris L. The interaction of TOGp with microtubules and tubulin. J Biol Chem. 2000 Jul 7;275(27):20748-53. doi: 10.1074/jbc.M002597200

Hood FE, Williams SJ, Burgess SG, Richards MW, Roth D, Straube A, Pfuhl M, Bayliss R, Royle SJ. Coordination of adjacent domains mediates TACC3-ch-TOG-clathrin assembly and mitotic spindle binding. J Cell Biol. 2013 Aug 5;202(3):463-78. doi: 10.1083/jcb.201211127

van der Vaart B, Manatschal C, Grigoriev I, Olieric V, Gouveia SM, Bjelic S, Demmers J, Vorobjev I, Hoogenraad CC, Steinmetz MO, Akhmanova A. SLAIN2 links microtubule plus end-tracking proteins and controls microtubule growth in interphase. J Cell Biol. 2011 Jun 13;193(6):1083-99. doi: 10.1083/jcb.201012179

Cimini D, Wan X, Hirel CB, Salmon ED. Aurora kinase promotes turnover of kinetochore microtubules to reduce chromosome segregation errors. Curr Biol. 2006 Sep 5;16(17):1711-8. doi: 10.1016/j.cub.2006.07.022

Zaytsev AV, Mick JE, Maslennikov E, Nikashin B, DeLuca JG, Grishchuk EL. Multisite phosphorylation of the NDC80 complex gradually tunes its microtubule-binding affinity. Mol Biol Cell. 2015 May 15;26(10):1829-44. doi: 10.1091/mbc.E14-11-1539

Wimbish RT, DeLuca JG. Hec1/Ndc80 Tail Domain Function at the Kinetochore-Microtubule Interface. Front Cell Dev Biol. 2020 Feb 26;8:43. doi: 10.3389/fcell.2020.00043

Kucharski TJ, Hards R, Vandal SE, Abad MA, Jeyaprakash AA, Kaye E, Al-Rawi A, Ly T, Godek KM, Gerber SA, Compton DA. Small changes in phospho-occupancy at the kinetochore-microtubule interface drive mitotic fidelity. J Cell Biol. 2022 Sep 5;221(9):e202107107. doi: 10.1083/jcb.202107107

DeLuca KF, Lens SM, DeLuca JG. J Cell Sci. 2011 Feb 15;124(Pt 4):622-34. doi: 10.1242/jcs.072629

Hindriksen S, Lens SMA, Hadders MA. The Ins and Outs of Aurora B Inner Centromere Localization. Front Cell Dev Biol. 2017 Dec 22;5:112. doi: 10.3389/fcell.2017.00112

Carmena M, Wheelock M, Funabiki H, Earnshaw WC. The chromosomal passenger complex (CPC): from easy rider to the godfather of mitosis. Nat Rev Mol Cell Biol. 2012 Dec;13(12):789-803. doi: 10.1038/nrm3474

Klein UR, Nigg EA, Gruneberg U. Centromere targeting of the chromosomal passenger complex requires a ternary subcomplex of Borealin, Survivin, and the N-terminal domain of INCENP. Mol Biol Cell. 2006 Jun;17(6):2547-58. doi: 10.1091/mbc.e05-12-1133

Kitajima TS, Hauf S, Ohsugi M, Yamamoto T, Watanabe Y. Human Bub1 defines the persistent cohesion site along the mitotic chromosome by affecting Shugoshin localization. Curr Biol. 2005 Feb 22;15(4):353-9. doi: 10.1016/j.cub.2004.12.044

De Antoni A, Maffini S, Knapp S, Musacchio A, Santaguida S. A small-molecule inhibitor of Haspin alters the kinetochore functions of Aurora B. J Cell Biol. 2012 Oct 15;199(2):269-84. doi: 10.1083/jcb.201205119

Kelly AE, Ghenoiu C, Xue JZ, Zierhut C, Kimura H, Funabiki H. Survivin reads phosphorylated histone H3 threonine 3 to activate the mitotic kinase Aurora B. Science. 2010 Oct 8;330(6001):235-9. doi: 10.1126/science.1189505

Kawashima SA, Tsukahara T, Langegger M, Hauf S, Kitajima TS, Watanabe Y. Shugoshin enables tension-generating attachment of kinetochores by loading Aurora to centromeres. Genes Dev. 2007 Feb 15;21(4):420-35. doi: 10.1101/gad.1497307

Bakhoum SF, Cantley LC. The Multifaceted Role of Chromosomal Instability in Cancer and Its Microenvironment. Cell. 2018 Sep 6;174(6):1347-1360. doi: 10.1016/j.cell.2018.08.027

Santaguida S, Amon A. Short- and long-term effects of chromosome mis-segregation and aneuploidy. Nat Rev Mol Cell Biol 16, 473–485 (2015). https://doi.org/10.1038/nrm4025

Hara, M., and Fukagawa, T. (2018). Kinetochore assembly and disassembly during mitotic entry and exit. Current opinion in cell biology 52, 73-81. 10.1016/j.ceb.2018.02.005.

Mellone, B.G., and Fachinetti, D. (2021). Diverse mechanisms of centromere specification. Current biology : CB 31, R1491-R1504. 10.1016/j.cub.2021.09.083.

Earnshaw WC, Rothfield N. Identification of a family of human centromere proteins using autoimmune sera from patients with scleroderma. Chromosoma. 1985;91(3-4):313-21. doi: 10.1007/BF00328227

Tomkiel J, Cooke CA, Saitoh H, Bernat RL, Earnshaw WC. CENP-C is required for maintaining proper kinetochore size and for a timely transition to anaphase. J Cell Biol. 1994 May;125(3):531-45. doi: 10.1083/jcb.125.3.531

Fukagawa T, Brown WR. Efficient conditional mutation of the vertebrate CENP-C gene. Hum Mol Genet. 1997 Dec;6(13):2301-8. doi: 10.1093/hmg/6.13.2301

Kalitsis P, Fowler KJ, Earle E, Hill J, Choo KH. Targeted disruption of mouse centromere protein C gene leads to mitotic disarray and early embryo death. Proc Natl Acad Sci U S A. 1998 Feb 3;95(3):1136-41. doi: 10.1073/pnas.95.3.1136

Fukagawa T, Pendon C, Morris J, Brown W. CENP-C is necessary but not sufficient to induce formation of a functional centromere. EMBO J. 1999 Aug 2;18(15):4196-209. doi: 10.1093/emboj/18.15.4196

Klare K, Weir JR, Basilico F, Zimniak T, Massimiliano L, Ludwigs N, Herzog F, Musacchio A. CENP-C is a blueprint for constitutive centromere-associated network assembly within human kinetochores. J Cell Biol. 2015 Jul 6;210(1):11-22. doi: 10.1083/jcb.201412028

Kato H, Jiang J, Zhou BR, Rozendaal M, Feng H, Ghirlando R, Xiao TS, Straight AF, Bai Y. A conserved mechanism for centromeric nucleosome recognition by centromere protein CENP-C. Science. 2013 May 31;340(6136):1110-3. doi: 10.1126/science

Petrovic A, Keller J, Liu Y, Overlack K, John J, Dimitrova YN, Jenni S, van Gerwen S, Stege P, Wohlgemuth S, Rombaut P, Herzog F, Harrison SC, Vetter IR, Musacchio A. Structure of the MIS12 Complex and Molecular Basis of Its Interaction with CENP-C at Human Kinetochores. Cell. 2016 Nov 3;167(4):1028-1040.e15. doi: 10.1016/j.cell.2016.10.005

Rago F, Gascoigne KE, Cheeseman IM. Distinct organization and regulation of the outer kinetochore KMN network downstream of CENP-C and CENP-T. Curr Biol. 2015 Mar 2;25(5):671-7. doi: 10.1016/j.cub.2015.01.059

Bonner MK, Haase J, Swinderman J, Halas H, Miller Jenkins LM, Kelly AE. Enrichment of Aurora B kinase at the inner kinetochore controls outer kinetochore assembly. J Cell Biol. 2019 Oct 7;218(10):3237-3257. doi: 10.1083/jcb.201901004

Kline SL, Cheeseman IM, Hori T, Fukagawa T, Desai A. The human Mis12 complex is required for kinetochore assembly and proper chromosome segregation. J Cell Biol. 2006 Apr 10;173(1):9-17. doi: 10.1083/jcb.200509158

McNairn AJ, Chuang CH, Bloom JC, Wallace MD, Schimenti JC. Female-biased embryonic death from inflammation induced by genomic instability. Nature. 2019 Mar;567(7746):105-108. doi: 10.1038/s41586-019-0936-6

Kemp CJ. Multistep skin cancer in mice as a model to study the evolution of cancer cells. Semin Cancer Biol. 2005 Dec;15(6):460-73. doi: 10.1016/j.semcancer.2005.06.003

Abel EL, Angel JM, Kiguchi K, DiGiovanni J. Multi-stage chemical carcinogenesis in mouse skin: fundamentals and applications. Nat Protoc. 2009;4(9):1350-62. doi: 10.1038/nprot.2009.120

Liu D, Vader G, Vromans MJ, Lampson MA, Lens SM. Sensing chromosome bi-orientation by spatial separation of aurora B kinase from kinetochore substrates. Science. 2009 Mar 6;323(5919):1350-3. doi: 10.1126/science.1167000

Zaytsev AV, Sundin LJ, DeLuca KF, Grishchuk EL, DeLuca JG. Accurate phosphoregulation of kinetochore-microtubule affinity requires unconstrained molecular interactions. J Cell Biol. 2014 Jul 7;206(1):45-59. doi: 10.1083/jcb.201312107

Long AF, Udy DB, Dumont S. Hec1 Tail Phosphorylation Differentially Regulates Mammalian Kinetochore Coupling to Polymerizing and Depolymerizing Microtubules. Curr Biol. 2017 Jun 5;27(11):1692-1699.e3. doi: 10.1016/j.cub.2017.04.058

Stumpff J, von Dassow G, Wagenbach M, Asbury C, Wordeman L. The kinesin-8 motor Kif18A suppresses kinetochore movements to control mitotic chromosome alignment. Dev Cell. 2008 Feb;14(2):252-62. doi: 10.1016/j.devcel.2007.11.014

Watanabe Y. Temporal and spatial regulation of targeting aurora B to the inner centromere. Cold Spring Harb Symp Quant Biol. 2010;75:419-23. doi: 10.1101/sqb.2010.75.035

Wang F, Ulyanova NP, van der Waal MS, Patnaik D, Lens SM, Higgins JM. A positive feedback loop involving Haspin and Aurora B promotes CPC accumulation at centromeres in mitosis. Curr Biol. 2011 Jun 21;21(12):1061-9. doi: 10.1016/j.cub.2011.05.016

Dewar H, Tanaka K, Nasmyth K, Tanaka TU. Tension between two kinetochores suffices for their bi-orientation on the mitotic spindle. Nature. 2004 Mar 4;428(6978):93-7. doi: 10.1038/nature02328

Lampson MA, Renduchitala K, Khodjakov A, Kapoor TM. Correcting improper chromosome-spindle attachments during cell division. Nat Cell Biol. 2004 Mar;6(3):232-7. doi: 10.1038/ncb1102

Kapoor TM, Mayer TU, Coughlin ML, Mitchison TJ. Probing spindle assembly mechanisms with monastrol, a small molecule inhibitor of the mitotic kinesin, Eg5. J Cell Biol. 2000 Sep 4;150(5):975-88. doi: 10.1083/jcb.150.5.975

Abe Y, Sako K, Takagaki K, Hirayama Y, Uchida KS, Herman JA, DeLuca JG, Hirota T. HP1-Assisted Aurora B Kinase Activity Prevents Chromosome Segregation Errors. Dev Cell. 2016 Mar 7;36(5):487-97. doi: 10.1016/j.devcel.2016.02.008

Parrinello S, Samper E, Krtolica A, Goldstein J, Melov S, Campisi J. Oxygen sensitivity severely limits the replicative lifespan of murine fibroblasts. Nat Cell Biol. 2003 Aug;5(8):741-7. doi: 10.1038/ncb1024

Suzuki A, Badger BL, Salmon ED. A quantitative description of Ndc80 complex linkage to human kinetochores. Nat Commun. 2015 Sep 8;6:8161. doi: 10.1038/ncomms9161

Walstein K, Petrovic A, Pan D, Hagemeier B, Vogt D, Vetter IR, Musacchio A. Assembly principles and stoichiometry of a complete human kinetochore module. Sci Adv. 2021 Jun 30;7(27):eabg1037. doi: 10.1126/sciadv.abg1037

Salimian KJ, Ballister ER, Smoak EM, Wood S, Panchenko T, Lampson MA, Black BE. Feedback control in sensing chromosome biorientation by the Aurora B kinase. Curr Biol. 2011 Jul 12;21(13):1158-65. doi: 10.1016/j.cub.2011.06.015

Cheeseman IM, Hori T, Fukagawa T, Desai A. KNL1 and the CENP-H/I/K complex coordinately direct kinetochore assembly in vertebrates. Mol Biol Cell. 2008 Feb;19(2):587-94. doi: 10.1091/mbc.e07-10-1051

Kimura H, Hayashi-Takanaka Y, Goto Y, Takizawa N, Nozaki N. The organization of histone H3 modifications as revealed by a panel of specific monoclonal antibodies. Cell Struct Funct. 2008;33(1):61-73. doi: 10.1247/csf.07035

Ando S, Yang H, Nozaki N, Okazaki T, Yoda K. CENP-A, -B, and -C chromatin complex that contains the I-type alpha-satellite array constitutes the prekinetochore in HeLa cells. Mol Cell Biol. 2002 Apr;22(7):2229-41. doi: 10.1128/MCB.22.7.2229-2241.2002

Nozawa RS, Nagao K, Masuda HT, Iwasaki O, Hirota T, Nozaki N, Kimura H, Obuse C. Human POGZ modulates dissociation of HP1alpha from mitotic chromosome arms through Aurora B activation. Nat Cell Biol. 2010 Jul;12(7):719-27. doi: 10.1038/ncb2075

Cong L, Ran FA, Cox D, Lin S, Barretto R, Habib N, Hsu PD, Wu X, Jiang W, Marraffini LA, Zhang F. Multiplex genome engineering using CRISPR/Cas systems. Science. 2013 Feb 15;339(6121):819-23. doi: 10.1126/science.1231143

Mátés L, Chuah MK, Belay E, Jerchow B, Manoj N, Acosta-Sanchez A, Grzela DP, Schmitt A, Becker K, Matrai J, Ma L, Samara-Kuko E, Gysemans C, Pryputniewicz D, Miskey C, Fletcher B, VandenDriessche T, Ivics Z, Izsvák Z. Molecular evolution of a novel hyperactive Sleeping Beauty transposase enables robust stable gene transfer in vertebrates. Nat Genet. 2009 Jun;41(6):753-61. doi: 10.1038/ng.343

Schindelin J, Arganda-Carreras I, Frise E, Kaynig V, Longair M, Pietzsch T, Preibisch S, Rueden C, Saalfeld S, Schmid B et al. Fiji: an open-source platform for biological-image analysis. 2012 Jun 28. Nature methods 9, 676-682. 10.1038/nmeth.2019.

Hashimoto M, Yamashita Y, Takemoto T. Electroporation of Cas9 protein/sgRNA into early pronuclear zygotes generates non-mosaic mutants in the mouse. Dev Biol. 2016 Oct 1;418(1):1-9. doi: 10.1016/j.ydbio.2016.07.017

Doench JG, Fusi N, Sullender M, Hegde M, Vaimberg EW, Donovan KF, Smith I, Tothova Z, Wilen C, Orchard R, Virgin HW, Listgarten J, Root DE. Optimized sgRNA design to maximize activity and minimize off-target effects of CRISPR-Cas9. Nat Biotechnol. 2016 Feb;34(2):184-191. doi: 10.1038/nbt.3437

Sanson KR, Hanna RE, Hegde M, Donovan KF, Strand C, Sullender ME, Vaimberg EW, Goodale A, Root DE, Piccioni F, Doench JG. Optimized libraries for CRISPR-Cas9 genetic screens with multiple modalities. Nat Commun. 2018 Dec 21;9(1):5416. doi: 10.1038/s41467-018-07901-8

Concordet JP, Haeussler M. CRISPOR: intuitive guide selection for CRISPR/Cas9 genome editing experiments and screens. Nucleic Acids Res. 2018 Jul 2;46(W1):W242-W245. doi: 10.1093/nar/gky354

Nishimura K, Fukagawa T, Takisawa H, Kakimoto T, Kanemaki M. An auxin-based degron system for the rapid depletion of proteins in nonplant cells. Nat Methods. 2009 Dec;6(12):917-22. doi: 10.1038/nmeth.1401

Nishimura K, Fukagawa T. An efficient method to generate conditional knockout cell lines for essential genes by combination of auxin-inducible degron tag and CRISPR/Cas9. Chromosome Res. 2017 Oct;25(3-4):253-260. doi: 10.1007/s10577-017-9559-7

Nishimura K, Yamada R, Hagihara S, Iwasaki R, Uchida N, Kamura T, Takahashi K, Torii KU, Fukagawa T. A super-sensitive auxin-inducible degron system with an engineered auxin-TIR1 pair. Nucleic Acids Res. 2020 Oct 9;48(18):e108. doi: 10.1093/nar/gkaa748

Moran EC, Liu L, Zasadzinska E, Kestner CA, Sarkeshik A, DeHoyos H, Yates JR, Foltz D, Stukenberg PT. Mitotic R-loops direct Aurora B kinase to maintain centromeric cohesion. 2021 Jan 15;bioRxiv 10.1101/2021.01.14.426738

Iemura K, Tanaka K. Chromokinesin Kid and kinetochore kinesin CENP-E differentially support chromosome congression without end-on attachment to microtubules. Nat Commun. 2015 Mar 6;6:6447. doi: 10.1038/ncomms7447

Thévenaz P, Ruttimann UE, Unser M. A pyramid approach to subpixel registration based on intensity. IEEE Trans Image Process. 1998;7(1):27-41. doi: 10.1109/83.650848

Potapova T, Gorbsky GJ. The Consequences of Chromosome Segregation Errors in Mitosis and Meiosis. Biology (Basel). 2017 Feb 8;6(1):12. doi: 10.3390/biology6010012

Messin LJ, Millar JB. Role and regulation of kinesin-8 motors through the cell cycle. Syst Synth Biol. 2014 Sep;8(3):205-13. doi: 10.1007/s11693-014-9140-z. Epub 2014 Mar 23

Luboshits G, Benayahu D. MS-KIF18A, new kinesin; structure and cellular expression. Gene. 2005 May 23;351:19-28. doi: 10.1016/j.gene.2005.02.009

Peters C, Brejc K, Belmont L, Bodey AJ, Lee Y, Yu M, Guo J, Sakowicz R, Hartman J, Moores CA. Insight into the molecular mechanism of the multitasking kinesin-8 motor. EMBO J. 2010 Oct 20;29(20):3437-47. doi: 10.1038/emboj.2010.220

Lin Y, Wei YL, She ZY. Kinesin-8 motors: regulation of microtubule dynamics and chromosome movements. Chromosoma. 2020 Jun;129(2):99-110. doi: 10.1007/s00412-020-00736-7

Varga V, Leduc C, Bormuth V, Diez S, Howard J. Kinesin-8 motors act cooperatively to mediate length-dependent microtubule depolymerization. Cell. 2009 Sep 18;138(6):1174-83. doi: 10.1016/j.cell.2009.07.032

Häfner J, Mayr MI, Möckel MM, Mayer TU. Pre-anaphase chromosome oscillations are regulated by the antagonistic activities of Cdk1 and PP1 on Kif18A. Nat Commun. 2014 Jul 22;5:4397. doi: 10.1038/ncomms5397

Huang Y, Yao Y, Xu HZ, Wang ZG, Lu L, Dai W. Defects in chromosome congression and mitotic progression in KIF18A-deficient cells are partly mediated through impaired functions of CENP-E. Cell Cycle. 2009 Aug 15;8(16):2643-9. doi: 10.4161/cc.8.16.9366

Marquis C, Fonseca CL, Queen KA, Wood L, Vandal SE, Malaby HL, Clayton JE, Stumpff J. Chromosomally unstable tumor cells specifically require KIF18A for proliferation. Nat Commun 12, 1213 (2021). https://doi.org/10.1038/s41467-021-21447-2

Fonseca CL, Malaby HLH, Sepaniac LA, Martin W, Byers C, Czechanski A, Messinger D, Tang M, Ohi R, Reinholdt LG, Stumpff J. Mitotic chromosome alignment ensures mitotic fidelity by promoting interchromosomal compaction during anaphase. J Cell Biol. 2019 Apr 1;218(4):1148-1163. doi: 10.1083/jcb.201807228

Alushin GM, Musinipally V, Matson D, Tooley J, Stukenberg PT, Nogales E. Multimodal microtubule binding by the Ndc80 kinetochore complex. Nat Struct Mol Biol. 2012 Nov;19(11):1161-7. doi: 10.1038/nsmb.2411

Mitchison T, Evans L, Schulze E, Kirschner M. Sites of microtubule assembly and disassembly in the mitotic spindle. Cell. 1986 May 23;45(4):515-27. doi: 10.1016/0092-8674(86)90283-7

Tanaka TU, Desai A. Kinetochore-microtubule interactions: the means to the end. Curr Opin Cell Biol. 2008 Feb;20(1):53-63. doi: 10.1016/j.ceb.2007.11.005

Rieder CL. The structure of the cold-stable kinetochore fiber in metaphase PtK1 cells. Chromosoma. 1981;84(1):145-58. doi: 10.1007/BF00293368

Tolić IM. Mitotic spindle: kinetochore fibers hold on tight to interpolar bundles. Eur Biophys J. 2018 Apr;47(3):191-203. doi: 10.1007/s00249-017-1244-4

DeLuca JG, Dong Y, Hergert P, Strauss J, Hickey JM, Salmon ED, McEwen BF. Hec1 and nuf2 are core components of the kinetochore outer plate essential for organizing microtubule attachment sites. Mol Biol Cell. 2005 Feb;16(2):519-31. doi: 10.1091/mbc.e04-09-0852

Dudka D, Noatynska A, Smith CA, Liaudet N, McAinsh AD, Meraldi P. Complete microtubule-kinetochore occupancy favours the segregation of merotelic attachments. Nat Commun. 2018 May 23;9(1):2042. doi: 10.1038/s41467-018-04427-x

Sen O, Saurin AT, Higgins JMG. The live cell DNA stain SiR-Hoechst induces DNA damage responses and impairs cell cycle progression. Sci Rep. 2018 May 21;8(1):7898. doi: 10.1038/s41598-018-26307-6

Yang J, Ikezoe T, Nishioka C, Tasaka T, Taniguchi A, Kuwayama Y, Komatsu N, Bandobashi K, Togitani K, Koeffler HP, Taguchi H, Yokoyama A. AZD1152, a novel and selective aurora B kinase inhibitor, induces growth arrest, apoptosis, and sensitization for tubulin depolymerizing agent or topoisomerase II inhibitor in human acute leukemia cells in vitro and in vivo. Blood. 2007 Sep 15;110(6):2034-40. doi: 10.1182/blood-2007-02-073700

Janssen A, van der Burg M, Szuhai K, Kops GJ, Medema RH. Chromosome segregation errors as a cause of DNA damage and structural chromosome aberrations. Science. 2011 Sep 30;333(6051):1895-8. doi: 10.1126/science.1210214

Mayr MI, Hümmer S, Bormann J, Grüner T, Adio S, Woehlke G, Mayer TU. The human kinesin Kif18A is a motile microtubule depolymerase essential for chromosome congression. Curr Biol. 2007 Mar 20;17(6):488-98. doi: 10.1016/j.cub.2007.02.036

Janssen LME, Averink TV, Blomen VA, Brummelkamp TR, Medema RH, Raaijmakers JA. Loss of Kif18A Results in Spindle Assembly Checkpoint Activation at Microtubule-Attached Kinetochores. Curr Biol. 2018 Sep 10;28(17):2685-2696.e4. doi: 10.1016/j.cub.2018.06.026

Quinton RJ, DiDomizio A, Vittoria MA, Kotýnková K, Ticas CJ, Patel S, Koga Y, Vakhshoorzadeh J, Hermance N, Kuroda TS, Parulekar N, Taylor AM, Manning AL, Campbell JD, Ganem NJ. Whole-genome doubling confers unique genetic

vulnerabilities on tumour cells. Nature. 2021 Feb;590(7846):492-497. doi: 10.1038/s41586-020-03133-3

Hain KO, Colin DJ, Rastogi S, Allan LA, Clarke PR. Prolonged mitotic arrest induces a caspase-dependent DNA damage response at telomeres that determines cell survival. Sci Rep. 2016 May 27;6:26766. doi: 10.1038/srep26766

Acknowledgement

Life as a graduate student has been challenging, but I believe it is a precious opportunity to explore the world of science. I am deeply grateful for the chance to study in the Fukagawa Lab.

First and foremost, I would like to thank my supervisor, Professor Fukagawa. I am very fortunate to have him as my advisor. He is a knowledgeable and brilliant teacher who generously shares his time and patience, providing invaluable support for my research. I couldn’t have made any progress without his guidance.

I’d also like to express my appreciation to Hara-san. I learned to take science seriously and with dedication from him. Thanks to his helpful discussions, suggestions and teaching, I was able to make progress in my work.

I also want to thank Hirano-san has also been a tremendous help. As my first teacher in molecular biology techniques and fluorescence microscopy, he has been incredibly kind and patient, helping me resolve many issues during my experiments.

I am thankful to all the members of the laboratory for their kindness and support. Takenoshita-san provided many helpful suggestions. Asakawa-san, Ariyoshi-san, Shreyas-san, and Hori-san offered professional advice kindly, and Fukuoka-san, Kubota-san, and Kondo-san managed the essential tasks that allowed us to focus more on our experiments. Thanks to Cao-san, Jiang-san, Yamaguchi-san, Miao-san, Sha-san, Zhou-san, and Li-san. Their support helped me adapt quickly to lab life.

I would also like to thank all members of the Hiraoka lab. I am deeply grateful to Professor Hiraoka for accepting me into FBS. Ogawa-san and Tcuchiya-san guided me through my first project and showed great care for my well-being, dedicating time and patience to help me improve academically.

Without everyone's help, I could not have made progress in my research. I will never forget their support and kindness.

Achievement

Publication

Weixia Kong, Masatoshi Hara, Yurika Tokunaga, Kazuhiro Okumura, Yasuhiro Hirano, Jiahang Miao, Yusuke Takenoshita, Masakazu Hashimoto, Hiroshi Sasaki, Toshihiko Fujimori, Yuichi Wakabayashi, and Tatsuo Fukagawa. CENP-C-Mis12 complex establishes a regulatory loop through Aurora B for chromosome segregation. **(under review)**

Tsuchiya M, **Kong WX**, Hiraoka Y, Haraguchi T, Ogawa H. TBK1 inhibitors enhance transfection efficiency by suppressing p62/SQSTM1 phosphorylation. Genes Cells. 2023 Jan;28(1):68-77.

Zhang WC, Cui YY, Du Y, Yang Y, Fang T, Lu FF, **Kong WX,** Xiao CJ, Shi J, Reid LM, He ZY. Liver cell therapies: cellular sources and grafting strategies. Front Med. 2023 Jun;17(3):432-457. doi: 10.1007/s11684-023-1002-1. Epub 2023 Jul 4. PMID: 37402953.

Kong WX, Zhu H, Jiang XX, Li H, Liu YL, Wu Y, Zhang Y, Mao N. Involvement of MAPK pathway in the osteoblastic differentiation of mouse mesenchymal stem cells. *Journal of Experimental Hematology*. 2010, 18(4): 981-5. (Article in Chinese)

Kong WX, Jiang XX, Mao N. Immunoregulatory function of mesenchymal stem cells and application of mesenchymal stem cells in therapy of autoimmune disease. *Journal of Experimental Hematology*. 2009, 17(6): 1605-8. (Review in Chinese)

Presentation

1. 5/6/2024 – 6/6/2024 World presentation and poster presentation at FBS retreat.
2. 25/1/2024 – 26/1/2024 Oral presentation at 2nd Joint meeting.
3. 12/6/2023 – 12/8/2023 Poster presentation in the 46th Annual Meeting of the Molecular Biology Society of Japan (MBSJ).
4. 11/30/2022 – 12/2/2022 Poster presentation in the 45th Annual Meeting of the Molecular Biology Society of Japan (MBSJ).